NOVEL BIOCOMPATIBLE/ANTIMICROBIAL MATERIALS BASED ON NITRIC OXIDE RELEASE/GENERATION

By

Wenyi Cai

A dissertation submitted in partial fulfillment
of the requirements for the degree of
Doctor of Philosophy
(Chemistry)
in the University of Michigan
2013

Doctoral Committee:

Professor Mark E. Meyerhoff, Chair
Professor Zhan Chen
Associate Professor Nicolai Lehnert
Professor Steven P. Schwendeman
Associate Professor Chuanwu Xi

2013

Dedication

To my parents

Xuexiang Cai

Hongfang Yang

Acknowledgements

First and foremost, I would like to thank my advisor, Dr. Meyerhoff, for providing me with the opportunity to work under his guidance and gain enthusiasm from his resourceful ideas and passion about science. I'm especially thankful for his patience, encouragement, and initiation of new collaborations throughout my PhD research.

I'm also thankful to my dissertation committee members, Dr. Zhan Chen, Dr. Nicolai Lehnert, Dr. Steven P. Schwendeman and Dr. Chuanwu Xi for providing me with all their advice and lab facilities during my PhD research. In particular, I'd like to thank Professor Chuanwu Xi and Dr. Jianfeng Wu from the School of Public Health, who collaborated with us and provided us with their invaluable expertise and facilities for all the antimicrobial and antibiofilm studies. I am also grateful to Professor Schwendeman and his student, Dr. Yajun Liu, for their expertise and advice related to the PLGA project. Professor Lehnert and his student, Dr. Anna Merkle, kindly provided me with guidance and the tris(2-pyridylmethyl)amine synthesized in their lab. Professor Zhan Chen and his students assisted me with all the contact angle measurements.

In addition to my advisor and my committee, there were also a number of other people who provided invaluable assistance during my PhD research. I appreciate the help from Professor Arthur Ashe, who gave me guidance and provided me with his lab facilities for the synthesis of carboxyl-ebselen. I also want to thank Terry Major and Kelly Koch in the Extracorporeal Membrane Oxygenation (ECMO) lab at the University of Michigan Medical School for providing me with blood samples, as well as Dr. Hitesh Handa and Elizabeth Brisbois for providing me with the diazeniumdiolate species that was used in this dissertation research. In addition, I'd like to thank Kitty Zhang, the intelligent undergraduate student who worked with me to investigate the RSNO decomposition catalytic activity of CuO nanoparticles-based polyurethane films.

I also need to thank all the past and present members in the Meyerhoff group for their help and support throughout my graduate studies: Dr. Jun Yang, Dr. Kun Liu, Dr. Lin

Wang, Dr. Wansik Cha, Dr. Qinyi Yan, Dr. Dongxuan Shen, Dr. Laura Zimmerman, Dr. Natalie Crist, Dr. Kebede Gemene, Dr. Lajos Höfler, Dr. Gary Jensen, Dr. Dipankar Koley, Bo Peng, Andrea Bell, Elizabeth Brisbois, Alex Wolf, Si Yang, Alex Ketchum, Ren Hang and Zheng Zheng. In particular, I'd like to thank Dr. Kun Liu who taught me how to do organic synthesis when I first joined the group. I thank her for her patience throughout the Cu(II)-cyclen project. I want to thank Dr. Jun Yang for her guidance during my rotation project, as well as her undergrad Saman Mirkazemi, who started the pioneering work of RSe-based Layer-by-Layer films in the lab. I also want to give my special thanks to Elizabeth Brisbois, who provided me with the diazeniumdiolate, helped me with the pH measurements during the revision of a manuscript and also helped me with the revisions of my thesis.

Finally, I would like to thank my parents, Xuexiang Cai and Hongfang Yang, for their unconditional love and understanding during my graduate studies. I'm also grateful to my uncle Haoliang Sun, my aunt Hsiuting Huang and her sister Hsiuchin Huang who treat me like family and took care of me during my time as a graduate student in Michigan.

Table of Contents

List of Figures

List of Schemes

List of Tables

List of Abbreviations

AbsNO	*S*-nitrosoalbumin
Alg	Alginate
BB	BromothymolBlue
BP	Bromocresol Purple
cAMP	Cyclic Adenosine Monophosphate
CDC	Centers for Disease Control and Prevention
C-ebselen	Carboxyl-Ebselen
cGMP	Cyclic Guanosine Monophosphate
Cu(II)-cyclen	Cu(II)-1,4,7,10-Tetraazacyclododecane
Cu(II)-DTTCT	Cu(II)-Dibenzo-[e,k]-2,3,8,9-Tetraphenyl-1,4,7,10-Tetraaza-Cyclododeca-1,3,7,9-Tetraene
CV	Cyclic Voltammograms
CySH	Cysteine
CysNO	*S*-nitrosocysteine
DBHD	Dibutyhexyldiamine
DBHD/N_2O_2	Dibutyhexyldiamine Diazeniumdiolate
DIC	N,N'-diisopropylcarbodiimide
E. coli	*Escherichia coli*
Ebselen	2-Phenyl-1,2-benzisoselenazol-3-(2H)-one
EDC	1-(3-Dimethylaminopropyl)-3-ethylcarbodiimide
e-PEI	Carboxyl-ebselen Immobilized Polyethyelenimine
EPR	Electron Paramagnetic Resonance
FTSC	Fluorescein-5-thiosemicarbazide
GPx	Glutathione Peroxidase
GSH	Glutathione
GSNO	*S*-nitrosoglutathione
H_2O_2	Hydrogen Peroxide
HEPES	4-(2-hydroxyethyl)-1-piperazineethanesulfonic acid
ICP-HRMS	Inductively Coupled Plasma High-Resolution Mass Spectrometry
ICP-OES	Inductively Coupled Plasma - Optical Emission Spectroscopy
KTpClPB	Potassium Tetrakis(4-Chlorophenylborate)
Lb	Luria Bertani
LbL	Layer-by-Layer
MES	2-(N-morpholino)ethanesulfonic acid

N_2O_3	Dinitrogen Trioxide
NADPH	Nicotinamide Adenine Dinucleotide Phosphate
NHS	N-hydroxysuccinimide
NO_2	Nitrogen Dioxide
NO	Nitric Oxide
NOA	Nitric Oxide Analyzer
NONOate	Diazeniumdiolate
NOS	Nitric Oxide Synthase
NPs	Nanoparticles
$O_2^{\bullet-}$	Superoxide
$ONOO^-$	Peroxynitrite
P.aeruginosa	*Pseudomonas aeruginosa*
PBS	Phosphate Buffered Saline
PDDA	Poly(dially dimethyl ammonium chloride)
PEDs	Phosphodiesterases
PEG	Poly(ethylene glycol)
PEI	Polyethylenimine
PEMS	Polyelectrolytes Multilayers
PI-3	Phosphoinositide-3
PLGA	Poly(lactic-co-glycolic) Acid
PLL	Poly (lactic acid)
PRP	Platelet-Rich Sheep Plasma
PU	Polyurethane
PVC	Poly (vinyl chloride)
RB	Rhodamine B
RSNOs	*S*-nitrosothiols
S. aureus	*Staphylococcus aureus*
S. epidermidis	*Staphylococcus epidermidis*
SeCA	Selenocystamine
SeDPA	3, 3'-Dipropionicdiselenide
SEM	Scanning Electron Microscope
sGC	Soluble Guanylyl Cyclase
SNAP	*S*-nitroso-N-acetylpenicillamine
SR	Silicone Rubber
THF	Tetrahydrofuran
TPA	tris(2-pyridylmethyl)amine
vWF	von Willebrand Factor
XRD	X-ray Diffraction

Abstract

Novel Biocompatible/Antimicrobial Materials
Based on Nitric Oxide Release/Generation

By

Wenyi Cai

Chair: Mark E. Meyerhoff:

Thrombus formation and bacterial infection are two major problems that are associated with indwelling biomedical devices. In this dissertation work, coatings that are capable of releasing or generating nitric oxide (NO), a potent anti-platelet and antimicrobial agent, have been developed to solve the biocompatibility issues.

First, diazeniumdiolate doped-poly(lactic-*co*-glycolic acid) (PLGA)-based NO release coatings with controllable NO release profiles can be prepared with lifetimes of up to 15 d at room temperature (23 °C) and 10 d at 37 °C. The NO release coatings exhibit significant antibiofilm properties after one week incubation in a CDC biofilm reactor, which provided both renewable nutrient sources and shear forces. In particular, compared to a silicone rubber surface, an NO release film with a base layer of 30 wt% dibutyhexyldiamine diazeniumdiolate (DBHD/N_2O_2) mixed with poly(lactic acid) (PLL) exhibited ~ 98.4% reduction in biofilm biomass of *S. aureus* and ~ 99.9% reduction for *E. coli* at 37 °C.

NO can also be generated from endogenous NO donors such as *S*-nitrosothiols (RSNOs) by utilizing catalytic materials. A carboxyl-ebselen-based layer-by-layer (LbL) film was fabricated by alternatively assembling carboxyl-ebselen linked

polyethylenimine (e-PEI) and alginate (Alg) onto substrates followed by salt annealing and cross-linking. After soaking in sheep blood for 24 h, a polyurethane catheter coated with $(\text{e-PEI/Alg})_{50}$ exhibit an NO flux of 3×10^{-10} mol cm^{-2} min^{-1} in a reservoir containing physiological levels of RSNO and thiols. The LbL film is also capable of generating superoxide ($O_2^{\bullet-}$), a potent antimicrobial agent. *In-vitro* antimicrobial tests demonstrated that a $(\text{e-PEI/Alg})_{50}$ film is capable of killing 98.2 % *E. coli* in solution and reducing ~87% *E. coli* surface coverage within 2 h at 37 °C.

In addition, a novel CuO nanoparticle-doped polyurethane film with less leaching of copper and minimized toxicity issue compared with a similar film doped with Cu^0 nanoparticles is prepared. The film is capable of catalytically generating NO for 16 days at 37 °C.

With their proven potential antithrombotic or antimicrobial properties, the developed NO release and NO generation coatings are expected to improve the biocompatibility of indwelling surfaces, reduce the medical cost and save patients' lives.

Chapter 1 Introduction

Thrombus formation and bacterial infection are two common problems that lead to dysfunction of indwelling biomedical devices such as catheters, vascular grafts and stents. As a potent antiplatelet and endogenous antimicrobial agent, nitric oxide (NO) has been shown to prevent thrombus formation,[1] reduce bacterial adhesion on surfaces[2] and disperse existing biofilms through signaling.[3, 4] Therefore, an artificial surface that is able to release or generate NO is expected to provide a potential solution for common biocompatibility issues that create risk for patients. While polymer coatings that contain NO donors are able to release NO from the polymeric materials, NO generation materials are a group of catalytic coatings that are able to convert endogenous NO donors, such as *S*-nitrosothiols (RSNOs), into NO.

In this dissertation work, both strategies are employed to improve the biocompatibility of polymeric surfaces. Firstly, a diazeniumdiolate-doped poly(lactic-*co*-glycolic acid) (PLGA)-based NO release coating with a controllable NO release pattern is shown to prevent biofilm formation under various conditions.[5] In contrast, for new organoselenium-based NO generation materials, the antimicrobial activity is attributed to the superoxide ($O_2^{\bullet-}$) production coming from the reaction between the selenolate and oxygen.[6] In this thesis, the NO generation and superoxide ($O_2^{\bullet-}$) production capability of an ebselen (non-toxic RSe species)-based Layer-by-Layer (LbL) coating is demonstrated and the potential antithrombotic and antimicrobial property is proven by *in vi*tro experiments.[7] In addition, the catalytic activities of various NO generation coatings containing different copper species are examined. It will be shown that polyurethane films doped with CuO naoparticles can be used as alternatives to previously developed copper(II)-based NO generation coatings to produce simple and effective NO generation materials.

1.1 Thrombus Formation and Bacterial Infection Related Complications for Indwelling Biomedical Devices

Although indwelling biomedical devices have played a key role in the healthcare system to save patients' lives, developing a truly "biocompatible" device surface remains a challenge. The thrombogenic nature and susceptibility to bacterial infection of polymeric materials that are employed for indwelling biomedical devices often lead to device complications, and further cause problems such as significantly increased medical costs, long-term hospitalization, amputation or even patient death.

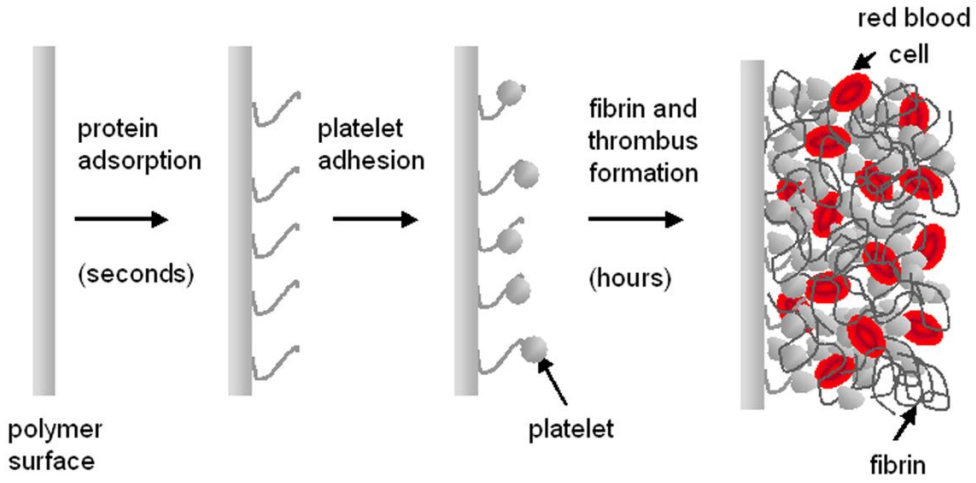

Figure 1.1. Thrombus formation on a foreign surface.[8]

As shown in **Figure 1.1**, when a device is implanted into the blood stream, adsorption of proteins including fibrinogen, fibronectin and von Willebrand Factor (vWF) will take place within seconds. These proteins will further interact with receptors on the plasma membranes of platelets and facilitate platelet adhesion, primarily through the binding of the glycoprotein GPIIb/IIIa receptor with fibrinogen, and GPIb with vWF.[9] Upon contacting the foreign surface, platelets become activated, which will further lead to conformation changes and the excretion of intracellular granulates containing the coagulation factors VII and XI, adhesion molecules P-selectin and vWF that will further

induce activation and aggregation of more platelets, facilitating the coagulation cascade, and eventually lead to thrombus formation on the foreign surface within hours.[9]

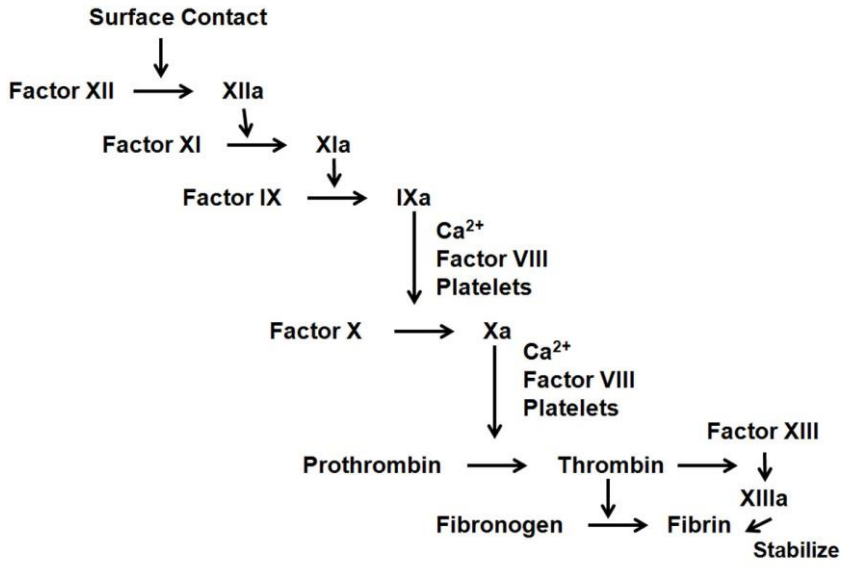

Figure 1.2. Surface initiated blood coagulation cascade (intrinsic system).[10]

The coagulation cascade contains a series of zymogen activation steps triggered through surface contact (intrinsic system) or tissue factor (extrinsic system). The implantation of a medical device (with a negatively charged surface created by the device material or protein absorption) will trigger the first step of the intrinsic pathway: the activation of the blood zymogen FXII (Hageman factor) into active enzyme FXIIa. The activation of FXII will further lead to the activation of Factor XI and eventually lead to the formation of thrombin through a series of zymogen activation steps (shown in **Figure 1.2**). Thrombin, the key enzyme that is capable of turning fibrinogen into fibrin, also activates Factor XIII, which will further cross-link and stabilize fibrin into an insoluble gel that traps platelets and red blood cells in a thrombus.

Thrombus formation can lead to significant consequences such as complete obstruction of stents,[10] occlusion of catheters[11] and small diameter vascular grafts,[12] errant results of implantable chemical sensors,[12] embolic complication with artificial hearts[13] and extensive blood damage during extracorporeal membrane oxygenation.[13] These types of complications occur at a rate between 2% to 10% depending on the device.[10]

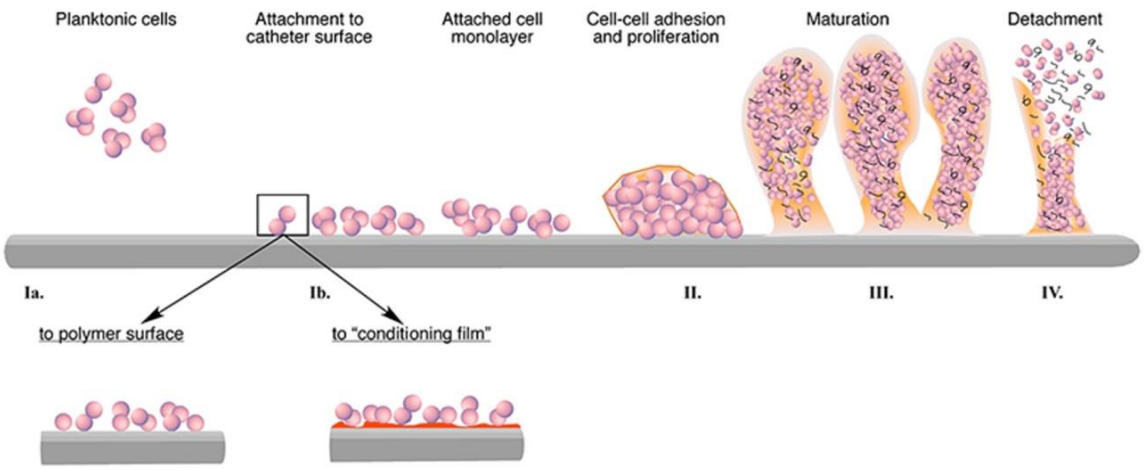

Figure 1.3. Four-step formation process of a biofilm.[14]

Bacterial infection, especially biofilm-induced infection, is another problem with indwelling devices. As shown in **Figure 1.3**, biofilm formation is a four-step process: 1) the attachment of planktonic bacterial cells onto the surface to form a cell monolayer; 2) the accumulation of bacterial cells resulting from increased cell adhesion and proliferation; 3) formation and maturation of a biofilm including production of extracellular polysaccharides; and 4) detachment of biofilm that will further lead to infection of new surfaces.[14] While the initial attachment occurs within 1~2 h and is reversible, after 2~3 h, irreversible adhesion will occur and further lead to biofilm formation after ~24 h.[2] Therefore, the biofilm community is capable of irreversibly colonizing the surface while retaining nutrients and protecting the microorganisms inside the matrix with the help of the extracellular polysaccharides. Once a biofilm is formed on indwelling device surfaces, it is difficult to kill the bacterial cells by conventional antibiotics due to their inability to penetrate well through the biofilm matrix and the heterogeneous chemical environment of the biofilm.[15] It is reported that in some cases, ~1000 fold dose of conventional antibiotics is necessary to treat bacterial cells in a biofilm compared to their planktonic forms.[2]

The annual infection rate in the United States is reported to be 4.3 % for orthopedic implants and 7.4 % for cardiovascular implants and the most common pathogens that cause bacterial infection include Gram-positive *Staphylococcus aureus (S. aureus)*, *Staphylococcus epidermidis (S. epidermidis)* and Gram-negative *Escherichia coli (E. coli)* and *Pseudomonas aeruginosa (P.aeruginosa).*[2] Although the infection rates vary widely with patients and devices, in some cases, the consequences can be severe and fatal.

In order to reduce the rate of device complication, various strategies have been used to improve the compatibility of an indwelling surface to prevent problems like thrombus formation and bacterial infection.

Since protein adsorption is an important initial stage for both thrombus and biofilm formation, one strategy is to create an antifouling surface that is capable of greatly reducing protein adsorption. For example, poly(ethylene glycol) (PEG) grafted surfaces have been widely used and have been proven to reduce thrombus formation[16] and biofilm formation.[17] This type of coating, however, tends to auto-oxidize at ambient conditions and gradually loses its anti-fouling functionality.[18] Recently, Semprus Biosciences Corp. (Cambridge, MA) has successfully developed an antifouling coating with long-term stability based on zwitterionic polysulfo- and polycarboxylbetaines.[19] The surface tightly binds water and forms a barrier that will prevent protein adsorption, thus greatly reducing thrombus and biofilm formation on the surface.

Another strategy is to immobilize antithrombotic or antimicrobial agents or sites on the surface to form a functional coating. For example, heparin-based coatings and devices have achieved both *in vitro* and *in vivo* success and have become commercially available to prevent thrombus formation.[20] However, for coatings that do not release antimicrobial agents, including coatings with immobilized polysaccharides, surfactants, polyelectrolytes multilayers (PEMs), positively charged polymer brushes, quaternary ammonium compounds or proteins,[21-24] the effectiveness varies with bacterial species[2, 18] and might be weakened through formation of conditioning films.

An alternative strategy is to use coatings that can release antimicrobial agents and co-immobilize antithrombotic agents. Although antibiotics such as cephalothin, carbenicillin, amoxicillin, cefamandol, gentamicin and vancomycin can be incorporated

into coatings to prevent infection,[25] the resistance of an increasing number of bacterial strains and biofilms to antibiotics has limited the practical application of most antibiotic-release coatings.[26] Therefore, novel antimicrobial agents have to be developed. Silver salts (e.g., silver sulfadiazine) have been applied widely into commercial coatings to prevent bacterial colonization on catheter surfaces[11] and a non-thrombogenic and biocidal coating has been fabricated by incorporating silver nanoparticles into surfaces with co-immobilized heparin.[27] However, the cytotoxicity and genotoxicity of silver-based species remain a potential issue. [22]

1.2 Antithrombotic and Antimicrobial Surface with Nitric Oxide Release

1.2.1 Nitric oxide as endogenous antithrombotic and antimicrobial agent

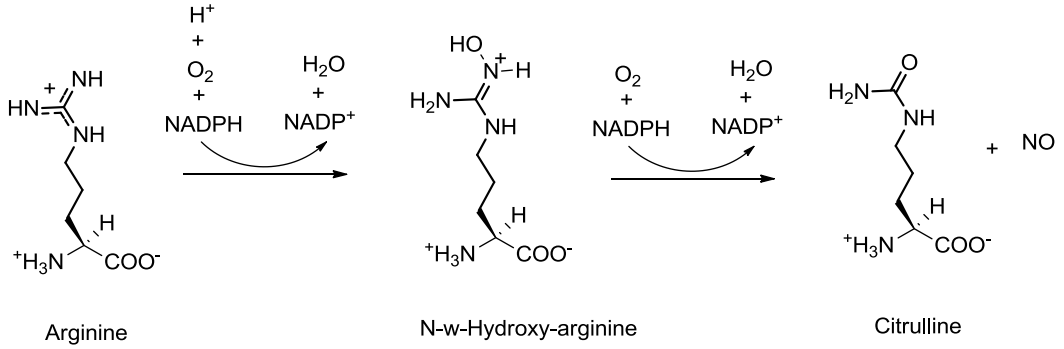

Figure 1.4. Biological production of nitric oxide.[28]

Nitric oxide (NO) is well recognized for its remarkable biological roles in the body including its antithrombotic, anti- cell proliferation, vasodilating, anti-microbial and anti-inflammatory effects.[29, 30] NO is enzymatically synthesized by nitric oxide synthase (NOS) through the conversion of L-arginine and oxygen into L-citrulline and NO with the help of nicotinamide adenine dinucleotide phosphate (NADPH) (see **Figure 1.4**).

Several isoforms of NOS have been identified including endothelial NOS (eNOS), neuronal NOS (nNOS) and induced NOS (iNOS),[31] and both eNOS and nNOS are also known as constitutive NOS (cNOS).[32] As a macrophage-derived form, iNOS is not expressed, but is induced by endotoxin and inflammatory mediators such as cytokines.[31]

While the functionality of cNOS is regulated by Ca^{2+} fluxes and further binding to calmodulin, iNOS functions independently of calcium and is able to release large amounts of NO continuously.[29] A healthy endothelial cell surface, with an NO flux of $0.5\sim4\times10^{-10}$ mol cm^{-2} min^{-1}, is known as the most non-thrombotic surface.[33] The amount of NO released per unit time from fully induced macrophages could be a thousand times higher than that released by NOS from endothelial cells,[29] which contributes to the important role of NO in the immune system and its antimicrobial and antiviral activity.

NO is reported to be an antiplatelet agent that is capable of preventing platelet adhesion,[34] aggregation[35] and recruitment[36] into a growing thrombus. The antiplatelet activity of NO contributes to the antithrombotic property of the endothelial cell surface. NO inhibits platelets through a cyclic guanosine monophosphate (cGMP) mediated signaling process by firstly binding to the heme moiety of soluble guanylyl cyclase (sGC), more specifically, NO-sensitive guanylyl cyclase (NO-GC),[37] and further causing an increase in cGMP and concurrent decrease in intracellular Ca^{2+}. Meanwhile, cGMP is able to increase cyclic adenosine monophosphate (cAMP) levels indirectly through phosphodiesterase III (PDE III), which will also cause a decreased Ca^{2+} flux. Since cGMP inhibits thrombin-mediated activation of phosphoinositide 3-kinase (PI-3 kinase) and both PI-3 kinase activation and Ca^{2+} are important in promoting the formation of an active conformation of glycoprotein IIb/IIIa on the outer platelet membrane, this will further decrease platelet association with fibrinogen and cause platelet disaggregation.[30]

As stated above, NO is also a potent antimicrobial agent. As a reactive free radical, NO is capable of interacting with reactive oxygen species such as hydrogen peroxide (H_2O_2) and superoxide ($O_2^{\bullet-}$) to form different antimicrobial agents, including peroxynitrite ($ONOO^-$), nitrogen dioxide (NO_2), dinitrogen trioxide (N_2O_3) and dinitrogen tetroxide (N_2O_4). These species can further cause oxidative stress and lead to DNA, protein or cell lipid membrane damage of most microbes.[38, 39] NO is also capable of nitrosating the cysteine or tyrosine residues of proteins to cause protein dysfunction.[2] In addition, NO can cause ion depletion and inhibit metabolic enzymes.[37] While a high level of NO produced by the immune system is able to kill microbes, low levels of NO have been reported to prevent biofilm formation and disperse established biofilms through a signaling process[4, 40-42] mediated by cyclic di-GMP (c-di-GMP). As a second

messenger, c-di-GMP regulates the transition from microbial biofilm to planktonic bacterial cells in response to cell-cell signals or environmental cues. Increased c-di-GMP levels facilitates the biofilm mode, and the decrease of c-di-GMP leads to biofilm dispersal.[4] Diguanylate cyclases (DGCs) and specific phosphodiesterases (PEDs) are responsible for the biosynthesis and degradation of c-di-GMP, respectively. Similar to the well-known NO/cGMP pathway that utilizes NO sensing domains in the eukaryotic system, it is reported that NO will also increase PEDs activity (e.g., binding to the heme of the PER-ARNT-SIM (PAS) domain present in some PDEs in *P. aeruginosa*[4]) and lead to a decrease in c-di-GMP levels, which will further lead to biofilm dispersal.[41, 43]

1.2.2 NO release coatings based on diazeniumdiolates (NONOates)

The antiplatelet, antimicrobial and antibiofilm properties of NO make it a potential candidate to solve the biocompatibility issues related with indwelling devices. However, since NO rapidly reacts with oxygen and is scavenged by oxyhemoglobin to form methaemoglobin and nitrate under *in vivo* conditions,[44] it is challenging to handle NO as a gas or a dissolved form in aqueous solution. Therefore, NO donors such as organic nitrates and nitrites, metal-NO complexes, diazeniumdiolates (NONOates) and *S*-nitrosothiols (RSNOs) have been utilized as more stable alternative forms of NO.[45-47] By incorporating synthetic NO donors into polymeric coatings, the coatings are capable of releasing NO at the surfaces and are thus termed NO release coatings. Artificial coatings with an NO flux that is equivalent or higher than that is produced by the healthy endothelium surfaces ($0.5\sim4 \times10^{-10}$ mol cm^{-2} min^{-1}), are expected to exhibit similar antithrombotic properties due to the antiplatelet effect of NO. The specific flux required for the antimicrobial property of an NO release surface has not yet been reported because it likely varies with different bacterial species.

N-diazeniumdiolates (NONOates) are one of the most widely used NO donors. As shown in **Figure 1.5A**, an N-diazeniumdiolate consists of a diolate group [$N(O^-)N=O$] bound to a nitrogen atom of a nucleophile, which can be a primary, secondary or polyamine.[48] One mole of N-diazeniumdiolate decomposes to release two moles of NO through a proton-driven mechanism (**Figure 1.5A**) and the half-life of the diazeniumdiolate species can range from seconds, hours, days or even weeks, depending

on the structure of the nucleophile.[46] Diazeniumdiolates such as proli/NONOate and spermine/NONOate (see structures in **Figure 1.5B**) with half-lives of 2 s and 5-50 min, respectively, in 0.1 M phosphate at pH 7.4 at 37 °C,[49] have been infused before the implantation of a device or incorporated into coatings to prevent thrombus formation.[48]

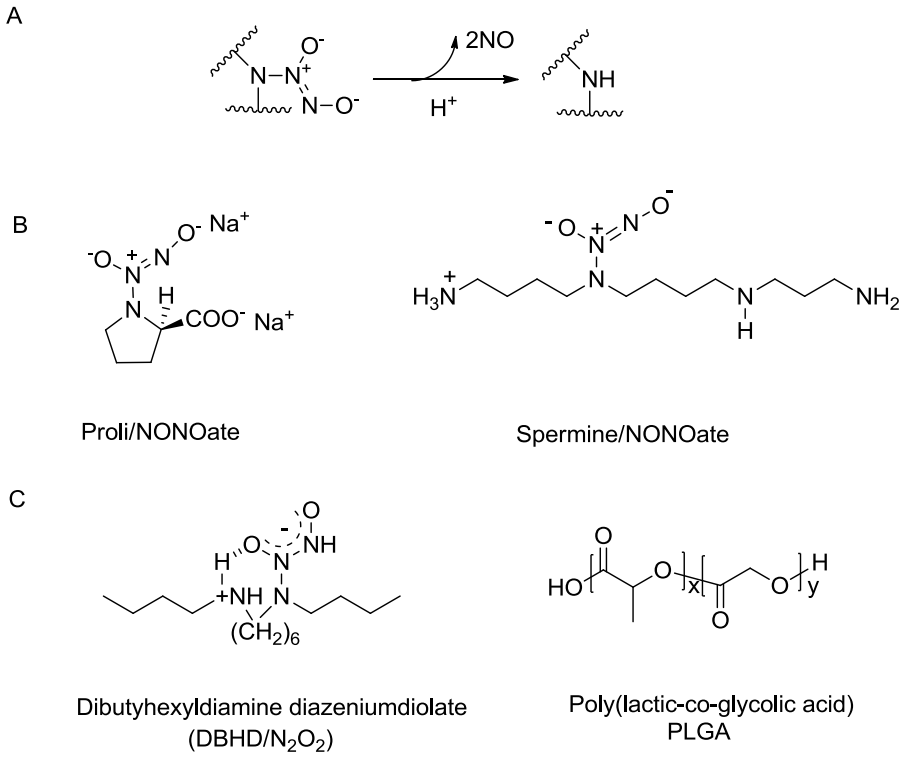

Figure 1.5. A) NO release mechanism from diazeniumdiolates; B) typical structures of small molecule diazeniumdiolates; C) structures of DBHD/N_2O_2 and PLGA.

To improve the stability of the NO release coating, diazeniumdiolates can be covalently attached onto the polymer backbone.[50-54] A facile way to prepare coatings is to dope lipophilic diazeniumdiolates into a polymer film and then further coat this layer with a top coat of polymer that decreases the leaching of the diazeniumdiolate or product amine, but allows rapid diffusion of NO out of the bilayer film.[53, 55, 56] Previously, our group has demonstrated that dibutyhexyldiamine diazeniumdiolate (DBHD/N_2O_2) (**Figure 1.5C**) can be used as a stable lipophilic NO donor in polymeric membranes to release NO with minimal leaching.[57] Due to the proton-driven NO release mechanism of diazeniumdiolates, the challenge of utilizing a DBHD/N_2O_2 doped coating lies in

controlling the NO release profile and extending its lifetime by controlling the pH within the polymeric material. Recently, poly(lactic-*co*-glycolic acid) (PLGA) (**Figure 1.5C)**, a biodegradable and biocompatible polymer that is approved by the U.S. Food and Drug Administration (FDA), was employed as a matrix to promote the NO release from DBHD/N_2O_2 incorporated coatings (with outer layer of polyurethane) and NO release intravascular glucose sensors based on such coatings exhibited greatly reduced thrombus formation when implanted into the veins of rabbits.[56]

1.2.3 NO release coatings based on *S*-nitrosothiols (RSNOs)

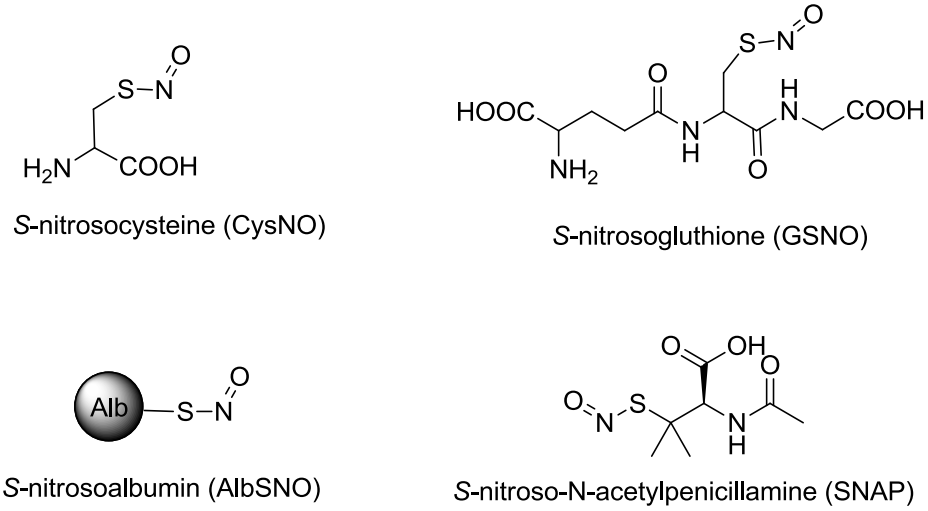

Figure 1.6. Structures of endogenous *S*-nitrosothiols and synthetic SNAP.

Although diazeniumdiolates are widely used as NO donors, they haven't been approved clinically.[46] *S*-nitrosothiols (RSNOs), which are also present endogenously, have gained popularity as NO donors in fabricating NO release coatings due to their low toxicity. **Figure 1.6** shows the structures of a group of endogenous RSNOs including *S*-nitrosocysteine (CysNO), *S*-nitrosoglutathione (GSNO) and *S*-nitrosoalbumin (AlbSNO). RSNOs can also be synthesized by nitrosation of thiols using nitrous acid as a carrier of NO^+ as shown in eq. 1.1a,[58] and the structure of *S*-nitroso-N-acetylpenicillamine (SNAP), a synthetic RSNO, is also shown in **Figure 1.6**. RSNOs can be converted into NO through heat, light or catalytic reactions, as shown in eq. 1.1b, and tertiary RSNOs are

more stable than primary ones.[59] However, Alb-SNO, which binds NO via a cysteine residue, is more stable than low molecular weight RSNOs.

$$RSH + HNO_2 \overset{H^+}{\rightleftharpoons} RSNO + H_2O \qquad (1.1a)$$

$$2\,RSNO \longrightarrow RSSR + 2\,NO \qquad (1.1b)$$

RSNOs can be doped[60] within or covalently[61-63] attached to polymers to fabricate NO release coatings. Despite the reduced toxicity, since most of the RSNO-release coatings rely on heat or light-induced RSNO decomposition, the in clinical application is limited due to the ineffectiveness of heat-induced RSNO decomposition under physiological conditions and the lack of access to light for indwelling biomedical devices. In addition, the instability of RSNOs in the presence of heat, light, pH change and trace metal ions also renders difficulties in the storage of these coatings.[58]

1.2.4 Antithrombotic and antimicrobial properties of NO release coatings

The antithrombotic and antimicrobial properties of NO release coatings have been demonstrated by both *in vitro* and *in vivo* tests. An NO release coating based on DBHD/N_2O_2, potassium tetrakis(4-chlorophenylborate) (KTpClPB) and poly(vinyl chloride) (PVC) has been coated onto a vascular graft and shown to significantly reduce thrombus formation compared to a control graft after implantation into a sheep model for 21 d.[57] When the toxic KTpClPB additive, which is important in extending the NO release lifetime, was replaced by PLGA, a biocompatible polymer, the antithrombotic property of the coating was also observed in a rabbit model.[56] It has also been demonstrated that NO release xerogel coatings are capable of reducing bacterial adhesion by both static[2] and parallel plate flow cell studies.[62] In addition, the NO release xerogel coating is capable of preventing biofilm formation by *S. aureus* in a subcutaneous animal model after 8 d of implantation.[64]

1.3 Antithrombotic and Antimicrobial Surfaces with Nitric Oxide Generation

Due to limited reservoir of NO donors that can be incorporated into the polymeric coatings, NO release materials normally have limited lifetime. An alternative strategy is

to use catalytic coatings that are capable of generating NO by converting endogenous NO donors, such as RSNOs, into NO and these types of coatings are thus called NO generation coatings.

1.3.1 NO generation from copper species

A series of copper-based materials including copper ion and Cu(II)-complexes are capable of converting RSNO into NO. In 1996, Williams and coworkers demonstrated the Cu^{+}, which is capable of forming a five- or six-membered ring-structured intermediate with RSNOs, is the key species in the RSNO decomposition mechanism by Cu^{2+} as shown in eq. 1.2.[58, 65]

$$2Cu^{2+} + 2RS^{-} \longrightarrow 2Cu^{+} + RSSR \qquad (1.2a)$$

$$Cu^{+} + RSNO \longrightarrow [X] \longrightarrow Cu^{2+} + RS^{-} + NO \qquad (1.2b)$$

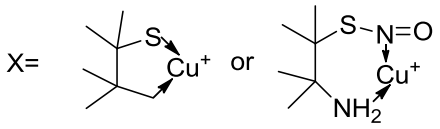

Based on this mechanism, Cu(II)-complexes including Cu(II)-DTTCT (DTTCT= dibenzo[e,k]-2,3,8,9-tetrapheny-1,4,7,10-tetraazacyclododeca-1,3,7,9-tetraene), Cu(II)-cyclen and Cu^{0} particles have been utilized in the fabrication of NO generation coatings. When reduced by a reducing agent, the reduced Cu(I) form of the Cu(II) complexes (see structures of Cu(II)-DTTCT and Cu(II)-cyclen in **Figure 1.7**) still have open coordination sites to interact with RSNO,[66-68] which contributes to their catalytic activity. The catalytic activity of Cu^{0} particles[69] comes from the production of Cu^{2+} through surface corrosion in solution.

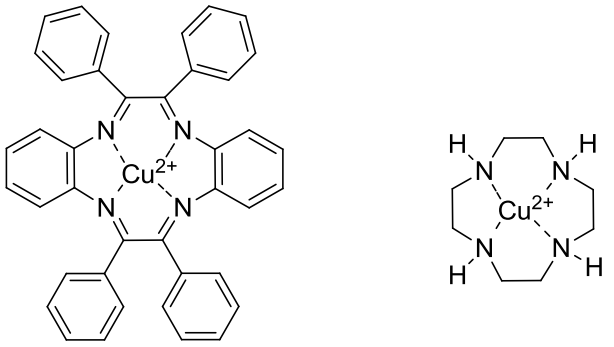

Cu(II)-DTTCT Cu(II)-cyclen

Figure 1.7. Structures of copper complexes including Cu(II)-DTTCT and Cu(II)-cyclen. (DTTCT= dibenzo[e,k]-2,3,8,9-tetrapheny-1,4,7,10-tetraazacyclododeca-1,3,7,9-tetraene).

1.3.2 NO generation and superoxide production from organoselenium species

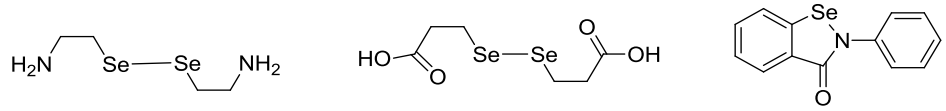

A. selenocystamine (SeCA) B. 3,3'-diselenodipropionic acid (SeDPA) C. ebselen

Figure 1.8. Structures of different organoselenium species.

Ever since the discovery that glutathione peroxidase (GPx), a selenoenzyme that protects cell from oxidation stress by reducing hydroperoxides using glutathione (GSH), can convert RSNO into NO,[70] organodiselenides including selenocystamine (SeCA, **Figure 1.8A**) and 3, 3'-dipropionicdiselenide (SeDPA, **Figure 1.8B**) that act as GPx mimics have been employed in developing NO generation materials.[71-73] The RSNO decomposition mechanism is shown in eqs. 1.3 a-d. In the presence of reducing agents at neutral pH, the diselenides can be converted into selenolates, which are the key intermediates that can reduce RSNOs into NO and thiolates.[71]

$$RSe\text{-}SeR + GSH \rightleftharpoons RSe\text{-}SG + RSe^- + H^+ \quad (1.3a)$$

$$RSe\text{-}SG + GSH \rightleftharpoons RSe^- + H^+ + GS\text{-}SG \quad (1.3b)$$

$$RSe^- + H^+ + R'S\text{-}NO \rightleftharpoons 1/2\ RSe\text{-}SeR + R'SH + NO \quad (1.3c)$$

$$RSe\text{-}SeR + 2R'S\text{-}NO \rightleftharpoons 2RSe\text{-}SR' + 2NO \quad (1.3d)$$

Interestingly, the reaction of selenolate with oxygen is also known to produce superoxide ($O_2^{\bullet-}$), which is able to inhibit bacterial adhesion to an organoselenium mediated surface.[74] Superoxide ($O_2^{\bullet-}$) is not very reactive itself, but the production of hydroxyl radical ($HO^{\bullet}$) through ion-mediated Haber-Weiss reaction (as shown in eq. 1.4 a-b) will further cause cell damage.[75]

$$H_2O_2 + Fe^{2+} \longrightarrow HO^{\bullet} + OH^- + Fe^{3+} \quad (1.4a)$$

$$Fe^{3+} + O_2^{\bullet-} \longrightarrow Fe^{2+} + O_2 \quad (1.4b)$$

Despite the RSNO decomposition catalytic activity and antimicrobial property of aliphatic selenium species, a recent study has shown that the reaction between aliphatic selenolates and oxygen is so fast that a significant amount of superoxide ($O_2^{\bullet-}$) and selenenyl radical (RSe•) are produced, and the accumulation of toxic peroxides and radical species through further reactions leads to the known toxicity of aliphatic selenium species.[76] Aliphatic selenium species are also known to trigger a thiol mediated one electron reduction of certain enzymes, such as cytochrome C, which also contributes to their toxicity.[77] Consequently, the *in vivo* toxicity of alkyldiselenides greatly limits their potential biomedical applications. Recently, a series of aromatic selenium species, with good GPx activity and reduced *in vivo* toxicity, have been developed. For example, the drug ebselen (2-phenyl-1,2-benzisoselenazol-3-(2H)-one, **Figure 1.8C**), is undergoing phase III clinic trials in Japan due to its low toxicity, anti-inflammatory and anti-oxidation properties.[77] The antimicrobial activity of ebselen and its derivatives have also been reported.[78-80] The catalytic activity of these species for RSNO decomposition, however, has not yet been examined.

1.3.3 Layer-by-Layer (LbL) assembly technique

Invented in 1966 by Iler and further developed in the 1990s by Dencher and co-workers, Layer-by-Layer (LbL) assembly has become a powerful and versatile technique for surface modification.[81, 82] As shown in **Scheme 1.1A**, this process starts with dipping a substrate in a polycation solution followed by several washing steps. This dipping and washing process is then repeated for the polyanion and a bilayer of the polycation and polyanion is then assembled onto the substrate based on electrostatic interaction as shown in **Scheme 1.1B**. This process can be further repeated to fabricate LbL films with desired

number of bilayers. The self-assembly nature and simplicity in the dip-coating procedures of this method enables the utilization of automatic LbL assembly systems and precise control of film properties. Based on electrostatic, hydrophobic and a variety of other interactions, this method is applicable for different building blocks and substrates. Given that various materials can be applied as the substrates, LbL assembly can be a universal and convenient method to apply coatings on biomedical devices. By utilizing chitosan,[84] heparin,[85, 86] silver species,[87] enzymes[88] or antibodies[89] as building blocks, LbL coatings with antifouling, anticoagulation and antimicrobial properties can be fabricated for biomedical applications. Via attachment of aliphatic diselenide species on to a polycation and utilizing alginate as the polyanion, the first NO generation coating based on the Layer-by-Layer technique has recently been developed.[72] The stability of the conventional LbL films, however, is highly related to factors such as temperature, ionic strength and pH, which is more important for weak polyelectrolyte-based LbL films.[90, 91] More homogeneous and stable LbL films can be obtained through annealing using salt, heat, pH changes[92, 93] or cross-linking the films.[90, 91]

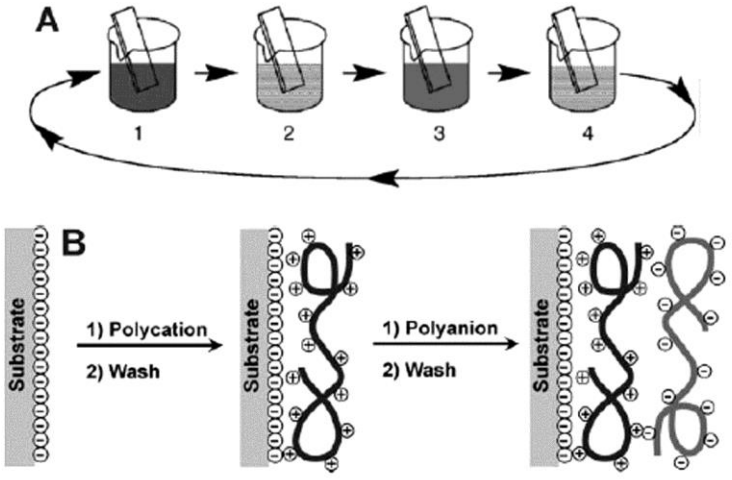

Scheme 1.1. Schematic illustration of A) experimental procedure of Layer-by-Layer assembly: 1 or 3 represents the soaking process in the polycation or polyanion solution, and 2 and 4 represent the washing process; B) formation of Layer-by-Layer film on a substrate based on electrostatic interaction.[83]

1.3.4 Antithrombotic and antimicrobial properties of NO generation coatings

The antithrombotic and antimicrobial properties of NO generation coatings have also been proven by both *in vitro* and *in vivo* tests. Firstly, all of the NO generation coatings based on organoselenium[72] or copper (II) complexes[66-68] are able to generate physiological levels of NO even after contacting with blood for prolonged periods, indicating potential for antithrombotic properties in clinical applications. The *in vivo* antithrombotic property of a Cu^0 particle-based NO generation coatings was demonstrated by using a porcine artery model with oxygen sensing catheters coated with the NO generation coatings.[69] In addition, synthetic RSNOs such as SNAP can be infused into blood to enhance the *in vivo* antithrombotic performance of NO generation coatings and this has been demonstrated using an *in vivo* extracorporeal circulation model.[94] Utilizing *in vitro* colony biofilm assays, the antibiofilm properties of a polymeric coating based on an organoselenium species loaded within polymethacrylate matrix against *S. aureus* and *P. aeruginosa* was also reported.[95] Similar technology was developed by Selenium, Ltd. (Austin, TX)[96, 97] and has been commercialized.

1.4 Statement of Dissertation Research

The primary goal of this dissertation work is to develop antithrombotic and antimicrobial coatings based on NO release and NO generation materials. While, previous research in this group has focused on the antithrombotic properties of NO release coatings, this dissertation work investigates and demonstrates the antibiofilm properties of NO release coatings based on diazeniumdiolates (NONOate) in PLGAs. In addition, two types of NO generation coatings based on novel catalysts including ebselen and CuO nanoparticles are also developed and these coatings are aimed at reducing the toxicity issues and improving the life-time of NO generation coatings.

In Chapter 2, NO release coatings with tunable NO release profiles are reported based on a previously described DBHD/N_2O_2 in PLGA system.[56] The NO release mechanism is studied by incorporating pH sensitive probes into the films, utilizing the observed colors to compare the pH changes and further correlating the color changes with the NO release patterns. The antibiofilm properties of the coatings against different bacterial

species are studied using a CDC biofilm reactor at different temperatures. This work has been published in *Biomaterials* in 2012[5] and presented at a national conference.[98]

To reduce the toxicity issue of Se-based NO generation coatings, in Chapter 3, a carboxyl derivative of the drug ebselen was synthesized and the RSNO decomposition catalytic activity of different organoselenium species were compared. A Layer-by-Layer film containing the ebselen species was fabricated and is shown to be capable of generating NO and producing superoxide ($O_2^{\bullet-}$). The potential antithrombotic, antimicrobial and antibiofilm properties of the film are also studied. This work has been published in *Biomaterials* in 2011[7] and presented at two national conferences.[99, 100]

In Chapter 4, the differences between the RSNO decomposition catalytic activity of Cu(II)-cyclen and Cu(II)-cyclen polyurethane conjugates are compared and the mechanism is examined. A CuO nanoparticle-based polyurethane film is also proposed as an alternative to previously developed NO generation materials based on copper-based catalyst. The long-term catalytic activity of the new CuO nanoparticles-based coating is also examined.

Conclusions and future directions are present in Chapter 5. The potential synthesis route of attaching the ebselen derivative onto polyurethane and utilizing of a novel copper ligand to substitute cyclen is discussed and the combination of NO generation materials with RSNO releasing coating is also proposed in this chapter.

In the appendix of this dissertation, a fully biodegradable NO release film is fabricated by incorporating a spermine-based diazeniumdiolate into a basic matrix composed of poly (lactic acid) (PLL) and $Ca(OH)_2$. This film is capable of releasing NO for 20 h and is expected to be further applied onto metal implants to solve infection problems.

1.5 References

1. Major, T. C.; Brant, D. O.; Reynolds, M. M.; Bartlett, R. H.; Meyerhoff, M. E.; Handa, H.; Annich, G. M. *Biomaterials* **2010,** 31, (10), 2736-2745.
2. Hetrick, E. M.; Schoenfisch, M. H. *Chem. Soc. Rev.* **2006,** 35, (9), 780-789.
3. Barraud, N.; Storey, M. V.; Moore, Z. P.; Webb, J. S.; Rice, S. A.; Kjelleberg, S. *Microbiol Biotechnol* **2009,** 2, (3), 370-378.
4. McDougald, D.; Rice, S. A.; Barraud, N.; Steinberg, P. D.; Kjelleberg, S. *Nat Rev Micro* **2012,** 10, (1), 39-50.
5. Cai, W. Y.; Wu, J. F.; Xi, C. W.; Meyerhoff, M. E. *Biomaterials* **2012,** 33, (32), 7933-7944.
6. Hofler, L.; Meyerhoff, M. E. *Anal. Chem.* **2011,** 83, (2), 619-624.
7. Cai, W. Y.; Wu, J. F.; Xi, C. W.; Ashe, A. J.; Meyerhoff, M. E. *Biomaterials* **2011,** 32, (31), 7774-7784.
8. Wu, Y. D.; Meyerhoff, M. E. *Talanta* **2008,** 75, (3), 642-650.
9. Schopka, S.; Schmid, T.; Schmid, C.; Lehle, K. *Materials* **2010,** 3, (1), 638-655.
10. Gorbet, M. B.; Sefton, M. V. *Biomaterials* **2004,** 25, (26), 5681-5703.
11. Dwyer, A. *Semin. Dialysis.* **2008,** 21, (6), 542-546.
12. Ratner, B. D. *Biomaterials* **2007,** 28, (34), 5144-5147.
13. Ratner, B. D. *J. Biomater. Sci.-Polym. Ed.* **2000,** 11, (11), 1107-1119.
14. Otto, M. *Front Biosci* **2004,** 9, 841-863.
15. Francolini, I.; Donelli, G. *FEMS Immunol. Med. Microbiol.* **2010,** 59, (3), 227-238.
16. Park, K.; Shim, H. S.; Dewanjee, M. K.; Eigler, N. L. *J. Biomater. Sci.-Polym. Ed.* **2000,** 11, (11), 1121-1134.
17. Dong, B. Y.; Manolache, S.; Wong, A. C. L.; Denes, F. S. *Polym. Bull.* **2011,** 66, (4), 517-528.
18. Banerjee, I.; Pangule, R. C.; Kane, R. S. *Adv. Mater.* **2011,** 23, (6), 690-718.
19. Zhang, Z.; Huval, C.; O'Shaughnessey, W. S.; William, S.; Hencke, M.; Squier, T.; Li, J.; Bouchard, M.; Loose, C. R. Layered non-fouling, antimicrobial antithrombogenic coatings US Patent 8,308,699, 2012.
20. Tanzi, M. C. *Expert Rev. Med. Devices* **2005,** 2, (4), 473-492.
21. Busscher, H. J.; Ploeg, R. J.; van der Mei, H. C. *Biomaterials* **2009,** 30, (25), 4247-8.
22. Campoccia, D.; Montanaro, L.; Arciola, C. R. *Biomaterials* **2006,** 27, (11), 2331-2339.
23. Lichter, J. A.; Van Vliet, K. J.; Rubner, M. F. *Macromolecules* **2009,** 42, (22), 8573-8586.
24. Knetsch, M. L. W.; Koole, L. H. *Polymers* **2011,** 3, 340-366.
25. Stigter, M.; Bezemer, J.; de Groot, K.; Layrolle, P. *J. Controlled Release* **2004,** 99, (1), 127-137.
26. Campoccia, D.; Montanaro, L.; Speziale, P.; Arciola, C. R. *Biomaterials* **2010,** 31, (25), 6363-6377.
27. Stevens, K. N. J.; Croes, S.; Boersma, R. S.; Stobberingh, E. E.; van der Marel, C.; van der Veen, F. H.; Knetsch, M. L. W.; Koole, L. H. *Biomaterials* **2011,** 32, (5), 1264-1269.

28. Jeremy, M. B.; John, L. T.; Lubert, S., *Biochemistry*. 6th ed.; W.H. Freeman and Company: New York, 2007; p 702.
29. Anggard, E. *Lancet* **1994,** 343, (8907), 1199-1206.
30. Walford, G.; Loscalzo, J. *J. Thromb. Haemost.* **2003,** 1, (10), 2112-2118.
31. Singh, S.; Evans, T. W. *Eur Respir J* **1997,** 10, (3), 699-707.
32. Bogdan, C. *Nat. Immunol.* **2001,** 2, (10), 907-916.
33. Vaughn, M. W.; Kuo, L.; Liao, J. C. *Am J Physiol Heart Circ Physiol* **1998,** 274, (6), H2163-H2176.
34. Roberts, W.; Michno, A.; Aburima, A.; Naseem, K. M. *J. Thromb. Haemost.* **2009,** 7, (12), 2106-2115.
35. Nong, Z. X.; Hoylaerts, M.; VanPelt, N.; Collen, D.; Janssens, S. *Circ. Res.* **1997,** 81, (5), 865-869.
36. Freedman, J. E.; Loscalzo, J.; Barnard, M. R.; Alpert, C.; Keaney, J. F.; Michelson, A. D. *J. Clin. Invest.* **1997,** 100, (2), 350-356.
37. Dangel, O.; Mergia, E.; Karlisch, K.; Groneberg, D.; Koesling, D.; Friebe, A. *J. Thromb. Haemost.* **2010,** 8, (6), 1343-1352.
38. Jones, M. L.; Ganopolsky, J. G.; Labbe, A.; Wahl, C.; Prakash, S. *Appl. Microbiol. Biotechnol.* **2010,** 88, (2), 401-407.
39. Zaki, M. H.; Akuta, T.; Akaike, T. *J Pharmacol Sci* **2005,** 98, (2), 117-129.
40. Barraud, N.; Hassett, D. J.; Hwang, S. H.; Rice, S. A.; Kjelleberg, S.; Webb, J. S. *J. Bacteriol.* **2006,** 188, (21), 7344-7353.
41. Barraud, N.; Schleheck, D.; Klebensberger, J.; Webb, J. S.; Hassett, D. J.; Rice, S. A.; Kjelleberg, S. *J. Bacteriol.* **2009,** 191, (23), 7333-7342.
42. Partridge, J. D.; Bodenmiller, D. M.; Humphrys, M. S.; Spiro, S. *Mol. Microbiol.* **2009,** 73, (4), 680-694.
43. Plate, L.; Marletta, M. A. *Mol. Cell* **2012,** 46, (4), 449-460.
44. Radi, R.; Beckman, J. S.; Bush, K. M.; Freeman, B. A. *J. Biol. Chem.* **1991,** 266, (7), 4244-4250.
45. Wang, P. G.; Xian, M.; Tang, X. P.; Wu, X. J.; Wen, Z.; Cai, T. W.; Janczuk, A. J. *Chem. Rev.* **2002,** 102, (4), 1091-1134.
46. Jen, M. C.; Serrano, M. C.; van Lith, R.; Ameer, G. A. *Adv. Funct. Mater.* **2012,** 22, (2), 239-260.
47. Huerta, S.; Chilka, S.; Bonavida, B. *Int. J. Oncol.* **2008,** 33, (5), 909-927.
48. Miller, M. R.; Megson, I. L. *Br. J. Pharmacol.* **2007,** 151, 305-21.
49. Keefer, L. K. *ACS Chem. Biol.* **2011,** 6, (11), 1147-1155.
50. Zhang, H. P.; Annich, G. M.; Miskulin, J.; Osterholzer, K.; Merz, S. I.; Bartlett, R. H.; Meyerhoff, M. E. *Biomaterials* **2002,** 23, (6), 1485-1494.
51. Reynolds, M. M.; Hrabie, J. A.; Oh, B. K.; Politis, J. K.; Citro, M. L.; Keefer, L. K.; Meyerhoff, M. E. *Biomacromolecules* **2006,** 7, (3), 987-994.
52. Zhou, Z. R.; Meyerhoff, M. E. *Biomacromolecules* **2005,** 6, (2), 780-789.
53. Frost, M. C.; Reynolds, M. M.; Meyerhoff, M. E. *Biomaterials* **2005,** 26, (14), 1685-1693.
54. Zhou, Z. R.; Annich, G. M.; Wu, Y. D.; Meyerhoff, M. E. *Biomacromolecules* **2006,** 7, (9), 2565-2574.
55. Wu, B.; Gerlitz, B.; Grinnell, B. W.; Meyerhoff, M. E. *Biomaterials* **2007,** 28, (28), 4047-4055.

56. Yan, Q. Y.; Major, T. C.; Bartlett, R. H.; Meyerhoff, M. E. *Biosens. Bioelectron.* **2011,** 26, (11), 4276-4282.
57. Batchelor, M. M.; Reoma, S. L.; Fleser, P. S.; Nuthakki, V. K.; Callahan, R. E.; Shanley, C. J.; Politis, J. K.; Elmore, J.; Merz, S. I.; Meyerhoff, M. E. *J. Med. Chem.* **2003,** 46, (24), 5153-5161.
58. Williams, D. L. H. *Acc. Chem. Res.* **1999,** 32, (10), 869-876.
59. Al-Sa'doni, H. H.; Ferro, A. *Curr. Med. Chem.* **2004,** 11, (20), 2679-2690.
60. Amadeu, T. P.; Seabra, A. B.; de Oliveira, M. G.; Costa, A. M. A. *J. Eur. Acad. Dermatol. Venereol.* **2007,** 21, (5), 629-637.
61. Seabra, A. B.; da Silva, R.; de Oliveira, M. G. *Biomacromolecules* **2005,** 6, (5), 2512-2520.
62. Li, Y.; Lee, P. I. *Mol. Pharm.* **2010,** 7, (1), 254-266.
63. Hetrick, E. M.; Schoenfisch, M. H. *Biomaterials* **2007,** 28, (11), 1948-1956.
64. Nablo, B. J.; Prichard, H. L.; Butler, R. D.; Klitzman, B.; Schoenfisch, M. H. *Biomaterials* **2005,** 26, (34), 6984-6990.
65. Dicks, A. P.; Swift, H. R.; Williams, D. L. H.; Butler, A. R.; AlSadoni, H. H.; Cox, B. G. *J. Chem. Soc., Perkin Trans. 2* **1996**, (4), 481-487.
66. Oh, B. K.; Meyerhoff, M. E. *J. Am. Chem. Soc.* **2003,** 125, (32), 9552-9553.
67. Hwang, S.; Cha, W.; Meyerhoff, M. E. *Angew. Chem., Int. Ed.* **2006,** 45, (17), 2745-2748.
68. Hwang, S.; Meyerhoff, M. E. *Biomaterials* **2008,** 29, (16), 2443-2452.
69. Wu, Y.; Rojas, a.; Griffith, G.; Skrzypchak, a.; Lafayette, N.; Bartlett, R.; Meyerhoff, M. *Sens. Actuators, B* **2007,** 121, 36-46.
70. Hou, Y. C.; Guo, Z. M.; Li, J.; Wang, P. G. *Biochem. Biophys. Res. Commun.* **1996,** 228, (1), 88-93.
71. Cha, W.; Meyerhoff, M. E. *Biomaterials* **2007,** 28, 19-27.
72. Yang, J.; Welby, J. L.; Meyerhoff, M. E. *Langmuir* **2008,** 24, (18), 10265-10272.
73. Cha, W.; Meyerhoff, M. E. *Langmuir* **2006,** 22, 10830-6.
74. Tran, P. L.; Hammond, A. a.; Mosley, T.; Cortez, J.; Gray, T.; Colmer-Hamood, J. a.; Shashtri, M.; Spallholz, J. E.; Hamood, A. N.; Reid, T. W. *Appl. Environ. Microbiol.* **2009,** 75, 3586-92.
75. Benov, L. *Protoplasma* **2001,** 217, (1-3), 33-36.
76. Mugesh, G.; du Mont, W. W.; Sies, H. *Chem. Rev.* **2001,** 101, 2125-79.
77. Mugesh, G.; Singh, H. B. *Chem. Soc. Rev.* **2000,** 29, 347-357.
78. Pietka-Ottlik, M.; Wojtowicz-Mlociiowska, H.; Kolodziejczyk, K.; Piasecki, E.; Mlochowski, J. *Chem. Pharm. Bull.* **2008,** 56, (10), 1423-1427.
79. Chan, G.; Hardej, D.; Santoro, M.; Lau-Cam, C.; Billack, B. *J. Biochem. Mol. Toxicol.* **2007,** 21, (5), 252-264.
80. Billack, B.; Santoro, M.; Lau-Cam, C. *Microb Drug Resist* **2009,** 15, (2), 77-83.
81. Boudou, T.; Crouzier, T.; Ren, K.; Blin, G.; Picart, C. *Adv. Mater.* **2010,** 22, 441-67.
82. Li, Y.; Wang, X.; Sun, J. Q. *Chem. Soc. Rev.* **2012,** 41, (18), 5998-6009.
83. Tang, Z. Y.; Wang, Y.; Podsiadlo, P.; Kotov, N. A. *Adv. Mater.* **2006,** 18, (24), 3203-3224.
84. Bulwan, M.; Wojcik, K.; Zapotoczny, S.; Nowakowska, M. *J. Biomater. Sci.-Polym. Ed.* **2012,** 23, (15), 1963-1980.

85. Tan, Q. G.; Ji, J.; Barbosa, M. A.; Fonseca, C.; Shen, J. C. *Biomaterials* **2003,** 24, (25), 4699-4705.
86. Brynda, E.; Houska, M.; Jirouskova, M.; Dyr, J. E. *J Biomed Mater Res* **2000,** 51, (2), 249-257.
87. Fu, J. H.; Ji, J.; Fan, D. Z.; Shen, J. C. *J. Biomed. Mater. Res. A* **2006,** 79A, (3), 665-674.
88. Pavlukhina, S. V.; Kaplan, J. B.; Xu, L.; Chang, W.; Yu, X. J.; Madhyastha, S.; Yakandawala, N.; Mentbayeva, A.; Khan, B.; Sukhishvili, S. A. *ACS Appl. Mater. Inter.* **2012,** 4, (9), 4708-4716.
89. Luo, L. L.; Wang, G. X.; Li, Y. L.; Yin, T. Y.; Jiang, T.; Ruan, C. G. *J. Biomed. Mater. Res. A* **2011,** 97A, (4), 423-432.
90. Ott, P.; Gensel, J.; Roesler, S.; Trenkenschuh, K.; Andreeva, D.; Laschewsky, A.; Fery, A. *Chem. Mater.* **2010,** 22, (11), 3323-3331.
91. Boudou, T.; Crouzier, T.; Ren, K. F.; Blin, G.; Picart, C. *Adv. Mater.* **2010,** 22, (4), 441-467.
92. Yang, S.; Zhang, Y.; Zhang, X.; Guan, Y.; Xu, J.; Zhang, X. *ChemPhysChem* **2007,** 8, 418-24.
93. McAloney, R. a.; Dudnik, V.; Goh, M. C. *Langmuir* **2003,** 19, 3947-3952.
94. Major, T. C.; Brant, D. O.; Burney, C. P.; Amoako, K. A.; Annich, G. M.; Meyerhoff, M. E.; Handa, H.; Bartlett, R. H. *Biomaterials* **2011,** 32, (26), 5957-5969.
95. Tran, P. L.; Hammond, A. A.; Mosley, T.; Cortez, J.; Gray, T.; Colmer-Hamood, J. A.; Shashtri, M.; Spallholz, J. E.; Hamood, A. N.; Reid, T. W. *Appl. Environ. Microbiol.* **2009,** 75, (11), 3586-3592.
96. Reid, T.; Spallholz, J. E.; Devanathan, T. N.; Mosley, T. Anti-microbial orthodontic compositions and appliances and methods of production and use thereof US Patent 8,236,337, 2012.
97. http://www.selenbio.com/home.html
98. Cai, W.; Meyerhoff, M. E., Diazeniumbiolate-Doped Poly(lactic-co-glycolic acid)-Based Nitric Oxide Releasing Films as Antibiofilm Coating. In *Society for Biomaterials 2012 Fall Symposium*, New Orleans, LA, October 4-6, 2012.
99. Cai, W.; Meyerhoff, M. E., Carboxyl-Ebselen-Based Layer-by-Layer Coating for Nitric Oxide Generation. In *Society for Biomaterials 2011 annual meeting & Exposition*, Orlando, FL, April 13-16, 2011.
100. Cai, W.; Meyerhoff, M. E., Carboxyl-Ebselen-Based Layer-by-Layer Film: A Potential Antithrombotic and Antimicrobial Coating. In *BioInterface 2011 Annual Symposium*, Bloomington, MN, October 24-26, 2011.

Chapter 2 Diazeniumdiolate-Doped Poly(lactic-*co*-glycolic acid)-Based Nitric Oxide Release Films as Antibiofilm Coatings

2.1 Introduction

As discussed in Chapter 1, nitric oxide (NO) is an endogenous biocide that is produced in large quantities by macrophages and exhibits antimicrobial properties against a broad spectrum of bacteria. NO is able to kill bacterial cells through oxidative stress caused mainly by peroxynitrite ($^{-}$OONO), the product of the reaction of NO with superoxide ($O_2^{\bullet-}$). It is also able to nitrosate cysteine and tyrosine residues which will lead to dysfunction of bacterial proteins.[1] While a high level of NO is able to kill bacterial cells, a significantly lower level of NO is reported to prevent biofilm formation and disperse established biofilm through a signaling process,[2-5] which is described in detail in Chapter 1.

Although the antimicrobial and antibiofilm properties of NO release coatings have been studied previously, most *in vitro* studies have been performed under "static" conditions,[6] which are not normally correlated with the natural life cycle of bacteria.[7] Recently, the Schoenfisch group has used a parallel plate flow cell that creates shear forces to mimic the natural environment encountered by microbes, and studied the decrease in microbial attachment on NO release coatings after 2 h in PBS buffer.[6, 8] Compared to this and other previously reported systems, a flow-through CDC (Centers for Disease Control and Prevention) biofilm reactor, capable of creating both renewable nutrient sources and shear forces, is regarded as a standard tool to study biofilm formation under natural conditions for longer time periods with repeatable results.[7]

As described in Chapter 1, as one of the most widely used NO donors, diazeniumdiolates have been utilized to prepare NO release polymer coatings that prevent thrombus formation[9] and reduce bacterial adhesion.[1] A previously reported poly(lactic-

co-glycolic acid) (PLGA) and dibutyhexyldiamine diazeniumdiolate (DBHD/N_2O_2)-based NO release coating greatly reduced the toxicity issues and has been shown to reduce thrombus formation on intravascular glucose sensors in an *in vivo* rabbit model.[10] No previous study, however, has been conducted to correlate the change in pH within the PLGA-based bilayer film with the NO release profile, resulting in an unclear mechanism for PLGA as an NO release promoter. Further, such coatings have never been examined with respect to antimicrobial/antibiofilm behavior.

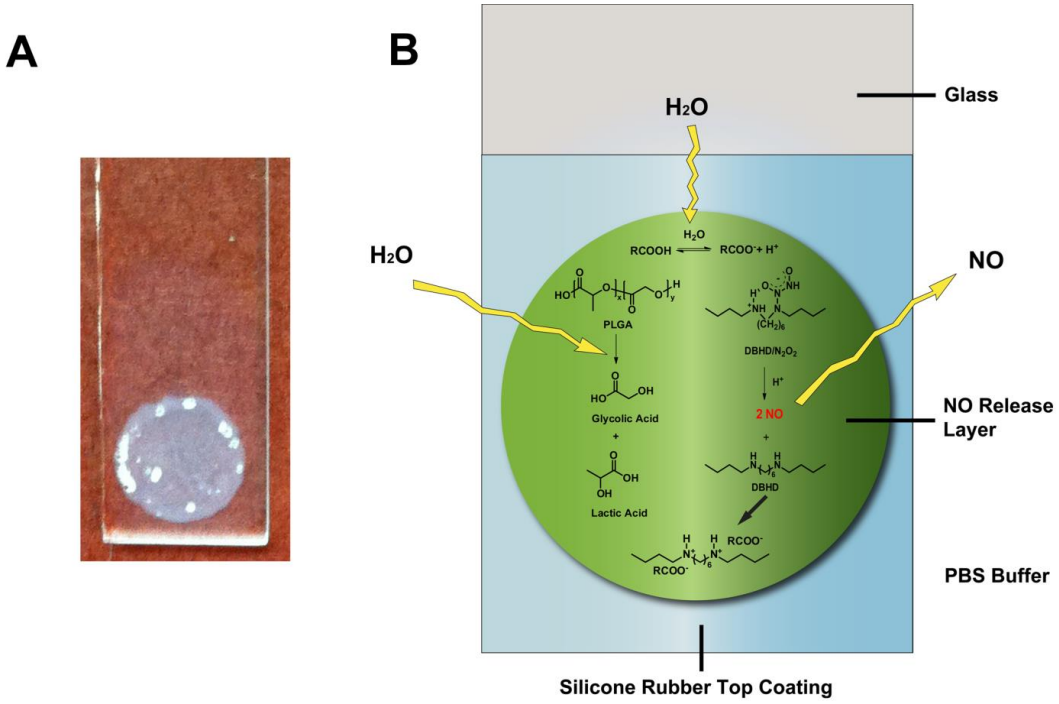

Figure 2.1. A) The appearance of dibutyhexyldiamine diazeniumdiolate (DBHD/N_2O_2) and poly(lactic-co-glycolic) acid (PLGA)-based NO release coating with a bi-layer structure on a glass slide; B) Schematic illustration of dibutyhexyldiamine diazeniumdiolate (DBHD/N_2O_2) and poly(lactic-co-glycolic) acid (PLGA)-based NO release coating and its cross-section.

Herein, a two-layered NO release coating with a base layer of DBHD/N_2O_2 doped in PLGA and a protective silicone rubber (SR) top coating (see **Figure 2.1A** for film configuration) is examined. The pH changes in the PLGA layer are visualized by incorporating a pH sensitive dye into the coating. By employing PLGAs with different hydrolysis rates as the inner matrix (possessing different ratios of lactic and glycolic acid

in the PLGA polymer), the NO release profile of this type of coating can be readily manipulated, which in turn, greatly impacts the NO release kinetics. The antibiofilm properties of these new NO release coatings against gram-positive *S. aureus* and gram-negative *E. coli* at room temperature (23 °C) and at physiological temperature (37°C) are evaluated after a one-week incubation in a CDC biofilm flow-reactor.

2.2 Experimental

2.2.1 Materials

Acid terminated poly(D, L-lactide-*co*-glycolide acid) (PLGA) 50:50 (a-50-50) (catalog number 719897) was purchased from Sigma-Aldrich (St. Louis, MO) and ester terminated PLGA e-50-50, e-75-25, e-PLL (with catalog numbers of 5050 DLG 7E, 7525 DLG 7E and 100 DL 7E, respectively) were purchased from SurModics Pharmaceuticals (Birmingham, AL). Silicone rubber RTV 3140 was obtained from Dow Corning Corporation (Midland, MI). Tecoflex polyurethane SG-80A was a gift from Lubrizol Advanced Materials (Cleveland, OH). Bromocresol purple was obtained from Fisher Scientific (Pittsburg, PA) and bromothymol blue was obtained from Sigma-Aldrich (St. Louis, MO). Phosphate buffered saline (PBS), pH 7.4, containing 137 mM NaCl, 2.7 mM KCl, 10 mM sodium phosphate, was used in all experiments. Tetrahydrofuran (THF) was obtained from Fisher Scientific (Pittsburgh, PA) and was distilled over sodium and benzophenone prior to use. All aqueous solutions were prepared with deionized water from a Milli-Q system (18 MΩ cm^{-1}; Millipore Corp., Billerica, MA). *Escherichia coli* K-12 MG16653 and *Staphylococcus aureus* ATCC 45330 were purchased from American Type Culture Collection. Luria Bertani (LB) agar and broth were products of Fisher Scientific Inc. (Pittsburgh, PA). DBHD/N_2O_2 was synthesized by treating N, N'-dibutyl-1, 6-hexanediamine (DBHD, Aldrich) with NO gas (80 psi, Cryogenic Gases (Detroit, MI)) at RT for three days as previously described.[11] DBHD/N_2O_2 and PLGA were stored in a desiccator at -20 °C before use.

2.2.2 Preparation of NO release films

Glass slides (0.9 × 5 cm) were cleaned by sonicating in acetone, deionized water and acetone sequentially and dried before use. Two hundred mg of a given type of PLGA was dissolved in 3 mL THF and 50 mg or 86 mg of DBHD/N_2O_2 was then added to the solution to form a dispersion containing 20 wt% or 30 wt% of the NO donor, respectively. The dispersion was then sonicated until a homogeneous dispersion was formed. Twenty five microliters of the dispersion was then cast in an O-ring (o.d.=7 mm) on a glass slide to form an NO-release base layer. The O-ring was then removed and the remaining layer was allowed to dry. This procedure was repeated another three times. Then, 100 μL of SR solution (160 mg mL^{-1} in THF) was then casted over the NO-release PLGA layer as a top coating. The NO release layer was fully covered by the top coating (see **Figure 2.1A**). The bilayer film was then dried in air for one day and in vacuum with desiccant for two days to remove residual solvent before testing. The diameter of the NO release layer was 7 mm. All the controls were prepared in the same way as the NO release films, except PLGA alone or PLGA mixed with DBHD was used as the base layer. In addition, for comparison, SR and polyurethane (PU) were also used to replace PLGA as matrices for the underlying layer.

The thickness of the top coating was optimized by evaluating the leaching of DBHD from films containing a base layer of 20 wt % DBHD mixed with a-50-50 PLGA with different top coating thicknesses using a Micromass LCT Time-of-Flight mass spectrometer. The solutions for MS spectra were prepared as follows: A solution (sol 1#) was prepared containing 5 mL methanol, 0.5 mL H_2O and 50 μL glacial acetic acid for dilution purposes. The MS spectra comparison is shown in **Figure 2.2**. Firstly, 1 μL DBHD was dissolved in 1 mL sol 1# to obtain the MS spectra of DBHD, which exhibits the peak of $[M+H]^+$ at 229.3 as shown in **Figure 2.2A**. For the leaching test, the films with different top coatings were soaked in 2 mL PBS buffer for two days at 37 °C and 20 μL soaking buffer was diluted by 1 mL sol 1#. From the comparison of spectra of **Figure 2.2B** and **Figure 2.2C**, it is obvious that a thicker coating with 100 μL SR is able to minimize leaching of DBHD from the film. Therefore, 100 μL SR was chosen for the top coating for all the NO release and control films. According to the peak height in the mass spectra, the total leaching of DBHD is < 54 μmol (<140 μmol · cm^{-2}). After two days, the leaching of the diamine is < 0.74% of the total DBHD incorporated into the

film. The NO release film should release less DBHD than the control due to the replacement of DBHD with DBHD/N_2O_2.

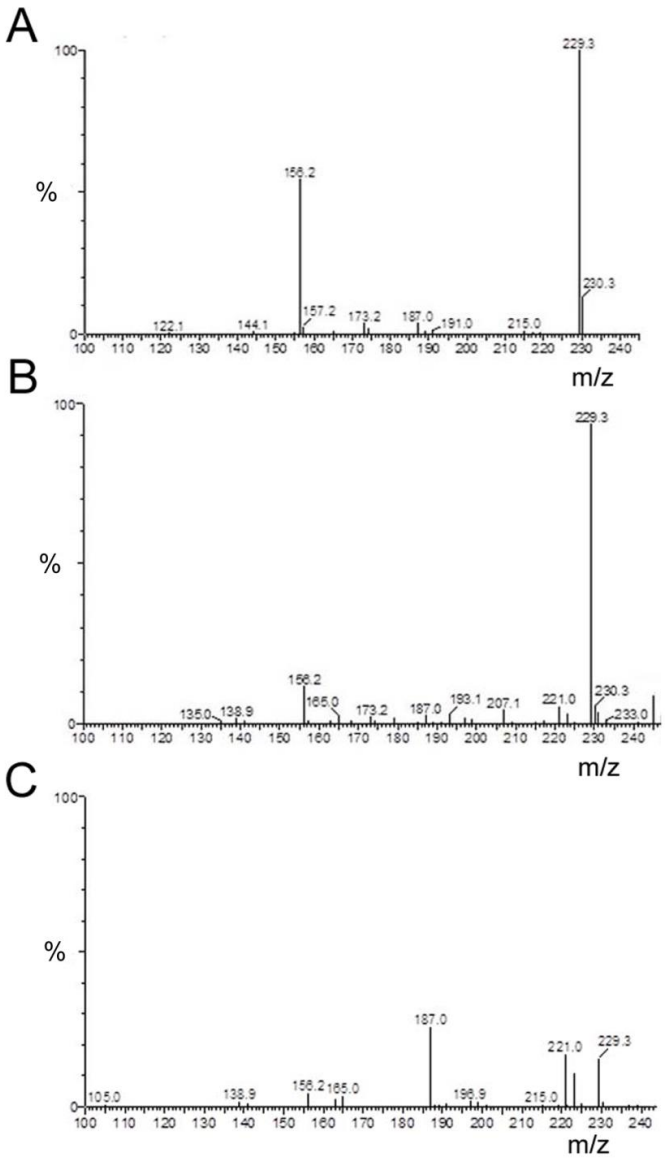

Figure 2.2. MS spectra of A) DBHD; B) soaking buffer for film using 100 μL of 20 wt% of DBHD mixed with a-50-50 PLGA as base layer and 50 μL SR as top coating; C) soaking buffer for film using the same base layer and 100 μL SR as top coating.

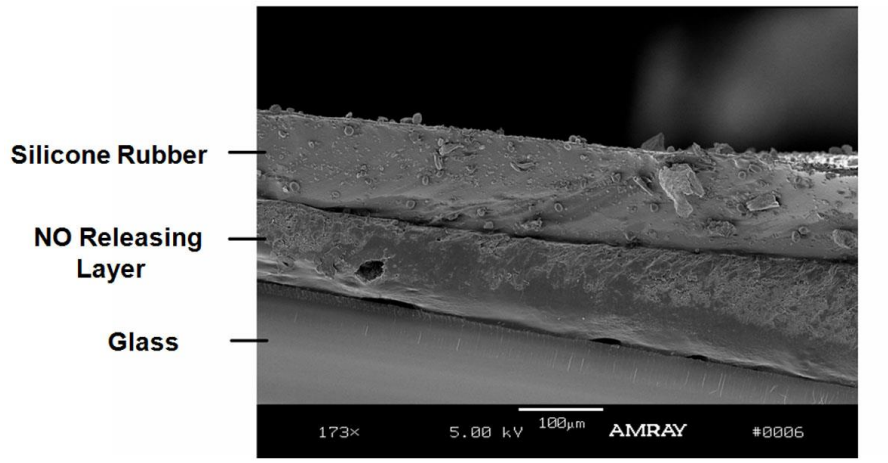

Figure 2.3. SEM image of a cross-section of a DBHD/N_2O_2-PLGA-SR-based NO release coating. The film has a two-layer configuration with a base layer of DBHD/N_2O_2 mixed in PLGA and silicone rubber as the top coating.

The thickness of the PLGA-based NO release layer as determined by Scanning Electron Microscope (SEM) was 100~130 μm and the thickness of the SR top coating was 120 μm (see **Figure 2.3**). SEM images were taken on an Amray FE 1900 Scanning Electron Microscope (SEM) at a working distance of 12 mm at 5 kV. The films were sputter-coated with gold for 30 s before imaging.

2.2.3 Evaluation of solution pH and pH changes in films

Ten microliters of 5 mM solutions of the pH probes (in THF) were added into 300 μL PBS buffers with pHs ranging from 3 to 8, respectively, in a round bottom 96-well microplate, and the image of the twelve wells was recorded to obtain the color chart of the two indicators. Dispersions were then prepared, as indicated in Section 2.2.2., and the indicator solutions were added to the NO release or control PLGA dispersions to reach a final concentration of 10 mmol kg^{-1}.[12] The colors of the dispersions were compared right after the dispersions were prepared. For in-situ pH assessment, the films were stored in pH 7.4 PBS in uncapped scintillation vials at R.T. (23 °C) or 37 °C. The solutions were replaced daily and the images of the films in PBS buffer were taken at different time points.

2.2.4 NO release measurements

The NO release profiles of the bilayer coatings were measured by purging N_2 into 2 mL PBS buffer solution, pH 7.4, in a glass cell protected from light and monitored using a chemiluminescence NO analyzer (NOA) (Sievers 280, Boulder, CO). The NOA calibration curve was obtained by adding nitrite to an acidified potassium iodide solution and plotting the integrated signal (ppb·s) vs. moles of NO that were introduced into the system.[13] The films were stored as described in Section 2.2.3, and the NO production was measured by the NOA and the NO fluxes at different time points were calculated using the calibration curve. The flux values were reported as average ± standard deviation calculated from the fluxes of two films with the same formulation.

2.2.5 *In vitro* antimicrobial test

Overnight LB (Luria Bertani) broth grown bacterial cultures were washed with 1×PBS buffer three times, and resuspended in 1×PBS buffer to make a final cell concentration at ~10^8 CFU/mL. Each NO release or control film was placed into a Corning 15-mL tube with 2 mL of the washed bacterial culture solution. The tube was incubated at 37 °C for 2 h or 24 h while horizontally shaking at 150 rpm. After incubation, the films were removed aseptically and the bacterial culture was serially diluted 10-fold in 1×PBS buffer and 50 µL of each dilution was plated onto an LB agar plate for viable bacterial counting. All the experiments were conducted in duplicate.

2.2.6 *In vitro* antibiofilm testing

A CDC flow bioreactor (Biosurface Technologies, Bozeman, MT) was used for the antibiofilm testing. The CDC bioreactor with its coupon holders was autoclaved before use. Coated slides were mounted on the coupon holders and the reactor was supplemented with 10% LB medium by a peristaltic pump with a continuous flow rate of 100 ml/h. Overnight bacterial cultures were diluted 1:100 and inoculated into the glass vessel of CDC reactor aseptically. The liquid growth medium was circulated through the vessel and shear force was generated by a magnetic stir bar rotated by a magnetic stir plate. Biofilms developed on the surface of coated slides were completely immersed into

the circulating culture. The CDC bioreactor was set up on the bench at room temperature (23 °C) or in an incubator at 37 °C.

After a 7 d incubation, coated slides were aseptically removed and individual slides were transferred to a petri dish for further staining with LIVE/DEAD® BacLight™ Bacterial Viability kit (L7012, Invitrogen, Carlsbad, CA) according to instructions in the reagent manual. Fluorescent images were acquired with a fluorescence microscope (Olympus 1X71, Center Valley, PA) equipped with Fluorescence Illumination System (X-Cite 120, EXFO) and filters for SYTO-9 (ex. 488 nm/em. 520 nm) and Propidium Iodide (ex. 535 nm/em. 617 nm) fluorescence. Images were obtained using an oil immersion 60 × objective lens. The slides were also examined under an Olympus FluoviewTM FV1000 confocal microscope (Olympus, Markham. Ontario) with Melles Griot Laser supply, detectors and appropriate filter sets. Three different spots on the NO release area of each film were randomly chosen to obtain both 2D and 3D images. Simulated 3D images were reconstructed using the Amira software package (Amira, San Diego, CA) and biofilm biomass values were quantified using the COMSTAT software (version 1) [14] with the threshold setting as 25.

2.3 Results and Discussion

2.3.1 Selecting pH-sensitive probes for film pH measurement

It is reported that at a given temperature, the decomposition of intramolecular zwitterionic diazeniumdiolates such as DBHD/N_2O_2 is pH dependent. The NO release rate decreases as the environmental pH increases.[11] Therefore, to understand and control the release profile of DBHD/N_2O_2-based NO release coatings, it is important to develop a method to monitor the pH change in the PLGA film.

Previously, our group demonstrated that the pH change of a DBHD/N_2O_2-based NO release PVC films could be evaluated by incorporating a chromoionophore and comparing the UV-Vis spectra of the film at different time points.[11] This method, however, suffers from the interferences from the light scattering signal due to the insolubility of DBHD/N_2O_2. Recently, the Schwendeman group developed a confocal flurescence microscope imaging method to directly quantify the microclimate pH

distribution in PLGA microspheres using a pH-sensitive probe.[15] As alternatives to fluorescence probes, pH indicators offer a facile, inexpensive and more convenient way to qualitatively visualize the pH changes.[16]

To effectively evaluate the film pH change within the NO release coating over a long period of time, the pH probe needs to be sensitive enough to change color during the NO release and the PLGA hydrolysis process. As shown in **Figure 2.1B**, within the NO release film, DBHD/N_2O_2 releases NO through a proton driven mechanism and produces the diamine DBHD, which will further increase the film pH. In contrast, the hydrolysis of PLGA that takes place simultaneously will cause a decrease in the film pH. Therefore, it is important for the indicator to change color according to these changes to visualize the acidic or basic environment created by the reactions within the polymeric coating. Furthermore, the amount of the pH indicator should also be well-controlled. While it is not sensitive enough to reflect a color change with too little pH probes incorporated, too much probe will also compete with the NO donor for available protons within the membrane and change the NO release profile.

Based on all of the above requirements, two sulfonphathaleins, bromocresol purple (BP) and bromothymol blue (BB), were selected as the pH-sensitive probes and added into the solutions or dispersions in a reported ratio[12] to evaluate their suitability as film pH indicators. As shown in the color chart in **Figure 2.4**, in PBS buffers with pH ranging from 3-8, the color of bromocresol purple (BP) changes from yellow to purple with the transition pH range of 5-6. For bromothymol blue (BB), on the other hand, the color changes from yellow to green and blue with a higher transition pH range of 6-8. The indicators were then added into different solutions or dispersions and the colors obtained were compared in **Figure 2.4**. First of all, a solution of 20% diamine DBHD in PLGA was used to represent an extreme case, in which all the NO was released from the NO donor DBHD/N_2O_2 while neglecting the hydrolysis of PLGA. In the real case, the film pH should be lower. Therefore, a good probe should at least be able to distinguish the difference between a mixture containing 20% of the NO donor DBHD/N_2O_2 in PLGA and a solution of 20% DBHD in PLGA.

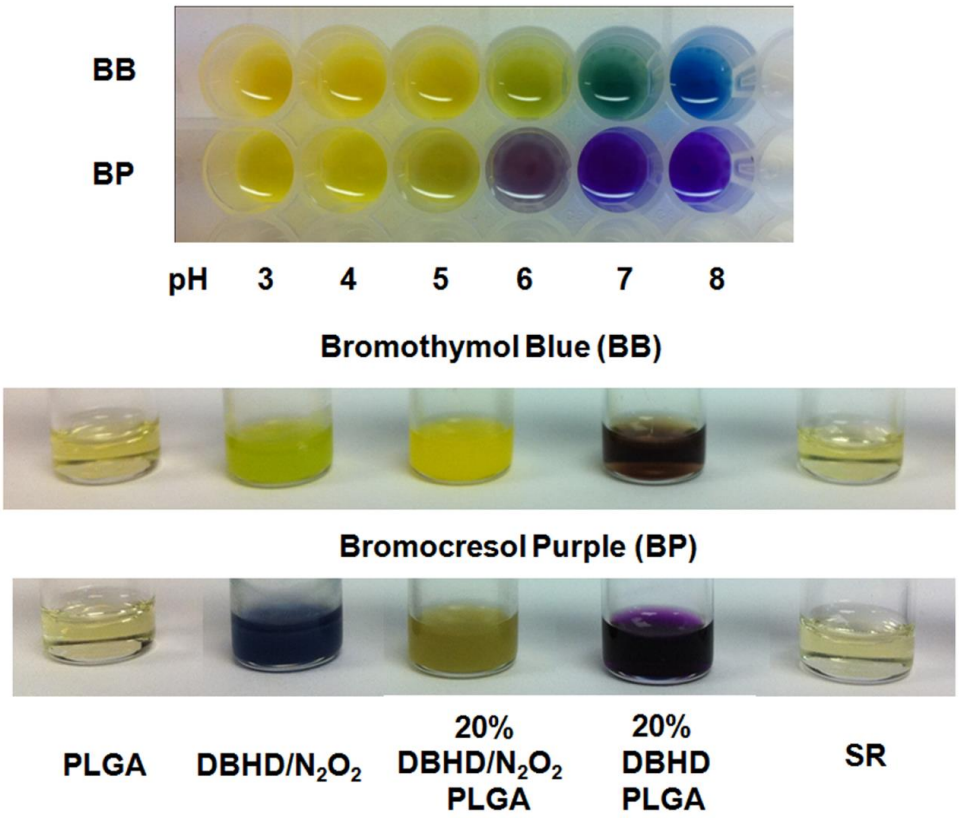

Figure 2.4. Comparison of color changes of bromothymol blue (BB) and bromocresol purple (BP) in different solutions or dispersions including pure PLGA, DBHD/N_2O_2, 20 wt% DBHD/N_2O_2 mixed in PLGA, 20 wt% DBHD in PLGA and silicone rubber THF solution (The concentration for all polymer solution is 200 mg/3 mL). a-50:50 lactide: glycolide PLGA is used for all the experiment. The indicator concentration is 10 mmol kg^{-1}. The colors of the solutions were compared rightly after the solutions were prepared. The color chart above indicates the variation of indicator colors with pH in PBS buffer.

As shown in **Figure 2.4**, for each of the indicators, a distinguishable color difference between the two mixtures is observed, indicating a much more basic environment once the NO is totally released. In addition, for both indicators, a suspension of DBHD/N_2O_2 exhibits a transition color totally different from the above two mixtures, indicating the sensitivity of both pH probes. It is also clear from the color difference that PLGA is the most acidic solution as previously reported.[15] Meanwhile, it is difficult to differentiate the acidity of PLGA and SR solutions due to the narrow transition pH range of both pH

probes. However, this does not affect their capability to be potentially used to indicate film pH changes in the NO release coatings.

2.3.2 Correlating film pH with NO release profile

As reported previously, the release of NO from DBHD/N_2O_2 will produce the diamine DBHD and further raise the film pH and decrease the NO release rate for diazeniumdiolates. Without any additives such as borate or PLGA to adjust the pH in the film, the NO fluxes of the NO release coatings are low and their lifetimes are short[10, 11]. Recently, our group demonstrated that PLGA can be used as a non-toxic alternative to the toxic potassium tetrakis(4-chlorophenyl)borate (KTpClPB), which is also an inhibitor to glucose oxidase, to promote the NO release of DBHD/N_2O_2 in a two-layered NO release coating[10]. However, since no study has been done to correlate the pH change of the films with the NO release profile, our understanding of this system is incomplete.

To further understand the system and to better control the NO release profile of this type of film, an NO release coating with a similar configuration was prepared. As shown in **Figure 2.1**, the coating used in this experiment has a two-layered configuration. In the inner layer, DBHD/N_2O_2 is embedded in the PLGA matrix and releases NO when water penetrates in. The outer layer is a SR top coating, which is used to protect the inner layer, extend the NO release time and prevent leaching of toxic species from the film into the surrounding solution. It is important that the SR top coating fully covers the entire NO release layer including the edges. Meanwhile, since a thin top coating will enhance the leaching of toxic diamine DBHD species and a thick top coating will impede the water uptake of the film thus the NO release, the thickness of the top coating should be optimized as indicated in the Experimental Section 2.2.2.

PLGA has been widely used in biomedical areas recently not only due to its biocompatibility, but also because of its controlled degradation achieved by the nature of innate acid or ester end groups as well as the lactide to glycolide ratio in the polymer chain.[17] Since the NO release of diazeniumdiolates is dependent on pH and temperature,[11] it is of interest to study the release profiles of the NO release films containing PLGA with different hydrolysis rates at different temperatures. Further, if the

lifetime of the NO release coatings can be extended to a week or longer, they can serve as models to study the antibiofilm effects of NO release coatings.

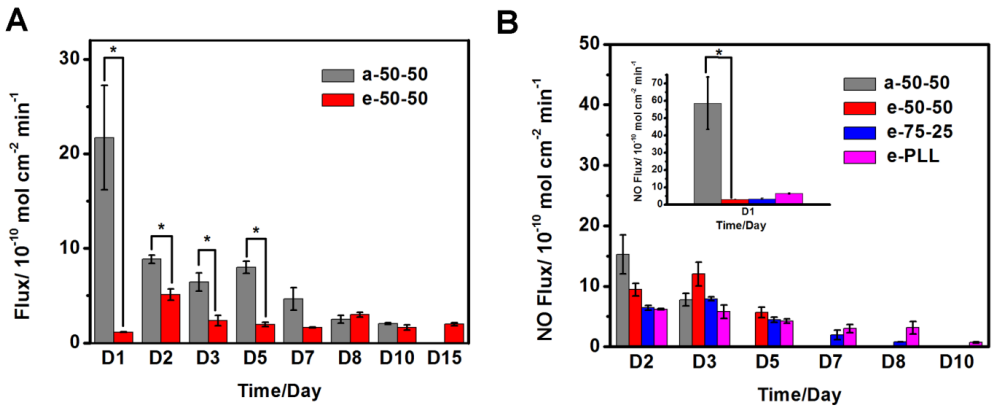

Figure 2.5. NO release profiles of NO release films with a base layer containing A) 20 wt% DBHD/N_2O_2 in a-50-50 and or e-50-50 at RT; B) 30 wt% DBHD/N_2O_2 in a-50-50, e-50-50, e-75-25 or e-PLL at 37 °C. The NO flux was recorded on a chemiluminescence NO analyzer (NOA). The fluxes presented are the average of two films (n=2). *, $P<0.05$ (the fluxes of a-50-50-based NO release films are significantly different from the fluxes of e-50-50-based films).

Therefore, the NO release profile and film pH change of two NO release coatings with 20% DBHD/N_2O_2 incorporated into two types of PLGA matrixes at RT (23 °C) were examined first. Both PLGAs had a lactide to glycolide ratio of 50:50, but the end group was acid and ester, respectively. The NO release profiles of the films were monitored daily until the depletion of the NO donor and the results are shown in **Figure 2.5A**. As shown in **Figure 2.5A**, while the film with the acid-capped PLGA (a-50-50) exhibits a steadily decreasing NO flux over time, there are no significant variations in the daily NO flux of the ester-capped PLGA (e-50-50)-based film except on the second and last day of the NO release period. Although the daily NO flux of the e-50-50-based film is lower compared to the film with the a-50-50, the NO release lifetime is extended from ten days to a fifteen-day period.

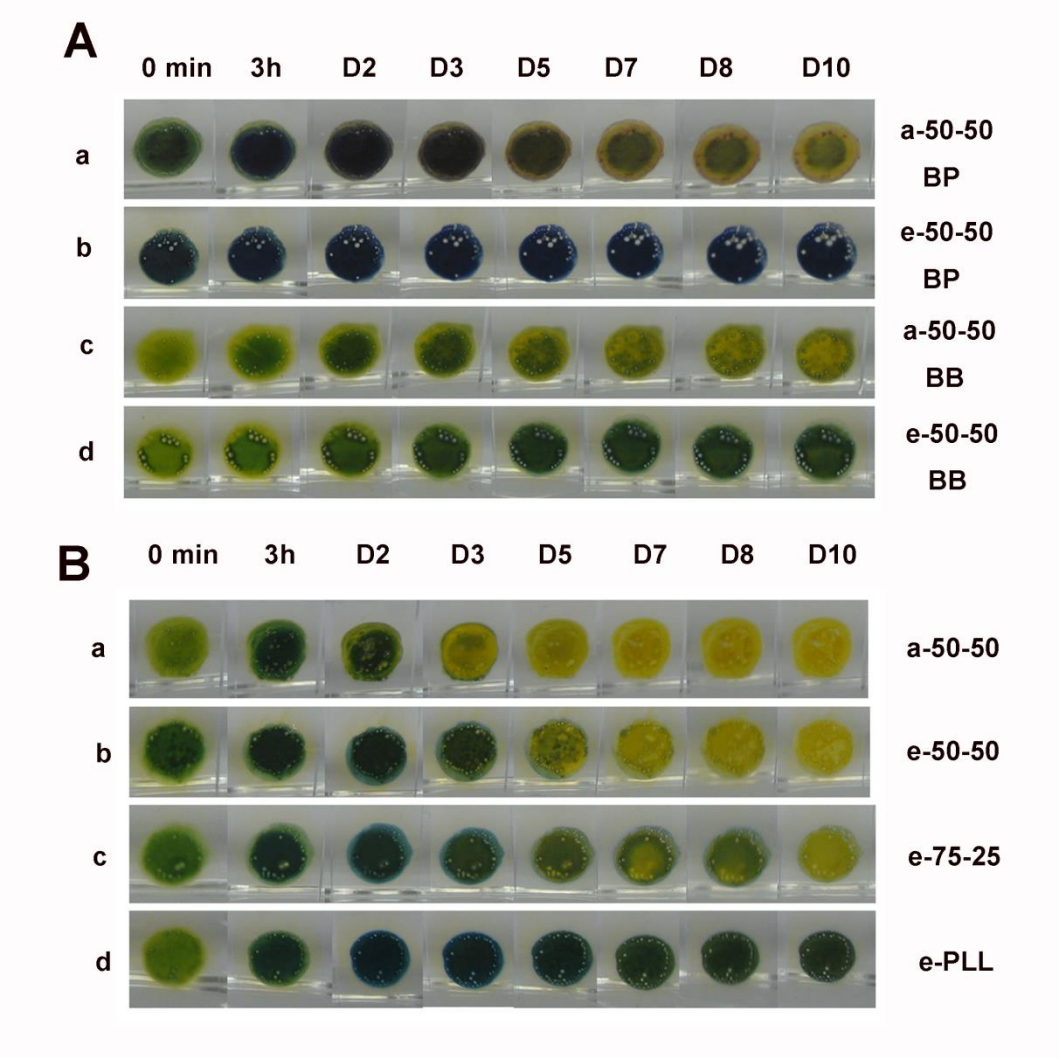

Figure 2.6. A) comparison of color changes of bromothymol blue (BB) or bromocresol purple (BP) doped NO release films containing a base layer of 20 wt% DBHD/N_2O_2 in a-50-50 and or e-50-50 at RT; B) comparison of color changes of bromothymol blue (BB) doped NO release films containing a base layer of 30 wt% DBHD/N_2O_2 in a-50-50, e-50-50, e-75-25 or e-PLL at 37 °C for 10d. D2, D3, D5, D7, D8, D10 represent day 2, day3, day 5, day 7, day 8 and day 10, respectively.

To further explain the NO release pattern, the two pH sensitive probes were further incorporated into the polymeric films to evaluate the pH changes in the coating over time. As shown in **Figure 2.6A**, as soon as the films are in contact with solution, both probes indicate a more basic environment for the e-50-50-based film due to the difference in their end groups. Within 3 h of NO release, an increase of the film pH has already been

observed for both films and it gets more obvious after a 24 h period. After the second day, however, due to the hydrolysis of PLGA, a gradual decrease in the film pH begins to be observed for the a-50-50-based film (**Figure 2.6A-a** and **Figure 2.6A-c**). The e-50-50, on the other hand, degrades much more slowly in the film, resulting in a much less obvious color change of the probe incorporated within the coating (**Figure 2.6A-b** and **Figure 2.6A-d**).

PLGA (ester-capped)	Lactide:glycolide	Lactide residual wt%	Glycolide residual wt%	Viscosity dL/g	Molecular weight (Mw)
5050 DLG 7E	50:50	1.0	0.2	0.80	132 KDa
7525 DLG 7E	75:25	1.5	0.1	0.71	114 KDa
100 DL 7E	100:0	3.1	0	0.70	106 KDa

Table 2.1. Information of ester-terminated PLGAs provided by the vendor.

Based on the above observations, a mechanism is proposed to further explain the difference in release profiles for the two NO release coatings. As shown in **Figure 2.1**, as soon as the NO release coating is in contact with solution, when water penetrates the SR outer layer and permeates into PLGA matrix, the carboxyl end groups and hydrolysis products of residual monomers present in the matrix will donate protons to the NO donors to release NO through a proton-driven mechanism. At a given temperature, the NO flux is highly dependent on the pH of the film, which is further related with the end group type and monomer residue ratio of the PLGA matrix. Therefore, the a-50-50 matrix shows a much higher initial NO flux compared to the e-50-50 with a limited ratio of monomer residues (see **Table 2.1**) to promote the initial NO release. Once NO is released, the diamine DBHD will remain in the film and form ammonium salts with the carboxyl groups in the PLGA matrix and this process will further facilitate the hydrolysis of PLGA to produce more protons and thus promote the NO release. However, even at a given temperature, it is still difficult to predict the NO flux at this stage because it is influenced by multiple factors including the water uptake of the coating, the NO donor

amount and the hydrolysis rate of PLGA within the films. For example, the highest NO flux for the e-50-50-based films is observed on the second day even though the coating pH is higher compared to the first day. This might due to either the hydrolysis of e-50-50 that provides more protons that are quickly consumed by the NO donor or the increased water uptake of the film on the second day. Due to its fast hydrolysis rate, the gradually decreased daily NO flux observed for the a-50-50-based coating is most likely due to the gradual depletion of NO donors within the film. The steady daily NO flux for the e-50-50-based coating, on the other hand, is most likely results from the slow hydrolysis rate of the PLGA matrix that further stabilizes the pH within the film.

The RT experimental results indicate that the hydrolysis rate of PLGA can be used to control the release profile of the NO release coatings. While PLGA with fast hydrolysis rate creates high NO flux, PLGA with slower hydrolysis rate can extend the NO release lifetime. At 37 °C, both the NO release rate of diazeniumdiolates and the hydrolysis rate of PLGA will be elevated. Since it is reported that a slower hydrolysis rate can be achieved by increasing the lactide ratio in the PLGA polymer chains,[17] e-PLGAs with a lactide to glycolide ratio of 75:25 (e-75-25) and poly(lactic acid) (e-PLL) were also used to prepare the NO release coatings used at 37 °C. **Figure 2.5B** shows the NO release profiles for four films containing 30 wt% DBHD/N_2O_2 doped into a-50-50, e-50-50, e-75-25 or e-PLL at 37 °C. The NO release profiles are consistent with the prediction from the RT experimental results. The films are able to release NO for three, five, eight and ten days for a-50-50, e-50-50, e-75-25 or e-PLL, respectively. The slower the PLGA hydrolysis rate, the longer the NO release lasts. Due to the introduction of slower hydrolyzed PLGAs, bromothymol blue (BB), with a higher transition pH range, was used to evaluate the film pH change for the four coatings at 37 °C. As shown in **Figure 2.6B**, similar to the RT observations, the release of NO firstly increases the film pH and the further hydrolysis of PLGA provides additional protons to the NO donors as well as lowers the film pH. From these comparisons, it is obvious that the hydrolysis rates of PLGAs are different within the coatings. While for the a-50-50 (**Figure 2.6B-a**), the hydrolysis of PLGA has already created a very acidic environment on the third day that contributes to the depletion of all the NO donors, the film pH of the e-PLL coating (**Figure 2.6B-d**), in contrast, is elevated due to the production of DBHD and remains

almost neutral for ten days due to the slow hydrolysis of the PLL matrix. For e-50-50 and e-75-25, the hydrolysis of PLGA causes an apparent color change, indicating an acidic environment on the fifth (**Figure 2.6B-c**) and seventh day (**Figure 2.6B-d**), respectively.

The initial NO flux at a given temperature, however, is not related to the hydrolysis rate of the polymer, but the initial film pH. The acid capped PLGA, a-50-50, should be the one that creates the most acidic environment. For the ester-capped PLGAs, as listed in **Table 2.1**, the monomer residue percentages are in the order of e-PLL > e-75-25 > e-50-50. Therefore, the initial pH of the films are in the order of a-50-50 < e-PLL < e-75-25 < e-50-50, which is further supported visually by comparing the film colors at 0 min (film pH a<d<c<b shown in **Figure 2.6B**). The order of the initial NO flux of the four films, as shown in **Figure 2.5B** (D1), is consistent with the film acidity order, which further supports that at a given temperature, the initial NO flux is highly dependent on the film pH. Thus, it is also possible to control the initial NO flux of the films by controlling the end groups and monomer residues within the PLGA polymer matrix. Therefore, PLGA acts as not only a promoter, but also a controller of the NO release within the coatings.

The NO release profiles and film pH of films containing other matrices such as SR and PU instead of PLGA in the base layer were also studied and the results are shown in **Figure 2.7**. The difference between the PLGA matrix and SR or PU lies in that the other two matrices lack the initial acid residues or the capability to hydrolyze to produce protons for the NO donor. Therefore, when the control films with a base layer of 30 wt% DBHD/N_2O_2 doped in SR and PU are placed into 37 °C PBS buffer, hardly any NO release is observed compared to films with various PLGAs incorporated (**Figure 2.7A**). Only a slight pH increase in the SR or PU-based film is observed over a one week period due to the production of DBHD, as shown in **Figure 2.7B**. This is a further proof of the important role of PLGA as both an NO release promoter and controller.

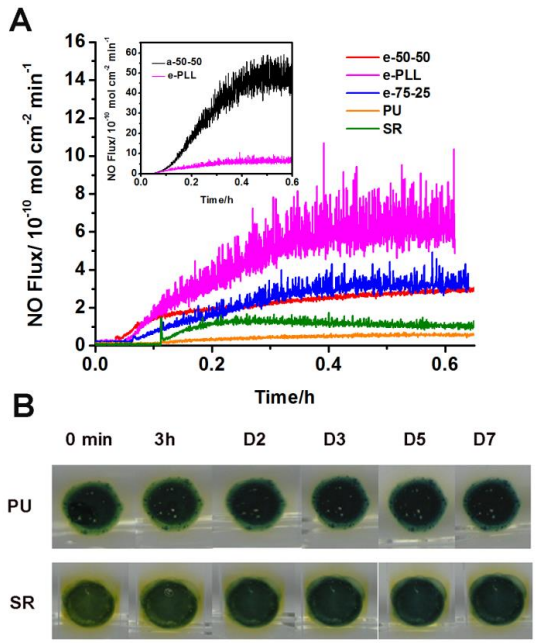

Figure 2.7. A) Initial NO release profiles of films with different polymers incorporated; B) pH changes of polyurethane and silicone rubber-based NO release films over a one week period. The control films are prepared in the same way as the PLGA-based NO release films except that SR or PU was used as the polymer matrix for the base layer. Bromothymol blue (BB) was used as the pH indicator.

2.3.3 Antibiofilm properties of NO release films

Before any antibiofilm testing, an *in vitro* antimicrobial test was used to compare the influence of the NO release film and a series of control films on planktonic bacterial cells. The aim of the test was to study the "matrix" effect and further evaluate the leaching of toxic diamine DBHD. An NO release film with 20 wt% DBHD/N_2O_2 mixed with a-50-50 PLGA as the inner layer was chosen because PLGA with the fastest hydrolysis rate is most likely to have the above problems. Therefore, two controls were used in this test including a film with only PLGA (PLGA/SR) and a film with PLGA doped with 20 wt% diamine DBHD (20% DBHD) as the inner layer.

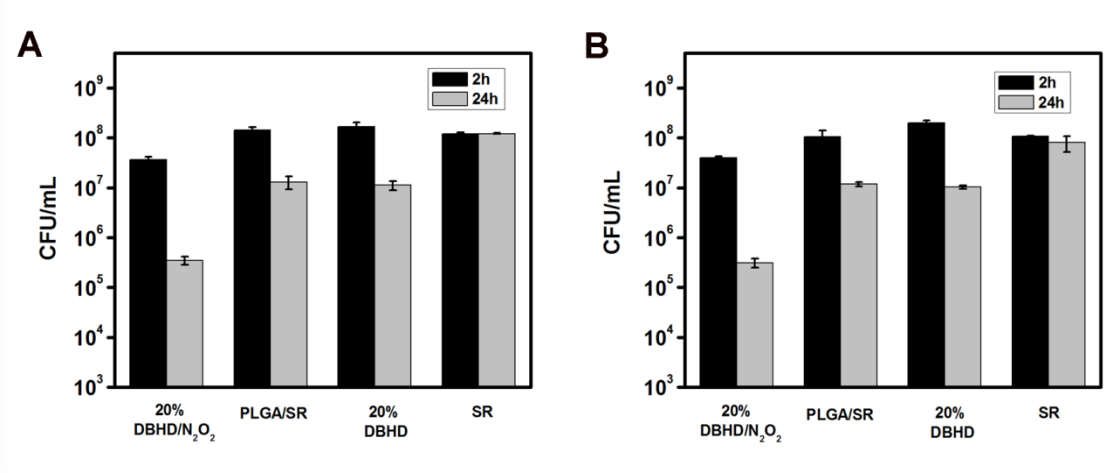

Figure 2.8. The antimicrobial killing effects of NO release films with a base layer of 20 wt% DBHD/N_2O_2 doped in a-50-50, control films with a base layer of a-50-50, 20 wt% DBHD doped in a-50-50 and control film with only SR top coating on A) *S. aureus*; B) *E. coli* after 2 h and 24 h incubation at 37 °C in 10^8 CFU/mL bacterial suspension.

As shown in **Figure 2.8**, when the NO release films and control films were placed into PBS buffer containing 10^8 CFU/mL *S. aureus* (**Figure 2.8A**) or *E. coli* (**Figure 2.8B**) at 37 °C for 2 h, the NO release films showed ~1 log killing (i.e., the number of viable cells was reduced from ~1.8×10^8 to ~3.7×10^7 CFU/mL for *S. aureus* and ~2.2×10^8 to ~5×10^7 CFU/mL for *E. coli*) compared to the controls that almost showed no changes. After 24 h exposure, with a continuous production of NO as the antimicrobial agent, 3 logs of killing of both *S. aureus* and *E. coli* (i.e., the number of viable cells was reduced from ~1.8×10^8 to ~3.5×10^5 CFU/mL for *S. aureus* and for ~2.2×10^8 to ~3.1×10^5 CFU/mL for *E. coli*) were observed. Compared to a control film that contains only a SR layer that exhibits almost no killing effect after 24 h exposure to bacterial suspension, the PLGA/SR or 20% DBHD control film showed ~1 log killing effect for both bacterial strains resulting from the "matrix" killing effect. However, this is much less than the NO release coatings, indicating NO, as reported, is a potent antimicrobial agent for both gram-positive *S. aureus* and gram-negative *E. coli*.[1] If there is a significant leaching of the diamine DBHD, the 20% DBHD control film should exhibit a much greater killing effect compared to either the NO release film or the PLGA/SR control. However, since both controls exhibit almost identical effect on planktonic bacterial cells, the minimized leaching of toxic DBHD from films with current configuration is further demonstrated.

When the same test was performed at RT (23 °C), however, none of the films exhibited any killing effect after 24 h incubation (data not shown). Thus indicates that higher temperature leads to faster hydrolysis of PLGA and enhanced release of NO, which also contributes to the "matrix" effect and antimicrobial effects of the NO release films.

Although the antibiofilm properties of NO release coatings have been proven by both *in vitro* and *in vivo* studies, there have been few examples that studied the influence of different NO release profiles on the antibiofim properties of NO release coatings over a time scale that is long enough to form a mature biofilm. For example, the Schoenfisch group has evaluated and demonstrated the antibiofilm property of NO release xerogel coatings against *S. aureus* in a subcutaneous animal model after eight days of implantation.[18] However, considering around 90% of the NO was released from their coating over the initial 24 h,[18] it will be difficult to study the influence of NO release profiles on the antibiofilm property of this type of film over an equivalent time scale. Similarly, although *in vitro* studies under both stagnant and dynamic conditions have shown that NO release catheters are able to prevent biofilm formation by *E. coli*, the NO release profile of the catheter is untunable and exhibits an initial "burst" of NO release.[19] Considering the complexity and time-scale of formation of a mature biofilm, the DBHD/N_2O_2 and PLGA-based NO release coating, with a tunable NO release profile over more than one week period offers an ideal model to study the influence of different NO release profiles on the antibiofilm properties of the coatings.

A CDC biofilm reactor was chosen as a tool for the study of the antibiofilm properties of the prepared NO release coatings because it is able to provide both shear forces and renewable nutrient sources that mimic an *in vivo* environment[7] and the film is continuously exposed to bacterial culture. It is also proven by statistical assessment to be a reliable tool for growing biofilms with repeatable results.[20] Compared to previously reported studies of microbial adhesion on NO release coatings in flowing systems for a short period of time with[19] or without[6, 8] nutrient sources, a seven-day biofilm test in a CDC biofilm reactor will better mimic a natural environment. Furthermore, the study of the antibiofilm properties of NO release coatings with tunable NO release profiles in a CDC biofilm reactor at different temperatures can provide further information to better utilize the NO release coatings for antibiofilm applications.

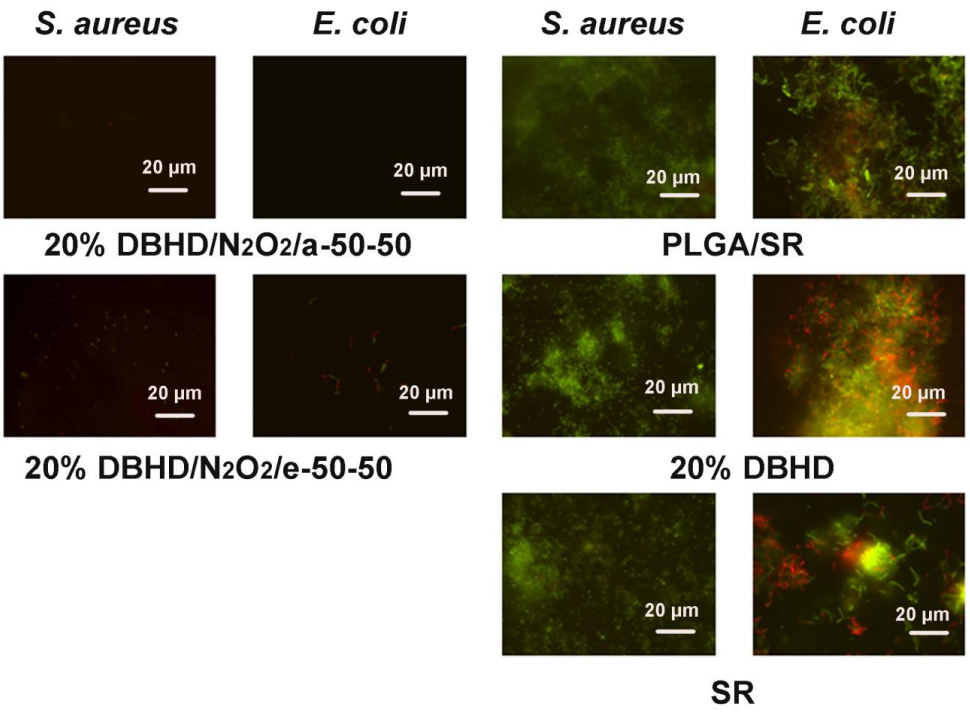

Figure 2.9. Representative fluorescent micrographs showing comparison of surfaces of NO release and control films after incubation at RT (23 ºC) for seven days in a CDC biofilm reactor containing *S. aureus* or *E. coli*. The NO release films containing a base layer of 20 wt% DBHD/N_2O_2 mixed with a-50-50 or e-50-50 PLGA matrix, and the NO release profile of the films are shown in **Figure 2.5**A. The controls include two films with base layers of a-50-50 PLGA or a-50-50 PLGA mixed with 20 wt% DBHD and a film with only a SR layer. Bacterial cells were stained with Bacterial LIVE/DEAD staining dyes and viable cells shown as green fluorescent dots while dead or membrane damaged cells shown as red fluorescence dots in the images.

Therefore, the NO release films and corresponding controls were first incubated in a CDC biofilm reactor at RT (23 °C) with gram-positive *S. aureus* or gram-negative *E. coli* cultures for seven days. On the eighth day, the films were taken out of the reactor and stained with bacterial LIVE/DEAD dyes to visualize the growth of biofilm on different surfaces. The NO release profiles of the films are shown in **Figure 2.5**, and **Figure 2.9** shows the representative fluorescent micrographs of the surfaces of the NO release and control films after the antibiofilm test in the CDC reactor. As shown in **Figure 2.9**, for all the control films including PLGA/SR, 20% DBHD and SR, the surfaces are fully colonized by mostly viable *S. aureus* or *E. coli* cells (shown as green dots). In contrast,

NO release films containing a base layer of 20 wt% DBHD/N_2O_2 doped in either a-50-50 or e-50-50 PLGA exhibit clean surfaces. Compared to the a-50-50 PLGA-based NO release film that barely exhibit any observable bacterial cells on the surface, a small amount of bacterial cells are still observable on the e-50-50 PLGA-based film surface for both *S. aureus* and *E. coli*. This might be attributed to the differences in the daily NO flux of the two films (see **Figure 2.5A**) with the film having a higher NO flux exhibiting a better antibiofilm effect. To gain a better view and quantification of biofilm structure and biomass, 3D images were reconstructed based on the confocal images. The 3D images representing *S. aureus* biofilm formation on different surfaces at RT are shown in **Figure 2.10A** and the quantitative analysis data are listed in **Table 2.2**. Similar to the fluorescent micrographs, the 3D images also confirm the significant antibiofilm effect of the NO release coatings. As shown in **Figure 2.10A**, thick, dense and carpet-like biofilms containing mostly living *S. aureus* cells are developed on the surfaces of all the control films with some variations in the biofilm structures between the SR surface and the other two controls. The surface of the NO release films, on the other hand, barely has any bacterial cell attachment, indicating significant antibiofilm effect due to the NO release from the film. The biofilm biomass values quantified from the 3D images are listed in **Table 2.2**. Even for the e-50-50-based NO release film, with a less effective antibiofilm effect, more than 99.9% reduction of the biofilm biomass is obtained and similar results are also obtained for *E. coli*, as listed in **Table 2.2**. Interestingly, while neither of the NO release films exhibit observable antimicrobial effect in the antimicrobial test at RT, the antibiofilm property of each is significant, even for the e-50-50 PLGA-based NO release film with a relatively low NO flux. Viable cell counts before and after the antibiofilm test indicated that after one week growth in the medium, the bacterial concentration is ~100 times higher than the initial concentration (i.e., the viable cell counts increases from ~1×10^6 CFU/mL to ~2.7×10^8 CFU/mL for both *S. aureus* and *E. coli*). Due to the short lifetime of NO, it is impossible for it to diffuse far enough to kill all the planktonic bacterial cells in solution, especially if there's limited amount of NO production. This might contribute to the low antimicrobial property for the NO release films at RT in the antimicrobial tests. However, since it is still possible for NO to interact with planktonic bacterial cells that are close enough to the coating surface, the

NO release coating is able to create a "bacterial inhibition zone" as previously reported,[19] which contributes to the observed antibiofilm effect for the NO release coatings. Furthermore, low levels of NO has been reported to induce the dispersal of diverse single-species and multi-species biofilms of gram-positive and gram-negative bacteria through signaling.[2, 21] Since the experimental results have also indicated the NO release coating with a low daily NO flux (**Figure 2.5A**, e-50-50) is able to prevent biofilm formation, the observed antibiofilm effect of NO release coating, might also arise from NO's potent biofilm dispersal effect.

Films		*S. aureus*	*E.coli*
		Biomass/$\mu m^{3}/\mu m^{2}$	Biomass/$\mu m^{3}/\mu m^{2}$
NO release	a-50-50	0±0	0±0
	e-50-50	$1.5\pm0.3\times10^{-3}$	$1.8\pm0.8\times10^{-3}$
Control	PLGA/SR	5.2±0.7	4.9±0.5
	20% DBHD	4.1±0.6	5.7±2.4
	SR	3.6±0.4	4.4±0.6

Table 2.2. Biofilm biomass in *S. aureus* and *E. coli* biofilm on PLGA-based bilayer films in CDC biofilm reactor at RT. Average values with standard deviations for n= 3 shown in the brackets were calculated from COMSTAT image analysis on CLSM images.

Films		*S. aureus*	*E.coli*
		Biomass/$\mu m^{3}/\mu m^{2}$	Biomass/$\mu m^{3}/\mu m^{2}$
NO release	a-50-50	$8.6\pm1.0\times10^{-3}$	$4.0\pm1.2\times10^{-3}$
	e-50-50	$8.3\pm3.6\times10^{-3}$	$1.3\pm0.5\times10^{-3}$
	e-75-25	$9.2\pm7.5\times10^{-3}$	$7.0\pm4.8\times10^{-4}$
	e-PLL	$9.4\pm6.0\times10^{-4}$	$1.6\pm0.6\times10^{-4}$
Control	PLGA/SR	$1.4\pm1.6\times10^{-2}$	$4.0\pm1.8\times10^{-1}$
	30% DBHD	$5.9\pm2.5\times10^{-2}$	$4.0\pm1.0\times10^{-1}$
	SR	$5.9\pm0.5\times10^{-2}$	$6.0\pm1.4\times10^{-1}$

Table 2.3. Biofilm biomass in *S. aureus* and *E. coli* biofilm on PLGA- or PLL-based bilayer films in CDC bioreactor at 37 °C. Average values with the standard deviations for n = 3 shown in the brackets were calculated from COMSTAT image analysis on CLSM images.

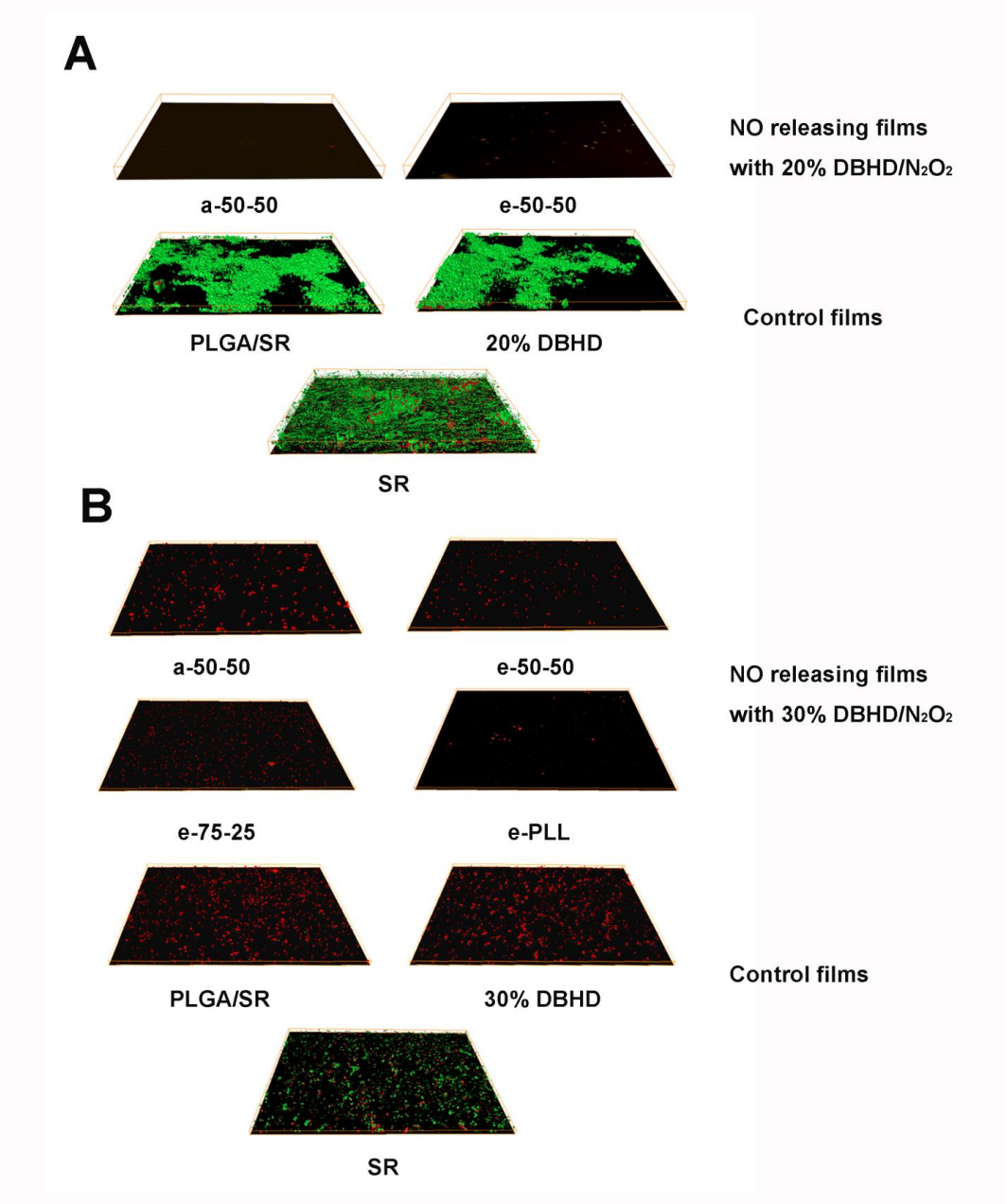

Figure 2.10. Three-dimensional images of *S. aureus* biofilm formed A) at RT on NO release films with a base layer of 20 wt% DBHD/N_2O_2 doped in a-50-50 or e-50-50 PLGA and control films with a base layer of a-50-50, a-50-50 mixed with 20 wt% DBHD or a control film with only a silicone rubber top coating. The dimension of the films are 142× 108 ×15 μm; B) at 37 °C on NO release film with a base layer of 30 wt% DBHD/N_2O_2 doped in a-50-50, e-50-50, e-75-25 or e-PLL PLGA matrix and control film with a base layer of a-50-50, a-50-50 mixed with 30 wt% DBHD and a film with only a silicone rubber top coating after incubation in a CDC biofilm reactor after seven days. The dimension of the films are 142 ×108 × 9 μm. Bacterial cells were stained with Bacterial LIVE/DEAD staining dyes and viable cells shown as green fluorescent dots while dead or membrane damaged cells shown as red fluorescence dots in the images.

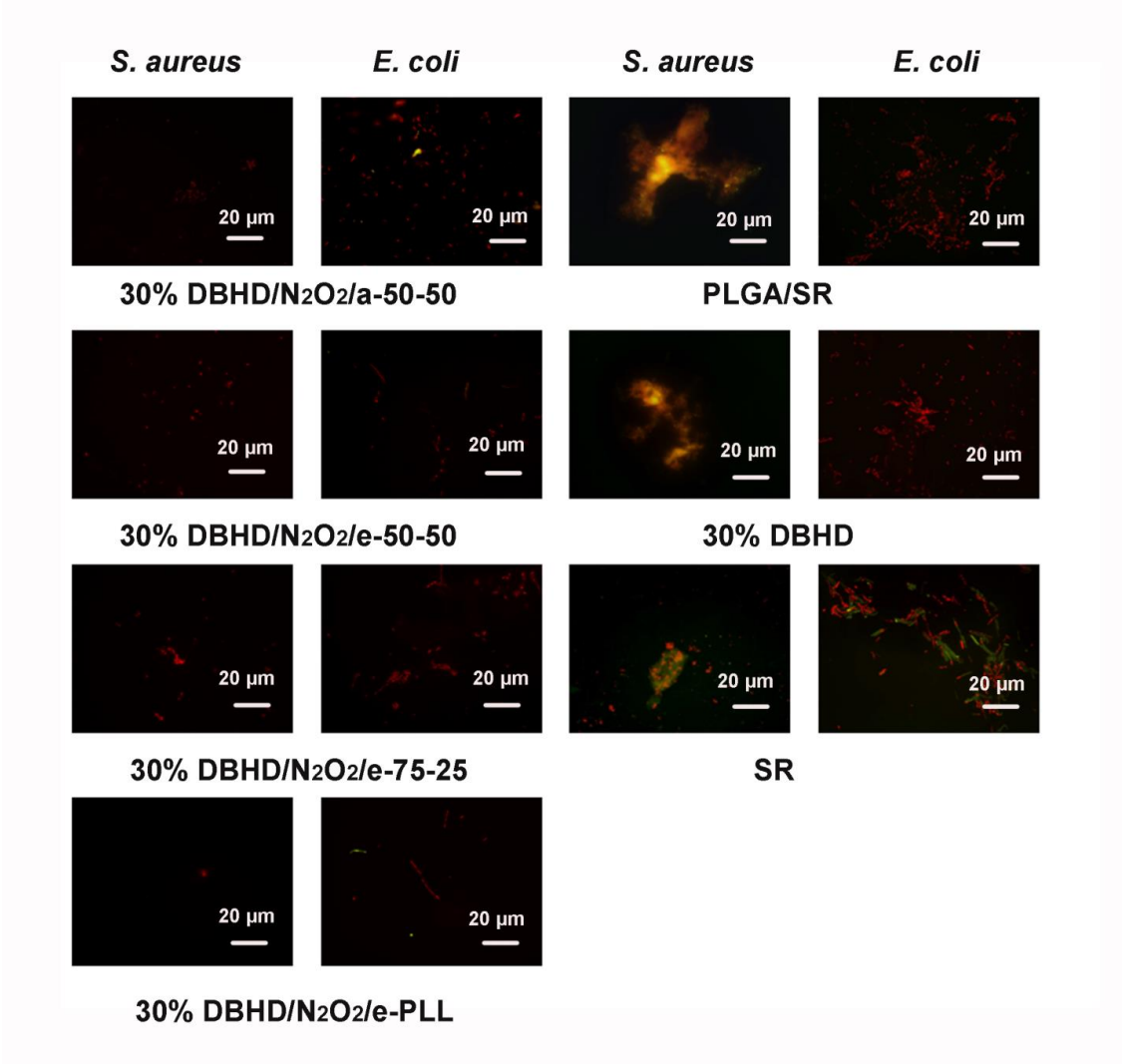

Figure 2.11. Representative fluorescent micrographs showing comparison of surfaces of NO release and control films after incubation for seven days at 37 ºC in a CDC biofilm reactor containing *S. aureus* or *E. coli*. The NO release films containing a base layer of 30 wt% DBHD/N_2O_2 mixed with a-50-50, e-50-50, e-75-25 or e-PLL PLGA matrix, and the NO release profile of the films are shown in **Figure 2.5B**. The controls include two films with base layers of a-50-50 PLGA or a-50-50 PLGA mixed with 30 wt% DBHD and a film with only a SR layer. Bacterial cells were stained with Bacterial LIVE/DEAD staining dyes and viable cells shown as green fluorescent dots while dead or membrane damaged cells are shown as red fluorescence dots in the images.

The antibiofilm properties of NO release coatings with different NO release profiles (shown in **Figure 2.5B**) were further evaluated at the physiological temperature of 37 °C and the representative fluorescent micrographs of bacterial adhesion on different surfaces after the antibiofilm test are shown in **Figure 2.11**. Compared to the SR surface that is

fully colonized by bacterial cells after the antibiofilm test at RT (see **Figure 2.9**), the biofilm formation on the same type of surface for either *S. aureus* or *E. coli* (**Figure 2.11**) is less obvious at 37 °C. This is similar to the observations in previous reports where *S. aureus*[22, 23] or *E. coli*[24] formed optimal biofilm coverage at lower temperature compared to physiological temperature. Different from the SR surface, the PLGA/SR and 30% DBHD control film surfaces exhibit more dead cells compared to viable cells, indicating a "matrix" killing effect occurs at 37 °C. However, for both *S. aureus* and *E. coli*, the NO release coating surfaces are much less colonized compared to the controls, indicating much better antibiofilm effect results via the NO released from the coatings. This is consistent with the observation in the previously described solution-based antimicrobial tests at 37 °C, where the NO release coatings exhibit much better killing effect on planktonic bacterial cells compared to the two controls that also exhibit a small "matrix" killing effect (**Figure 2.8**). In addition, high temperature might also increase the permeability of the cell membrane, which can also contribute to greater dead or membrane damaged cells observed on the surfaces.

The antibiofilm effects of different NO release coatings, however, vary with bacterial strains and the NO release profiles. A difference was also observed in the viable cell counts after one week incubation at 37 °C for different bacterial strains in the CDC biofilm reactor. While the viable cell counts for *S. aureus* increased from ~1.8×10^6 to ~ 8.6×10^9 CFU/mL, the growth of *E. coli* was slower (i.e., the viable cell counts increased from 1.6×10^6 to 4.6×10^8 CFU/mL). Therefore, the antibiofilm properties of the NO release films on different bacterial strains were compared separately. For *S. aureus*, with a faster growth rate, although the formation of *S. aureus* biofilms on all the control films can be clearly observed as shown (see **Figure 2.11**), only a few dead or membrane damaged bacterial cells are observed on the surfaces of NO release films with different NO release profiles. The antibiofilm effects are almost identical for all the NO release films regardless of the differences in the lifetime of the films. However, the e-PLL-based NO release film with the longest NO release lifetime (**Figure 2.5B**) exhibits a cleaner surface. The 3D images for *S. aureus* biofilm formation on different surfaces are shown in **Figure 2.10B** and the biomass values are quantified and listed in **Table 2.3**. Similar to the observations from the 2D images, the 3D images indicate that at RT, a denser and

more evenly distributed *S. aureus* biofilm is formed on a SR surface compared to 37 °C. The calculated *S. aureus* biofilm biomass values listed in **Table 2.3** for different surfaces further support the antibiofilm properties of NO release coatings. With a biofilm biomass reduction of ~ 98.4% compared to a silicone rubber control, the e-PLL-based NO release coating that is able to release NO for the longest time period is the most effective coating to prevent *S. aureus* biofilm formation at 37 °C. In contrast, a-50-50, e-50-50 and e-75-25 PLGA-based coatings all exhibit ~85% biofilm reduction despite the fact that the lifetime of films varies from three to eight days. One possible explanation for the better antibiofilm effect observed for e-PLL compared to the e-75-25-based NO release coating might be that there was a time lag between the evaluation of the NO flux and the removal of the film from the CDC reactor on the eighth day, so the e-75-25 PLGA-based NO release coating might stop releasing NO before its removal, which was not the case for the e-PLL-based coating.

When *E. coli* is used instead of *S. aureus,* the influences of different NO release profiles on the antibiofilm properties of the NO release films at 37 °C are more clearly observed. As shown in **Figure 2.11**, for all the control films, a high percentage of the surface is colonized by *E. coli* cell clusters. Compared to a SR surface where both viable and dead cells can be observed, most of the *E. coli* cells that are attached on either the PLGA or the 30% DBHD control films are dead or membrane damaged cells due to the "matrix" effect. Since the attachment of dead bacterial cells can trigger immune responses and inflammation,[25] an "ideal" antibiofilm coating should be able to prevent the attachment of both living and dead bacterial cells.[26] Compared to the controls, the NO release coatings exhibit different extents of antibiofilm properties due to their different NO release profiles (**Figure 2.5B**). It is obvious, however, that the NO release coatings with a longer lifetime exhibit a cleaner surface (**Figure 2.11**) and this effect is further supported by the *E. coli* biofilm biomass values listed in **Table 2.3**, which indicate the longer the NO release, the lower the *E. coli* biofilm biomass value. In particular, the e-PLL-based NO release coating was able to reduce the biofilm biomass by ~ 99.9%. However, for films with all the other PLGA, > 99% biofilm reduction was observed. Therefore, the combined DBHD/N_2O_2 and PLGA-based NO release coatings, especially those can release NO for a long period, are expected to be potential candidates

as antibiofilm coatings for indwelling devices. Needless to say, the current study is still limited because the one week antibiofilm test and ten day NO release at 37 °C are not long enough to meet the requirements for all possible indewelling devices. However, since our preliminary study indicated that the lifetime of the NO release coating could be extended by increasing the thickness of the NO release layer (data not shown), future work will focus on utilizing this type of coating with extended lifetime in animal models to evaluate the feasibility of applying such films as antibiofilm coatings for indwelling devices.

2.4 Conclusions

Nitric oxide release coatings with a bilayer configuration using DBHD/N_2O_2 doped within various PLGA materials were fabricated. By comparing the NO release profiles and film pH changes using PLGAs with different hydrolysis rates, it was shown that the specific chemical formulation of the PLGA used plays an important role as both a pH promoter and controller in the NO release mechanism. The new films with tunable NO release profiles were proven to prevent *S. aureus* and *E. coli* biofilm formation in a CDC flow bioreactor using a 7 d antibiofilm test. The proposed coatings are thus expected to be potentially applied on short-term indwelling devices such as catheters to prevent thrombus formation and bacterial infection issues and future work will focus on further extending the NO release lifetimes of the coatings and conducting appropriate *in vivo* studies.

2.5 References

1. Hetrick, E. M.; Schoenfisch, M. H. *Chem. Soc. Rev.* **2006,** 35, (9), 780-789.
2. McDougald, D.; Rice, S. A.; Barraud, N.; Steinberg, P. D.; Kjelleberg, S. *Nat Rev Micro* **2012,** 10, (1), 39-50.
3. Barraud, N.; Hassett, D. J.; Hwang, S. H.; Rice, S. A.; Kjelleberg, S.; Webb, J. S. *J. Bacteriol.* **2006,** 188, (21), 7344-7353.
4. Barraud, N.; Schleheck, D.; Klebensberger, J.; Webb, J. S.; Hassett, D. J.; Rice, S. A.; Kjelleberg, S. *J. Bacteriol.* **2009,** 191, (23), 7333-7342.
5. Partridge, J. D.; Bodenmiller, D. M.; Humphrys, M. S.; Spiro, S. *Mol. Microbiol.* **2009,** 73, (4), 680-694.
6. Hetrick, E. M.; Schoenfisch, M. H. *Biomaterials* **2007,** 28, (11), 1948-1956.
7. Williams, D. L.; Bloebaum, R. D. *Microsc. Microanal.* **2010,** 16, (2), 143-152.
8. Privett, B. J.; Nutz, S. T.; Schoenfisch, M. H. *Biofouling* **2010,** 26, (8), 973-983.
9. Frost, M. C.; Reynolds, M. M.; Meyerhoff, M. E. *Biomaterials* **2005,** 26, (14), 1685-1693.
10. Yan, Q. Y.; Major, T. C.; Bartlett, R. H.; Meyerhoff, M. E. *Biosens. Bioelectron.* **2011,** 26, (11), 4276-4282.
11. Batchelor, M. M.; Reoma, S. L.; Fleser, P. S.; Nuthakki, V. K.; Callahan, R. E.; Shanley, C. J.; Politis, J. K.; Elmore, J.; Merz, S. I.; Meyerhoff, M. E. *J. Med. Chem.* **2003,** 46, (24), 5153-5161.
12. Qin, Y.; Bakker, E. *Talanta* **2002,** 58, (5), 909-918.
13. Castegnaro, M.; Massey, R. C.; Walters, C. L. *Food Addit Contam* **1987,** 4, (1), 37-43.
14. Heydorn, A.; Nielsen, A. T.; Hentzer, M.; Sternberg, C.; Givskov, M.; Ersboll, B. K.; Molin, S. *Microbiology* **2000,** 146, 2395-2407.
15. Ding, A. G.; Schwendeman, S. P. *Pharm. Res.* **2008,** 25, (9), 2041-2052.
16. Li, L.; Li, S. M.; Sun, J. H.; Zhou, L. L.; Bao, X. G.; Zhang, H. G.; Zhang, F. S. *Proc Natl Acad Sci U S A* **2007,** 104, (27), 11192-6.
17. Li, S. M. *J Biomed Mater Res* **1999,** 48, (3), 342-353.
18. Nablo, B. J.; Prichard, H. L.; Butler, R. D.; Klitzman, B.; Schoenfisch, M. H. *Biomaterials* **2005,** 26, (34), 6984-6990.
19. Regev-Shoshani, G.; Ko, M.; Miller, C.; Av-Gay, Y. *Antimicrob. Agents Chemother.* **2010,** 54, (1), 273-279.
20. Goeres, D. M.; Loetterle, L. R.; Hamilton, M. A.; Murga, R.; Kirby, D. W.; Donlan, R. M. *Microbiology-Sgm* **2005,** 151, 757-762.
21. Barraud, N.; Storey, M. V.; Moore, Z. P.; Webb, J. S.; Rice, S. A.; Kjelleberg, S. *Microbiol Biotechnol* **2009,** 2, (3), 370-378.
22. Williams, D. L.; Woodbury, K. L.; Haymond, B. S.; Parker, A. E.; Bloebaum, R. D. *Curr. Microbiol.* **2011,** 62, (5), 1657-1663.
23. Rode, T. M.; Langsrud, S.; Holck, A.; Moretro, T. *Int J Food Microbiol* **2007,** 116, (3), 372-383.
24. Andersen, T. E.; Kingshott, P.; Palarasah, Y.; Benter, M.; Alei, M.; Kolmos, H. J. *J Microbiol Methods* **2010,** 81, (2), 135-140.
25. Cheng, G.; Xite, H.; Zhang, Z.; Chen, S. F.; Jiang, S. Y. *Angew. Chem., Int. Ed.* **2008,** 47, (46), 8831-8834.

26. Webb, J. S.; Thompson, L. S.; James, S.; Charlton, T.; Tolker-Nielsen, T.; Koch, B.; Givskov, M.; Kjelleberg, S. *J. Bacteriol.* **2003,** 185, (15), 4585-4592.

Chapter 3 Carboxyl-Ebselen-Based Layer-by-Layer Films as Potential Antithrombotic and Antimicrobial Coatings

3.1 Introduction

Nitric oxide release coatings have limited lifetimes due to their limited NO reservoirs that can be incorporated into the polymeric matrices and an attractive alternative is to use NO generation coatings, which are a group of catalytic coatings that are capable of generating NO from endogenous RSNOs. As described in Chapter 1, the toxicity issues of aliphatic organoselenium species have limited their application in developing NO generation and antimicrobial coatings and the RSNO decomposition catalytic activity of aromatic selenium species, such as ebselen (**Figure 3.1A**) and its derivatives with low toxicity have not been studied in detail to date.

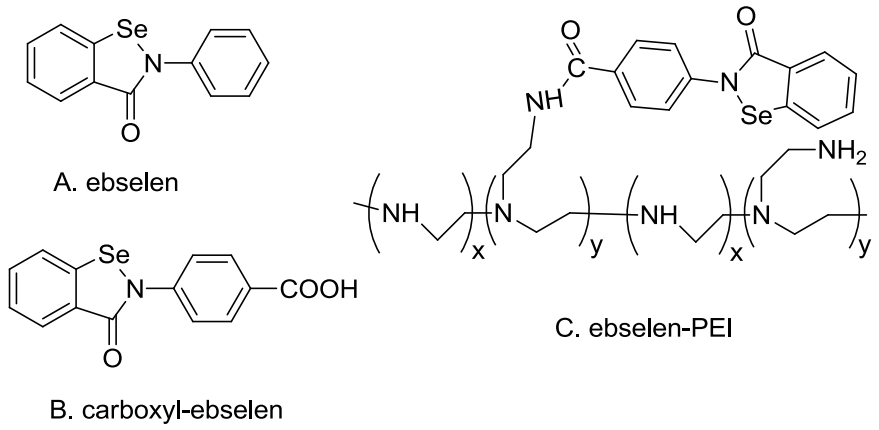

Figure 3.1. Structures of different aromatic organoselenium species.

In this chapter, the NO generating catalytic activity of different organoselenium species for RSNO decomposition is studied and compared. By covalently attaching carboxyl-ebselen (C-ebselen, **Figure 3.1B**) to polyethylenimine (PEI), ebselen-PEI (e-PEI, **Figure. 3.1C**), a new water-soluble NO generating polymer is obtained. C-ebselen-based LbL films are fabricated by alternatively assembling the resulting e-PEI and sodium alginate (Alg) onto a suitable substrate and further annealed to obtain a more robust and stable film with minimal Se leaching. The annealing mechanism is studied in detail. Finally, the NO generation and antimicrobial properties of the final LbL films are also examined.

3.2 Experimental

3.2.1 Materials

3,3'-diselenodipropionic acid (SeDPA) was synthesized using a reported method[1]. Ebselen, 1-(3-dimethylaminopropyl)-3-ethylcarbodiimide (EDC), N-hydroxysuccinimide (NHS), 2-(N-morpholino)ethanesulfonic acid (MES), rhodamine B (RB), fluorescein-5-thiosemicarbazide (FTSC), redistilled nitric acid (≥99.999% trace metals basis), polyethyleneimine (PEI, Mw 25 kD), sodium alginate (Alg, Mw 12-80 kD) and poly(dially dimethyl ammonium chloride) (PDDA, Mw 100-200 kD) were purchased from Sigma-Aldrich (St. Louis, MO). NMR reagents were from Cambridge Isotope Laboratories, Inc. (Andover, MA). *S*-nitrosoglutathione (GSNO) and *S*-nitrosocysteine (CysNO) were freshly prepared as previously reported[1]. Phosphate buffered saline (PBS), pH 7.4, containing 137 mM NaCl, 2.7 mM KCl, 10 mM sodium phosphate, was used in all experiments. All solutions were prepared with deionized water from a Milli-Q system (18 MΩ cm^{-1}; Millipore Corp., Billerica, MA). *Pseudomonas aeruginosa* (*P. aeruginosa*) PAO300, a *mucA22* derivative of PAO1 that constitutively overproduce alginate[2] was obtained from the University of Copenhagen, Denmark. *Escherichia coli* (*E. coli*) K-12 MG16653 and *Staphylococcus aureus (S. aureus)* ATCC 45330 were purchased from American Type Culture Collection. Luria Bertani (LB) agar and broth were products of Fisher Scientific Inc. (Pittsburgh, PA).

3.2.2 Synthesis of C-ebselen and immobilization of C-ebselen on PEI

C-ebselen was synthesized using a reported method[3] with the minor modification of using anhydrous acetonitrile[4] instead of ether as the solvent in the third step. ^{1}H NMR, ^{13}C NMR spectra and mass spectra of C-ebselen were recorded using a Varian MR400 MHz, Varian VNMRS 700 MHz spectrometer and a VG (Micromass) 70-250-S Magnetic sector mass spectrometer (EI, 70eV), respectively.

^{1}H NMR (400 MHz, DMSO-d_6): δ 12.92 (s, 1H, -COOH), 8.11-8.09 (d, *J*=8.0 Hz, 1H, ArH), 8.02-7.99 (d, *J*=8.8 Hz, 2H, ArH), 7.93-7.91 (d, *J*=7.6 Hz, 1H, ArH), 7.86-7.84 (d, *J*=8.4 Hz, 2H, ArH), 7.72-7.69 (t, *J*=7.6, 1H, ArH), 7.51-7.48 (t, *J*=7.4 Hz, 1H, ArH). ^{13}C NMR (176 MHz, DMSO-d_6): δ 166.72, 165.33, 144.07, 138.65, 132.65, 130.48, 128.59, 128.10, 127.17, 126.41, 125.87, 123.39. The ^{1}H NMR and ^{13}C NMR spectra are shown in **Figure 3.2**. EI-MS *m/z* $[M]^+$ calculated for $C_{14}H_9NO_3{}^{80}Se$, 319.0 (nominal mass), measured 319.1, measured isotope pattern matches predicted pattern for $C_{14}H_9NO_3Se$.

C-ebselen immobilized PEIs (e-PEI) with different Se contents were synthesized by EDC/NHS coupling of C-ebselen with PEI in pH 6.0 MES buffer. Carboxyl:-NH_2 molar ratios of 1:10 and 1:3 were selected for further studies. C-ebselen was first dissolved in MES buffer and 2 M NaOH solution was added till a clear yellow solution was formed. EDC and NHS were then added to the solution (molar ratio -COOH: EDC: NHS=1:6:4) and the clear solution became turbid after 5 min. A PEI solution in MES buffer was further added and the final pH was adjusted to 6.0 using 4 M HCl. The reaction was kept at room temperature for 12 h. The reaction mixture was then centrifuged and the polymers in the supernatant were further dialyzed (MWCO, 2 kD) against 0.05 M NaCl for 2 d and then Milli-Q water for 1 d. The e-PEI obtained was then lyophilized and the Se content was determined by inductively coupled plasma - optical emission spectroscopy (ICP-OES) on a Perkin-Elmer Optima 2000 DV (Perkin-Elmer, Wellesley, MA) to be 1.87 wt% and 4.14 wt%, respectively, for the two different e-PEI preparations.

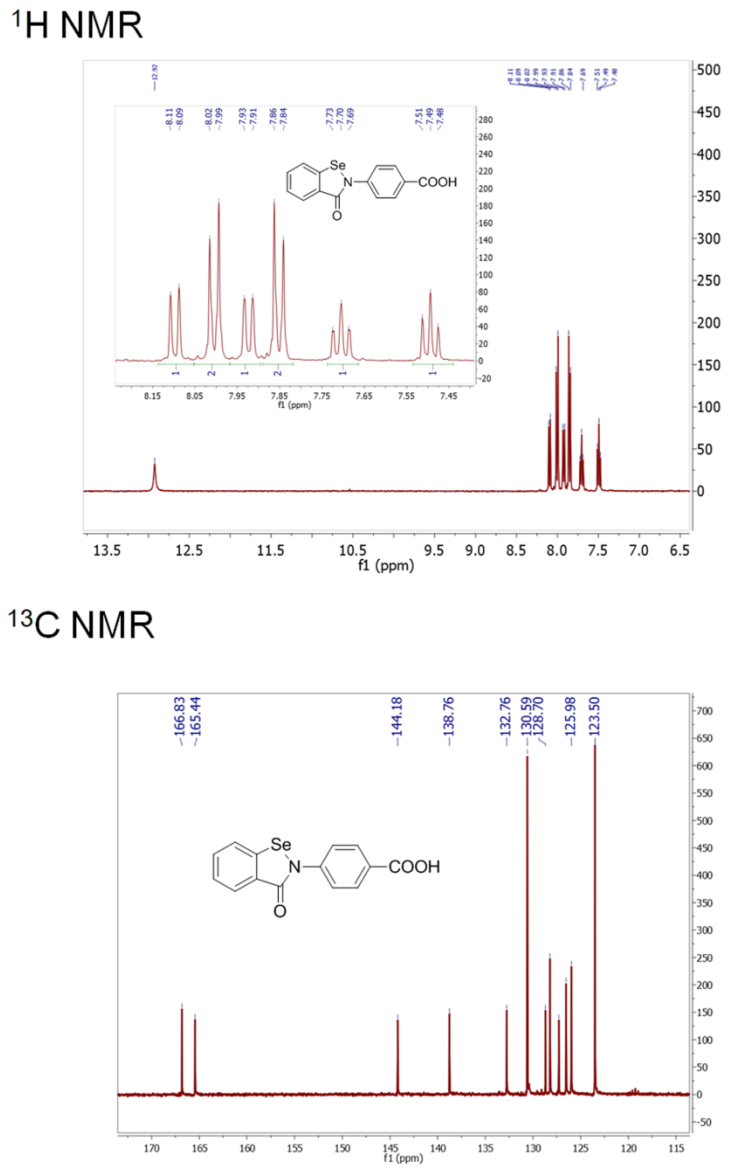

Figure 3.2. NMR spectra of carboxyl-ebselen in DMSO.

3.2.3 Labeling e-PEI and Alg with fluorophores

The e-PEI was labeled with RB and Alg was labeled with FTSC by the EDC/NHS reaction for 12 h in MES buffer, pH 6.0, using molar ratio EDC: fluorophore: NHS: -NH_2/–COOH = 1:1:1:20. The labeled polymer was then washed and dialyzed extensively in the dark before use.

3.2.4 Layer-by-Layer assembly of e-PEI/Alg

Glass and quartz slides were cleaned with piranha solution (7:3 H_2SO_4/30% H_2O_2) at 80 ºC before use (*Caution: the solution is extremely corrosive!*) and the LbL films were prepared by alternately dipping the substrates in 1 mg mL^{-1} e-PEI and Alg solutions in pH 7.4 PBS (10 min each) with three intermediate PBS washings (1 min each) using a homemade automated deposition system until the desired number of bilayers were assembled onto the substrate. The as prepared LbL films were further placed in a salt annealing solution (PBS buffer containing 1.5 M NaCl) for 1 min and then cross-linked for 12 h in a cross-linking solution (PBS buffer containing 1.5 M NaCl and EDC/NHS 50 mM).

3.2.5 Characterization of LbL films

3.2.5.1 UV-Vis spectra

The UV-Vis spectra of LbL films on quartz slides were recorded on a UV-Vis spectrophotometer (Lambda 35, Perkin-Elmer, MA). The quartz slides were placed vertically into a quartz cuvette containing 3 mL buffer solution and the UV-Vis spectra were recorded with a resolution of 1 nm. To record the spectra of the film after salt annealing, the film was placed in the salt annealing solution for 1 min and then transferred to another cuvette containing the annealing solution for recording the spectra.

3.2.5.2 NO generation detection

The catalytically generated NO from the LbL coatings was detected by purging N_2 into 2 mL pH 7.4 PBS solution in an NOA cell protected from light and monitored using a chemiluminescence NO analyzer (NOA) (Sievers 280, Boulder, CO). For the homogeneous experiments with different organoselenium species, the Se-based catalysts were dissolved in DMSO while reducing agent and RSNOs were freshly prepared in pH 7.4 PBS to form 5 mM solutions, respectively. Lyophilized e-PEI was dissolved as a 1 mg mL^{-1} solution in PBS. Glass slides with LbL coatings were soaked in PBS containing 100 μM EDTA, 100 μM GSH overnight before the NOA test. To monitor the effect of superoxide ($O_2^{\bullet-}$) scavenging, air instead of N_2 was used for the purging.

3.2.5.3 Scanning electron microscopy

Scanning electron microscopy (SEM) images were recorded on a Hitachi S-3200N scanning electron microscope (Hitachi High Technologies, Tokyo, Japan) at a working distance of 15 mm at 16 kV. Glass slides with the LbL coatings were dip-washed with Milli-Q water, dried in a desiccator overnight and then sputter-coated with gold for 30 s before imaging.

3.2.5.4 Optical microscopy and confocal laser scanning microscopy

Glass slides with LbL coatings were placed in CoverWell perfusion chambers (Sigma-Aldrich, St. Louis, MO) containing PBS buffer or the salt annealing solution for solution phase imaging. Optical microscopy images were recording on a Nikon Eclipse E600 POL optical microscope (Nikon Instruments, Inc., Melville, NY) using a 20× or a 40× objective lens. A Zeiss LSM 510-META confocal laser scanning microscope (Carl Zeiss Microimaging, Inc., Thoronwood, NY) was used for recording confocal images in PBS buffer or annealing solutions. The fluorophores were excited by an Argon laser at 488 nm and a HeNe laser at 543 nm and observed with a C-Apochromat 63× objective lens using two filters (505-550 nm, 560 nm). The images were scanned at a speed of 1.6 μs / pixel using a 12 bit plane mode. The image size was 1024×1024 pixels, which corresponds to an area of 143 μm ×143 μm.

3.2.5.5 Selenium content and Se leaching tests

Fresh LbL films on glass slides were digested using fuming nitric acid and further diluted to a 10 mL final volume and the Se content of the films was determined via inductively coupled plasma - optical emission spectroscopy (ICP-OES) on a Perkin-Elmer Optima 2000 DV (Perkin-Elmer, Wellesley, MA). The Se leaching test was done by placing a $(\text{e-PEI/Alg})_{100}$ film in 9 mL of PBS buffer containing 100 μM EDTA, 50 μM GSH and 50 μM GSNO at 37.5 °C in the dark for 24 h. Each day, the soaking solution was collected, diluted to 10 mL and replaced. After one week, the Se contents in the daily soaking solutions were measured with inductively coupled plasma high-resolution mass spectrometry (ICP-HRMS), using a Thermo Finnigan Element (Thermo Electron Corp., Schaumberg, IL).

3.2.6 *In vitro* blood test

Fresh heparinized (5 U mL^{-1}) sheep or pig whole blood was obtained from Extracorporeal Membrane Oxygenation (ECMO) Laboratory in the Medical School at the University of Michigan. The blood was centrifuged at 1300 rpm for 15 min to obtain platelet-rich sheep plasma (PRP). Kendall monoject veterinary polyurethane (PU) I.V. catheters (Tyco Healthcare) were first modified by annealed $(e\text{-}PEI/Alg)_{50}$ LbL films and then placed in PBS buffer, sheep plasma and whole sheep blood for 24 h at 4 °C, respectively. The catheters were dip washed by PBS before testing NO generation from RSNOs with the NOA. The NO generation from a solution of pH 7.4 PBS containing 100 μM EDTA, 10 μM CysNO and 20 μM CySH at 37.5°C was monitored. Six glass slides with the same coatings were also used for the experiment (duplicate for each soaking experiment) and after the NOA test, the LbL film on glass slides was digested by fuming nitric acid and the Se content was determined by ICP-OES. For long-term catalytic activity studies, the modified catheters were soaked in PBS buffer or pig blood for a week at 4 °C and the RSNO decomposition catalytic activity was then evaluated.

3.2.7 Detection of superoxide production by LbL films

Superoxide ($O_2^{\bullet-}$) produced from the LbL films constructed with e-PEI was detected using a previously reported lucigenin-derived chemiluminescence assay via a Shimadzu RF-1501 spectrofluorophotometer (Shimadzu, Columbia, MD).[5] Forty μL of 6.25 mM lucigenin (in DMSO) solution was mixed in 960 μL of glycine-NaOH buffer (0.05 M, pH=10) in semimicro disposable cuvettes. Annealed $(e\text{-}PEI/Alg)_{50}$, annealed $(PEI/Alg)_{50}$ and $(PDDA/Alg)_{50}$ films on glass slides were presoaked in 100 μM EDTA and 100 μM GSH PBS buffer overnight and then placed in the cuvettes to record the emission spectra. The chemiluminescence signal observed at 350-650 nm was integrated and the integrated intensity per unit area of the films was compared.

3.2.8 *In vitro* antimicrobial tests

Glass slides coated with LbL films were presoaked in PBS buffer containing 100 μM EDTA and 100 μM GSH before the antimicrobial tests in order to remove trace metal ions and reduce the catalytic sites into the selenolate form. Overnight LB-broth grown bacterial culture was washed with PBS buffer three times, and resuspended in PBS buffer

to make a final cell concentration at 10^5 or 10^8 CFU/mL, respectively. For solution phase antimicrobial tests, LbL films coated glass slides were placed into Corning 15-mL tubes with 2 mL of washed bacterial culture with or without addition of GSH solution. The tubes were incubated at 37.5 °C for 2 h or 24 h with horizontally shaking at 150 rpm. After incubation, coated slides were removed and the bacterial culture was serially 10-fold diluted in PBS buffer and 50 μL of each dilution was plated onto LB (Luria Bertani) agar plate for viable bacterial counting. Annealed $(\text{e-PEI/Alg})_n$, annealed $(\text{PEI/Alg})_{50}$ and glass controls in bacterial solution containing 0 or 20 μM GSH were also used to study the effect of bilayer numbers, while annealed $(\text{e-PEI/Alg})_{50}$, annealed $(\text{PEI/Alg})_{50}$ and glass controls in bacterial solution containing 0, 20 or 50 μM GSH were used to study the effect of different concentrations of reducing agent. Annealed $(\text{e-PEI/Alg})_{50}$ and glass controls were also used to study the influence of specific strains of different bacteria (including *E. coli*, *P. aeruginosa* and *S. aureus*) on the antimicrobial properties of the LbL films and the influence of RSNO addition. All the antimicrobial tests were conducted in duplicate.

For microscopic observation, glass slides with the annealed LbL films were placed in semi-micro disposable cuvettes and 0.5 mL of washed bacterial culture was added to a final cell concentration of 10^5 CFU/mL. GSH was added to reach a final concentration of 50 μM. The solution was incubated at 37.5 °C for 2 h with horizontally shaking at 150 rpm. After incubation, the LbL coated slides were removed and stained with fluorescent dyes (SYTO-9 and propidium iodide) for 20 min in dark according to the instructions of the LIVE/DEAD® BacLight™ Bacterial Viability kit (L7012, Invitrogen, Carlsbad, CA). Stained slides were observed with a fluorescence microscope (Olympus 1X71, Center Valley, PA) equipped with Fluorescence Illumination System (X-Cite 120, EXFO) and appropriate filter sets. Images were obtained using an oil immersion 60 × objective lens. Untreated glass slides were used as controls. Three images were taken for the same film and used for quantitative analysis. The images were analyzed using COMSTAT software (version 1)[6] with the threshold setting as 25 and the surface bacterial coverage and deal cell percentage for glass slide, $(\text{PEI/Alg})_{50}$ and $(\text{e-PEI/Alg})_{50}$ were compared.

3.2.9 *In vitro* antibiofilm test

A CDC biofilm reactor (Biosurface Technologies, Bozeman, MT) was used for the anti-biofilm test. CDC biofilm reactor with its coupon holders was autoclaved before use. Coated slides were mounted on coupon holders and the reactor was supplemented with 10% LB medium by a peristaltic pump with a continuous flow rate at 100 ml/h. Green Fluorescent Protein (GFP)-labeled *E. coli* culture was diluted 1:100 and inoculated into the glass vessel of CDC reactor aseptically. The liquid growth medium was circulated through the vessel and shear force was generated by a magnetic stir bar rotated by a magnetic stir plate. GSH was added to the circulating medium to reach a constant reducing agent concentration of 50 μM. Biofilms developed on the surface of coated slides were completely immersed into the circulated culture. After 7 d incubation at room temperature (23 °C), coated slides were aseptically removed and individual slide surfaces were inspected under a fluorescence microscope (Olympus 1X71, Center Valley, PA) equipped with Fluorescence Illumination System (X-Cite 120, EXFO). Images were obtained using an oil immersion 60 × objective lens.

3.3 Results and Discussion

3.3.1 Identifying the key intermediate for C-ebselen catalytic activity

Before working with LbL films, the homogeneous catalytic activity of C-ebselen for RSNO decomposition in solution phase was studied using GSH as the reducing agent in pH 7.4 PBS. EDTA was added to eliminate the interference from free metal ion-induced RSNO decomposition. As shown in **Figure 3.3**, this compound is able to generate NO from both GSNO (a) and CysNO (b). It has been reported that selenol or selenolate is the key intermediate for the RSNO decomposition by organodiselenide species.[1] For ebselen, the reaction with equal molar of GSH will first produce a GSH-selenenyl sulfide product, which will be further reduced to ebselen selenol in the presence of excess GSH (see reaction in **Figure 3.4a**). The presence of an ebselen selenol intermediate has been verified elsewhere.[7] The pKa for aliphatic selenols is ca 5.5,[1] and an arylselenol should have an even lower pKa due to reduced electron density on the selenium atom. Therefore, at pH 7.4, in the presence of excess GSH, C-ebselen is in its selenolate form. In a homogeneous experiment in which different amounts of free C-ebselen catalyst were

added into a solution containing 100 μM EDTA, 50 μM GSNO and 50 μM GSH, it was found that the NO generation was fastest when the molar ratio of GSH:C-ebselen = 2:1 (**Figure 3.4b**). When the molar ratio of GSH:C-ebselen was kept at 2:1, it was also found that the NO generation rate increased linearly with selenolate concentration (**Figure 3.4c**). Therefore, C-ebselen selenolate is expected to be the key intermediate for the RSNO decomposition activity.

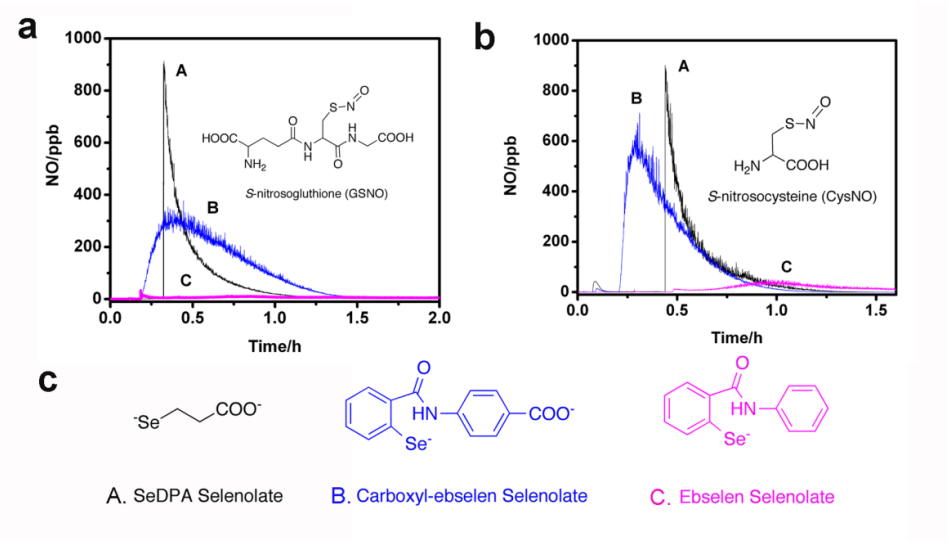

Figure 3.3. Catalytic NO generation profiles indicating comparison of the RSNO decomposition catalytic activity of C-ebselen (A), SeDPA (B) and ebselen (C) in homogeneous solution with 100 μM EDTA, 50 μM selenolate and 50 μM a) GSNO; b) CysNO; c) Structures of selenolate of SeDPA (A), C-ebselen (B) and ebselen (C).

3.3.2 Comparison of RSNO decomposition activity of SeDPA, C-ebselen and ebselen

The catalytic activities of SeDPA, C-ebselen and ebselen towards GSNO and CysNO decomposition were compared and are shown in **Figure 3.3a** and **Figure 3.3b**. When the selenolate concentrations are kept the same for all three catalysts, SeDPA exhibits the best catalytic activity. This is because aliphatic selenolates are better nucleophiles compared to aromatic ones due to the higher electron density on the Se atom. The reduced steric hindrance owing to the smaller size of the SeDPA selenolate also contributes to the improved catalytic activity (see structures in **Figure 3.3c**). C-ebselen, however, exhibits much better catalytic activity than ebselen. It is possible that this improvement arises from the better solubility of C-ebselen-selenolate in an aqueous

phase coming from the ionization of the carboxyl group at neutral pH. When CysNO, a smaller RSNO with less steric hindrance was used instead of GSNO, improved catalytic activity is observed for both C-ebselen and ebselen.

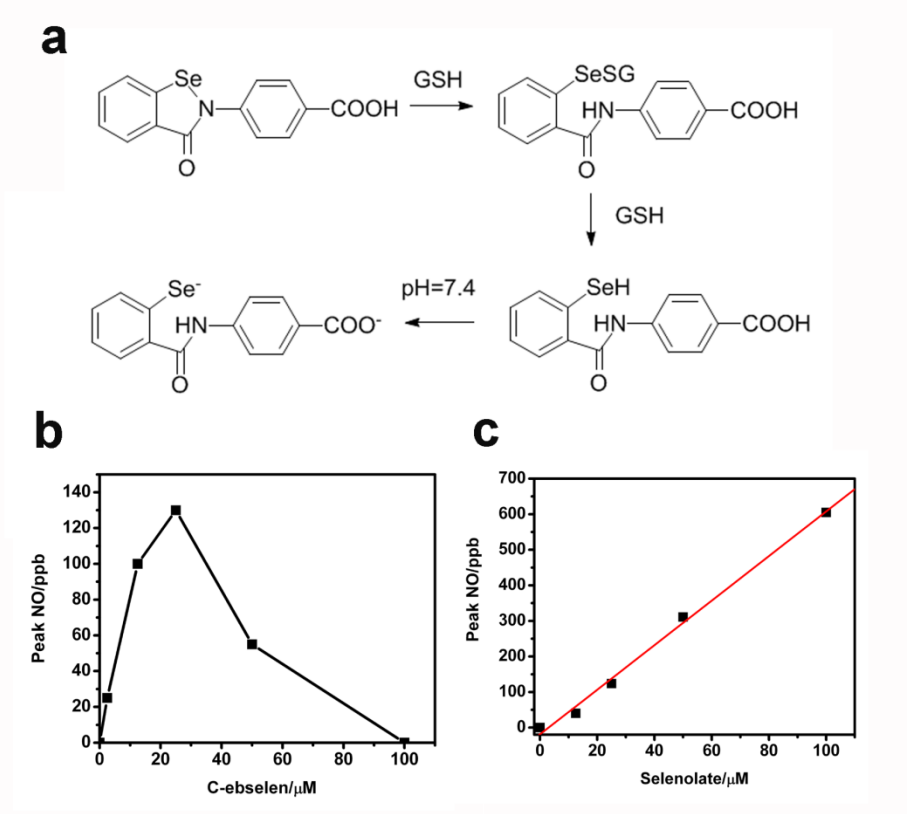

Figure 3.4. a) Stepwise reaction between carboxyl-ebselen and GSH; b) Influence of C-ebselen concentration on the NO generation in 100 μM EDTA, 100 μM GSH, 50 μM GSNO, pH 7.4 PBS. NO generation was fastest when C-ebselen:GSH=1:2, indicating selenolate is the key intermediate; c) Influence of selenolate concentration on the NO generation in 100 μM EDTA, 50 μM GSNO, pH 7.4 PBS. C-ebselen:GSH=1:2.

3.3.3 Catalytic activity of e-PEI

Ebselen-PEIs with different C-ebselen to $-NH_2$ molar ratios were synthesized and the Se content of the respective polymer was calculated from ICP-OES to be 1.87 wt% (e-PEI-2) and 4.14 wt% (e-PEI-4), respectively. **Figure 3.5a** inset shows the UV-Vis spectra of PEI (A), e-PEI-2 (B) and e-PEI-4 (C) at the same concentration (67 μg mL^{-1}) in pH 7.4 PBS buffer. Due to the introduction of ebselen segments, the spectra of e-PEI solutions exhibit two bands. While the absorption at 280 nm is from the benzene ring,

the absorption band at 350 nm is from the isoselenazol ring of the ebselen segments.[8] The ratio of C-ebselen moieties in the polymers calculated from the absorption differences at 280 nm was 2.2, which is consistent with the ICP results.

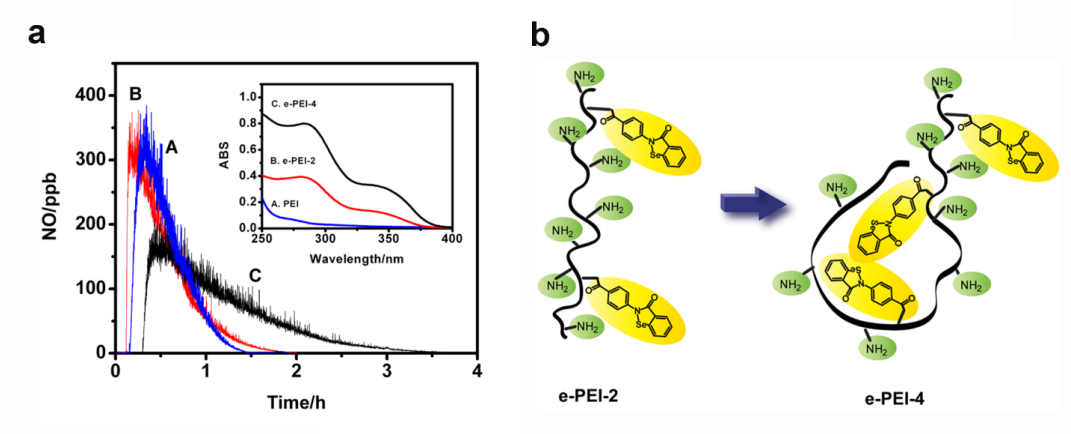

Figure 3.5. a) Catalytic NO generation profiles indicating comparison of RSNO decomposition catalytic activity of C-ebselen (A), e-PEI-2(B) and e-PEI-4 (C) in solution with 100 μM EDTA, 50 μM selenolate and 50 μM GSNO; inset shows the UV-Vis spectra of same concentration (67 μg/mL) of PEI (A), e-PEI-2 (B) and e-PEI-4 (C) in PBS buffer; b) Schematic illustration of possibility of formation of hydrophobic centers in e-PEI-4 that prevent access of GSH and GSNO to the catalytic sites.

The catalytic activities of e-PEI-2, e-PEI-4 and free C-ebselen were compared in pH 7.4 PBS containing 100 μM EDTA and 50 μM GSNO. The selenolate concentration was kept at 50 μM for both polymers and C-ebselen. As shown in **Figure 3.5a**, while e-PEI-2 shows catalytic activity equivalent to free C-ebselen, e-PEI-4 with a higher Se content, exhibits reduced catalytic activity. A proposed mechanism for the reduced catalytic activity is shown in **Figure 3.5b**. It is possible that as the hydrophobic ebselen segments become denser (from higher C-ebselen loading on to polymer), the conformation of the amphiphilic e-PEI polymer will change in solution to form hydrophobic centers that prevent the access of GSH and GSNO to the catalytic sites. In this case, not all the catalytic sites in e-PEI-4 can be fully used for catalytic RSNO decomposition, which may contribute to the reduced catalytic activity observed for this species. Since e-PEI-2 has better catalytic activity, it was used to fabricate all the LbL films reported herein.

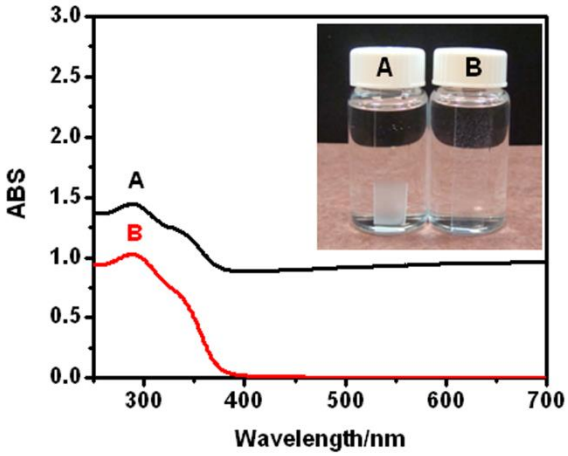

Figure 3.6. UV-Vis spectra of (e-PEI/Alg)$_{50}$ on quartz slides. A) unannealed film in PBS; B) film after salt annealing in salt annealing solution. Inset shows the appearance of the films.

3.3.4 Fabrication and annealing of LbL film

The initially prepared LbL films exhibit a cloudy appearance (**Figure 3.6**, inset A) and are not stable. As shown in **Figure 3.7a-A**, as soon as an unannealed (e-PEI/Alg)$_{50}$ is placed in PBS buffer containing 100 μM EDTA, 50 μM GSH and 50 μM GSNO, NO is generated due to the decomposition of the RSNO species by the catalytic sites in the LbL film. However, the NO generation continues even after the film is removed, indicating significant leaching of catalytic sites from the film into the reaction reservoir. The leaching is attributed to the heterogeneous nature of the unannealed film. As shown in **Figure 3.6A**, the UV-Vis spectrum of an unannealed (e-PEI/Alg)$_{50}$ exhibits large background signal from 400 nm to 700 nm, resulting from the light scattering of the heterogeneous film.[9] The heterogeneous nature of the unannealed film is further revealed by SEM images shown in **Figure 3.8A** and **Figure 3.8B.** The surface of the unannealed film is very rough, and it is composed of both vermiculate structures and particles. Based on this surface morphology, it is highly unlikely that the film is in a thermodynamically stable state. When this type of film is placed in solution for catalytic NO generation, chain rearrangements will likely take place to form a thermodynamically more stable structure, resulting in the leaching of the selenium species.

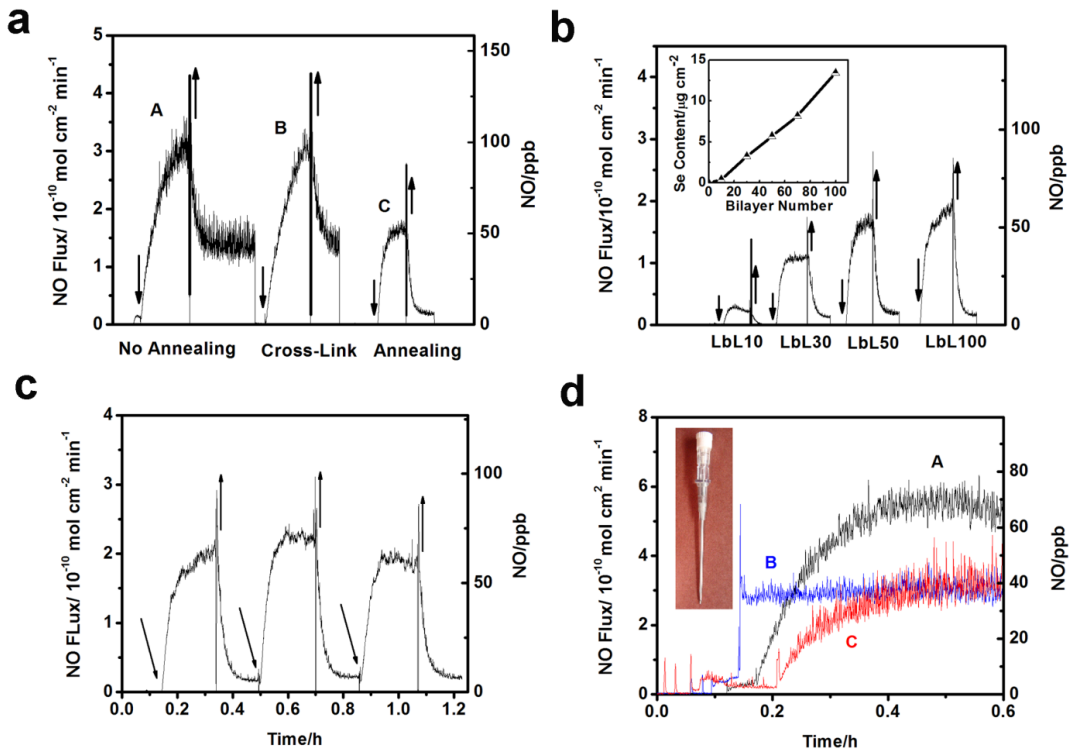

Figure 3.7. NO generation of a) $(e\text{-PEI/Alg})_{50}$ with no annealing (A), cross-link only (B) and two-step annealing (C) in 100 μM EDTA, 50 μM GSH, 50 μM GSNO at R.T.; b) NO generation of LbL films with different bilayers on glass slides in 100 μM EDTA, 50 μM GSH, 50 μM GSNO at R.T. (Inset: Se content of LbL films vs layer numbers.); c) NO generation of $(e\text{-PEI/Alg})_{100}$ in 100 μM EDTA, 50 μM GSH, 50 μM GSNO at R.T.; d) NO generation from $(e\text{-PEI/Alg})_{50}$ on polyurethane catheters (inset) in 100 μM EDTA, 20 μM CySH, 10 μM CysNO at 37.5 °C after 24 h soaking in PBS (A), sheep plasma (B) or sheep blood (C). The ↑or ↓arrow indicate the moment the film was placed in or taken out of the reaction reservoir.

Layer-by-layer assembly, as indicated by Yang, et al., contains two steps: adsorption and chain rearrangement.[9] While the former is a kinetically driven process that helps build the films, it also creates defects and results in thermodynamically unstable structures. Chain rearrangement, on the other hand, helps in healing the defects, but is a slow and inefficient process. To obtain a more robust and stable LbL film, it is necessary to heal the defects and change the heterogeneous nature of the initial film. Therefore, the mobility of the polymer chains within the LbL film must be enhanced, and chain

rearrangements have to take place to form a more homogeneous structure, which needs to be further stabilized. Based on this concept, a two-step annealing method was used to improve the stability of the LbL film and thereby to minimize the leaching of catalytic sites. As shown in **Figure 3.9**, in the first step of annealing, salt is used to partly break the ionic bonds, enhance the chain mobility of the polyelectrolytes and turn a heterogeneous film into a homogeneous one. In the second step, EDC/NHS is added to the annealing solution, so that the ionic bonds within the homogeneous film are turned into covalent linkages and the film is "locked" in its homogeneous state.

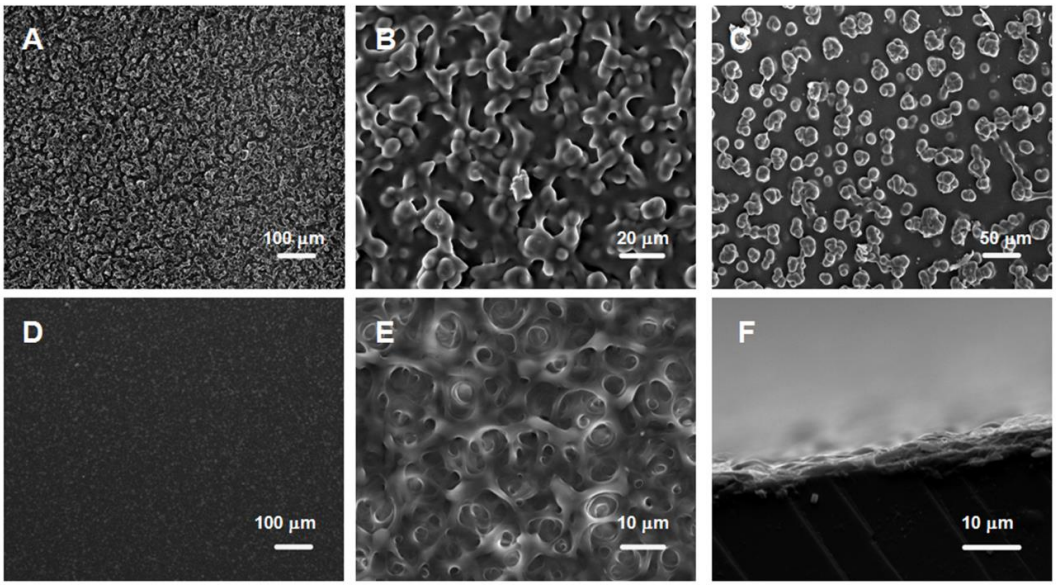

Figure 3.8. Scanning electron microscopy (SEM) images of $(e\text{-PEI/Alg})_{50.}$ A) B) without annealing; C) cross-link only; D) E) F) after two-step annealing.

Salt-induced annealing is a convenient, universal and effective method to improve the homogeneity of LbL films. When placed in the annealing solution, the unannealed $(e\text{-PEI/Alg})_{50}$ turned from cloudy to clear within 1 min (**Figure 3.6**, inset B). In addition, the background absorption in the UV spectra went back to zero (**Figure 3.6B**) after the salt annealing, indicating the formation of a homogeneous film. However, if the salt concentration is less than 1.5 M, the film remains cloudy. Since salt anneals the surface by temporarily breaking the electrostatic contacts and smoothing the surface, the change

will not happen immediately unless the salt concentration reaches a certain level of breaking enough contacts.[10]

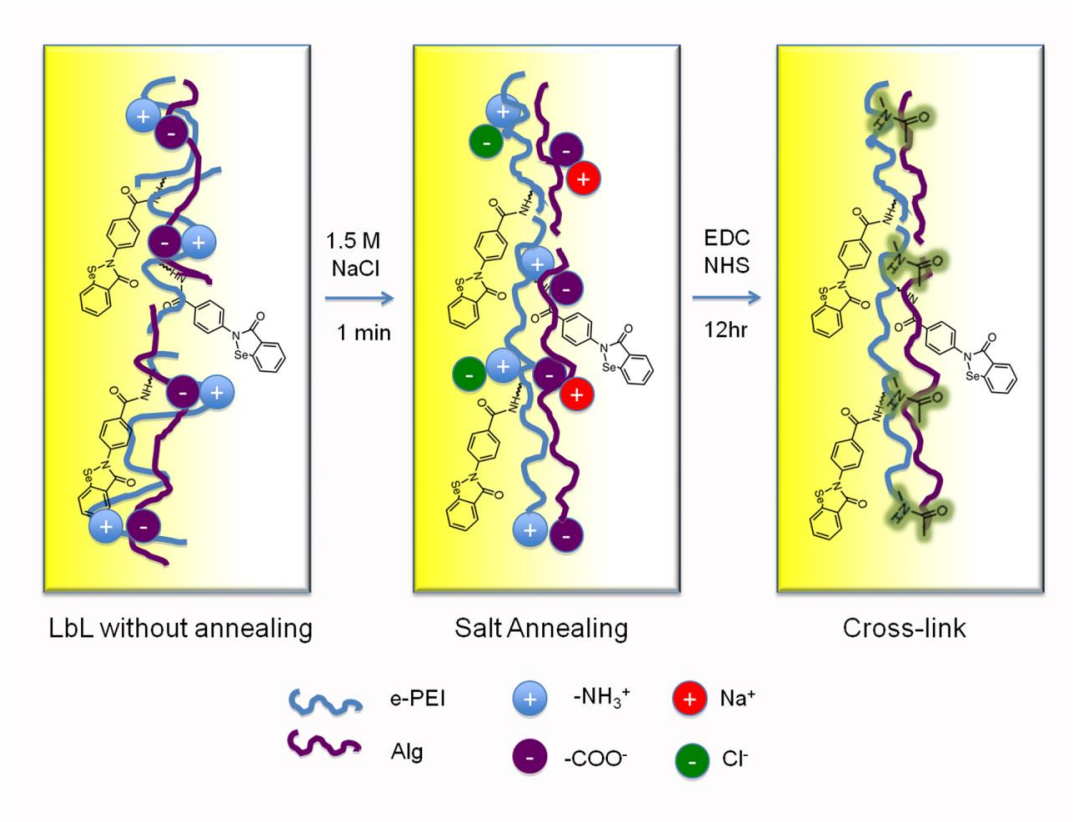

Figure 3.9. Schematic illustration of two-step annealing of LbL films including salt annealing and cross-linking.

To monitor the surface morphology change in solution during the annealing process, e-PEI and Alg were labeled with fluorophores and the surface morphology of the LbL films under different treatments were monitored using a confocal laser scanning microscope. As shown via the confocal images in **Figure 3.10A**, in PBS buffer, an unannealed (e-PEI/Alg)$_{50}$ shows a rough surface containing significant aggregates of micro-particle-domains. The morphology of e-PEI (red) and Alg (green) are the similar to each other, indicating the formation of polyion pairs throughout the film. The surface morphology of the film in PBS buffer is different from the dry state SEM images shown in **Figure 3.8A-B**, and this can be attributed to the polyelectrolyte conformation change from a stretched to a coiled conformation due to the reduced repulsion from the screening effect of salt.[11]

When the same film is placed in the salt annealing solution, the surface becomes smooth immediately as shown in **Figure 3.10B**. With the breakage of the ionic bonds, the microparticle domains are dissociated, allowing new and lower energy configurations to form. The salt annealing effect at solution phase is also observed by an optical microscope in **Figure 3.11**, and this is similar to a previously reported smoothing effect from salt annealing.[10]

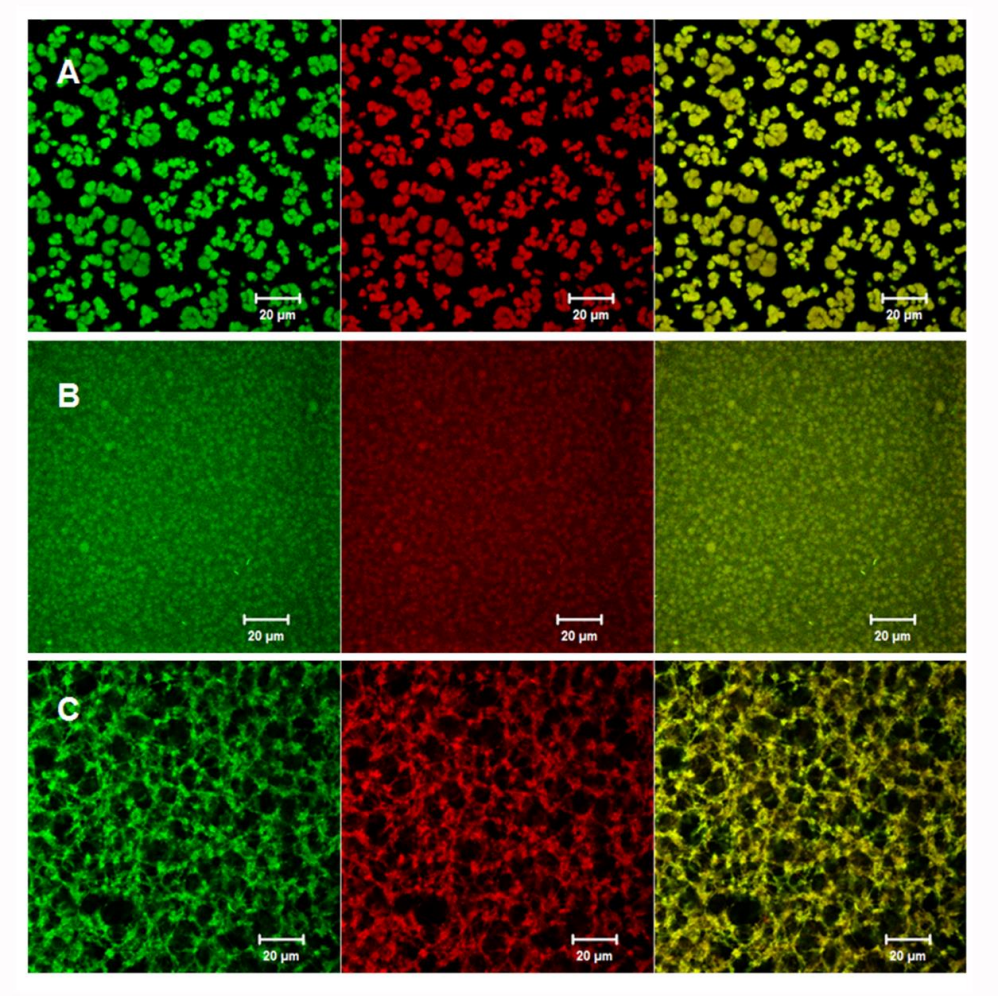

Figure 3.10. Confocal images of A) unannealed $(e\text{-PEI/Alg})_{50}$ in PBS; B) $(e\text{-PEI/Alg})_{50}$ after salt annealing in PBS containing 1.5M NaCl; C) $(e\text{-PEI/Alg})_{50}$ after two-step annealing in PBS, e-PEI (red), Alg (green).

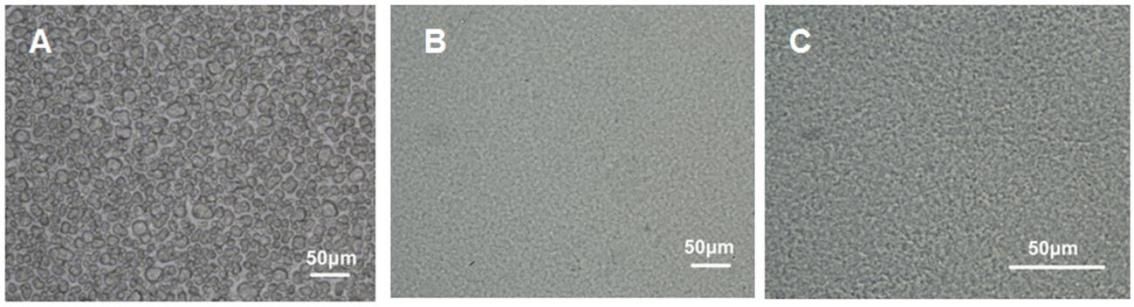

Figure 3.11. Optical microscope images of A) unannealed $(e\text{-}PEI/Alg)_{50}$ in PBS; B) $(e\text{-}PEI/Alg)_{50}$ after salt annealing in annealing solution; C) $(e\text{-}PEI/Alg)_{50}$ after two-step annealing in PBS.

Although salt-annealing produced more homogeneous LbL films, the films were fragile and swelled considerably after extended exposure to the annealing solution. Therefore, it is necessary to cross-link the film immediately after brief exposure. The cross-linking process is to "lock" the film in its homogeneous state by turning the ionic bonds into covalent linkages. However, cross-linking alone does not produce a stable film. As shown in **Figure 3.7a-B**, an $(e\text{-}PEI/Alg)_{50}$ film treated only by cross-linking shows similar NO generation pattern to an unannealed film, indicating that cross-linking alone does not solve the leaching problem. However, for a film treated with the two-step annealing process (**Figure 3.7a-C**), the NO detection signal goes back to nearly baseline once the film is removed from the reaction reservoir, indicating minimal leaching of Se species. The NO flux of the annealed film, however, is lower than the unannealed one. This is consistent with a decrease in the Se contents for the LbL films after the annealing treatment **(Figure 3.12a**). Therefore, the reduced NO flux is attributed to reduction in the total amount of e-PEI adsorption resulting from the increased screening of surface charges in a highly concentrated salt solution.[12] The surface morphology of the film with cross-linking only and the annealed films are compared in the SEM images shown in **Figure 3.8**. As can be seen in **Figure 3.8C**, similar to the surface morphology of unannealed $(e\text{-}PEI/Alg)_{50}$ in PBS buffer shown in **Figure 3.10A**, the surface of $(e\text{-}PEI/Alg)_{50}$ treated by cross-linking only possesses significant micro-particle aggregations. This is further proof that cross-linking alone can "lock" the film

morphology in solution phase by turning ionic bonds into covalent linkages. Although the cross-linking restricts the chain mobility of LbL films, due to the rough surface and structural instability, the cross-linked film still suffers from significant leaching problem. The annealed film, on the other hand, shows a flat and smooth surface as shown in **Figure 3.8D**. At higher magnification (**Figure 3.8E**), the entire film reveals a porous 3D structure, which is a thermodynamically stable network with minimal leaching. The film thickness for $(\text{e-PEI/Alg})_{50}$ is 3.5 μm (see **Figure 3.8F**). The porous structure of the annealed film in PBS buffer is also observed by confocal microscope images shown in **Figure 3.10C**, indicating the consistency of the surface morphology of the film in a dry state and in contact with a solution phase. The shift from a rough surface in PBS buffer to a smooth surface after the two-step annealing is also confirmed by optical microscope images shown in **Figure 3.11**. Compared to conventional LbL films, which are sensitive to environmental changes like pH and ionic strength, this type of film is a more stable and robust alternative.

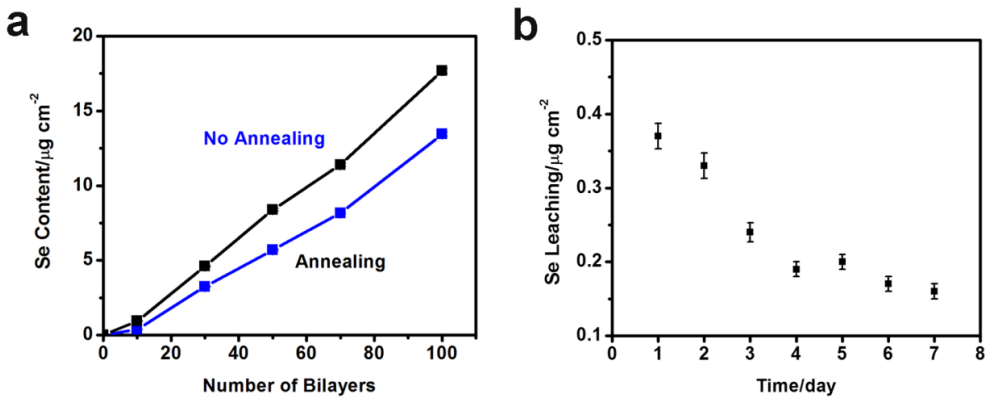

Figure 3.12. a) Comparison of Se content in LbL films before and after the annealing; b) Daily Se leaching from an annealed $(\text{e-PEI/Alg})_{100}$ in 100 μM EDTA, 50 μM GSH, 50 μM GSNO at 37.5 °C for a week.

3.3.5 NO generation and Se leaching from annealed LbL films

The NO flux of the LbL films can be controlled by the number of bilayers that are incorporated into the films. As shown in **Figure 3.7b** inset, the Se content of the LbL film grows exponentially with the number of bilayers within the films, which is

consistent with a previously reported growth for a PEI/Alg LbL film.[13] In a PBS buffer containing 100 μM EDTA, 50 μM GSH, 50 μM GSNO, the NO flux of the LbL film increases with increased number of bilayers, as shown in **Figure 3.7b** for $(e\text{-PEI/Alg})_{10}$, $(e\text{-PEI/Alg})_{30}$ and $(e\text{-PEI/Alg})_{50}$. However, when the catalyst content exceeds the substrate amount, the increase in the NO flux is less obvious as shown for $(e\text{-PEI/Alg})_{50}$ and $(e\text{-PEI/Alg})_{100}$. In these cases, it is likely that most of the RSNO substrate is consumed by the outer layers before it reaches the inner layers and reacts with the inner catalytic sites. To investigate the stability of the LbL films, $(e\text{-PEI/Alg})_{100}$ with the highest Se content was repeatedly inserted and taken out of the reaction reservoir. As shown in **Figure 3.7c**, no significant baseline signal increase is observed when the film is repeatedly taken out of the solution, indicating minimal leaching of Se species from the film.

The leaching of Se species from a $(e\text{-PEI/Alg})_{100}$ film was monitored every day for a week using ICP-MS and the Se daily leaching was found to be 0.15~0.4 μg cm^{-2} (**Figure 3.12b**). Considering the small area of most medical devices (e.g. the surface of a catheter surface is normally less than 10 cm^2), this value is far below the daily recommended intake of Se of 40 μg d^{-1}.[14]

3.3.6 *In vitro* blood soaking experiment for annealed LbL films

One of the advantages of LbL coatings lies in that they are applicable to a variety of substrates. To determine whether the C-ebselen-based LbL films are potentially useful as coatings for blood contacting medical devices, the LbL films were assembled onto polyurethane (PU) catheters (shown in **Figure 3.7d**, inset) and the NO fluxes of the catheters after 24 h soaking in PBS buffer, sheep plasma and whole sheep blood were compared. As shown in **Figure 3.7d-A**, in a reservoir of 20 μM CySH and 10 μM CysNO at 37.5 °C, an $(e\text{-PEI/Alg})_{50}$ coating on a polyurethane catheter with PBS soaking exhibits an NO flux of 5.5×10^{-10} mol cm^{-2} min^{-1} and the NO flux is 3×10^{-10} mol cm^{-2} min^{-1} for the film soaked in sheep plasma (**Figure 3.7d-B**) or whole blood (**Figure 3.7d-C**).

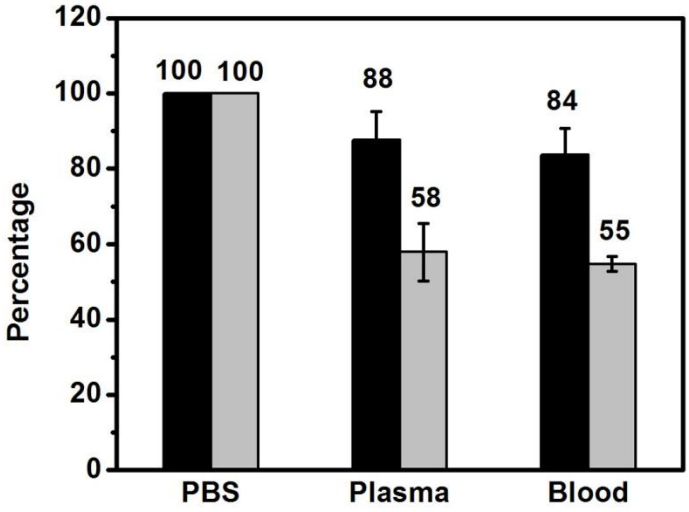

Figure 3.13. Comparison of Se content (black, left) and NO fluxes (light grey, right) of $(e\text{-PEI/Alg})_{50}$ on glass slides in 100 μM EDTA, 20 μM CySH, 10 μM CysNO in pH 7.4 PBS at 37.5 °C after 24 h soaking in PBS, sheep plasma and sheep blood.

To identify the reasons that contribute to the NO flux drop after blood or plasma soaking, the same experiments were conducted with $(e\text{-PEI/Alg})_{50}$ on glass slides and NO fluxes and the Se contents of films after different treatments were compared, as shown in **Figure 3.13**. Although the films retain more than 80% of the total catalytic sites after plasma or blood soaking, the NO flux is only 55~ 60% of films that are only soaked in PBS buffer. Therefore, the reduced NO flux is likely due to the combination of a loss of catalytic sites and protein adsorption on the LbL surfaces after plasma or blood soaking. In particular, protein adsorption might block the catalytic sites from interacting with thiols and RSNOs, and it might also scavenge NO generated from the films through nitrosation of any thiol groups. When the catheter modified with $(e\text{-PEI/Alg})_{50}$ was soaked in pig blood for one week and placed into PBS buffer containing 20 μM CySH and 10 μM CysNO at 37.5 °C, the NO flux hardly changed compared to the observation after 24 h (**Figure 3.14**). Indeed, the LbL-film-based catheters are still able to generate physiological level of NO that are comparable with the healthy endothelial cell surface

($0.5\sim4\times10^{-10}$ mol cm^{-2} min^{-1})[15] even after one-week blood soaking, indicating their potential antithrombotic properties.

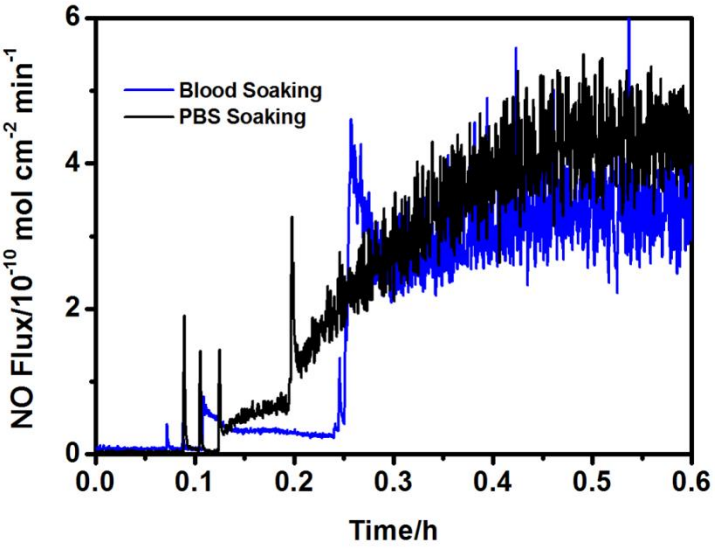

Figure 3.14. NO generation from $(e\text{-}PEI/Alg)_{50}$ on polyurethane catheters in 100 μM EDTA, 20 μM CySH, 10 μM CysNO at 37.5 °C after one week soaking in PBS buffer or pig blood.

3.3.7 Antimicrobial properties of annealed LbL films

The antimicrobial effect of aliphatic selenium species-based films have been reported and it is believed that superoxide ($O_2^{\bullet-}$) produced from the reaction of aliphatic selenolate with oxygen is responsible for the observed antimicrobial activity.[14] Due to reduced electron density on selenium atom, ebselen and its derivatives are reported to produce less superoxide ($O_2^{\bullet-}$), which also contributes to their reduced *in vivo* toxicity.[16] Since superoxide ($O_2^{\bullet-}$) is a potent antimicrobial agent which causes oxidation stress and DNA damage to bacterial cells, even a small amount of superoxide ($O_2^{\bullet-}$) production could lead to observable antimicrobial effects. Therefore, the superoxide production from $(e\text{-}PEI/Alg)_{50}$ and $(PEI/Alg)_{50}$ was assessed by a previously reported lucigenin-derived chemiluminescence assay.[5] A $(PEI/Alg)_{50}$ control produces 37% of the superoxide ($O_2^{\bullet-}$) that is produced by $(e\text{-}PEI/Alg)_{50}$ (**Figure 3.15**), indicating the introduction of only a

small percentage (1.87 wt% Se) of C-ebselen segments greatly increases the superoxide ($O_2^{\bullet-}$) production of the polymer matrix. The reason for the superoxide ($O_2^{\bullet-}$) production from the $(PEI/Alg)_{50}$ matrix without immobilized organoselenium sites is unknown. However, decreased superoxide ($O_2^{\bullet-}$) production from the LbL film was observed by the EDTA pre-soaking procedure or replacing PEI with PDDA as shown in **Figure 3.15**, suggesting that trace metal ions that are strongly bound to PEI are responsible for the observed production of superoxide ($O_2^{\bullet-}$) by the background LbL matrix components.

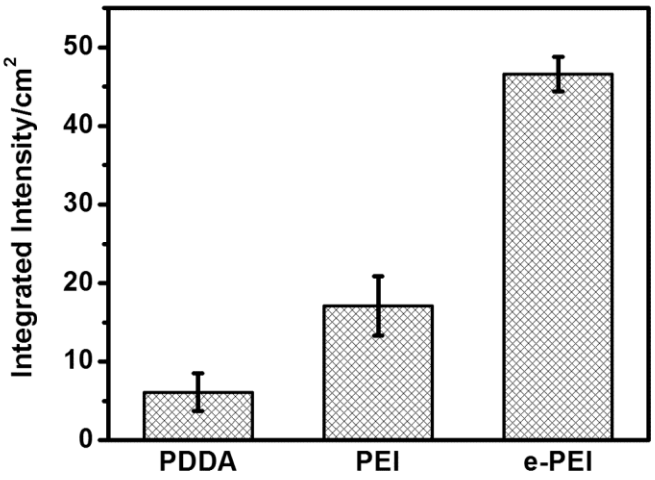

Figure 3.15. Detection of superoxide ($O_2^{\bullet-}$) produced from $(PDDA/Alg)_{50}$, $(PEI/Alg)_{50}$, $(e\text{-}PEI/Alg)_{50}$ using a lucigenin-assay in pH=10 glycine-NaOH buffer. No signal was observed for a bare glass.

The antimicrobial effects of ebselen and its derivatives have been reported,[17] and the effect is suggested to be related to the S-N bond within this species. Since ebselen tends to inhibit enzymes by interacting with their L-cysteine residues, the inhibition of enzymes such as H^+-ATPase[18] is reported to be one possible mechanism for the antimicrobial activity of ebselen and its derivatives.

For LbL films with covalently attached ebselen segments, the antimicrobial effects are expected to be related to both superoxide production and the surface interactions of immobilized ebselen sites with bacterial cells. In addition, since polyelectrolytes films have been reported to have antimicrobial functions by interacting with cell membranes,[19] the PEI/Alg backbone may also contribute to the antimicrobial effects observed with the

LbL films. Among all the possible factors, only superoxide ($O_2^{\bullet-}$) is likely to diffuse out of the LbL layer and kill the bacteria surrounding the LbL films in the bulk solution. Considering the small thicknesses of the LbL films (e.g., 3.5 μm for $(e\text{-PEI/Alg})_{50}$ as indicated by SEM image **Figure 3.8F**) and the short lifetime of superoxide ($O_2^{\bullet-}$), the killing effects are expected to take place in the localized vicinity of the film or in a contact-killing mode. Therefore, both the antimicrobial properties of the LbL films in solution and the surface bacterial attachment were evaluated.

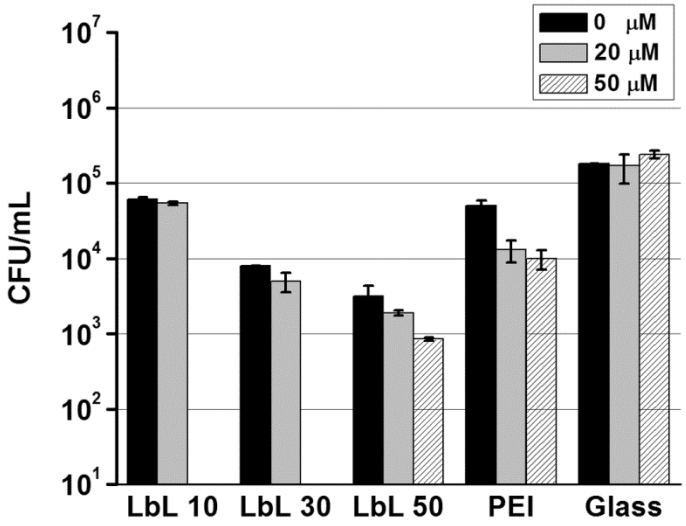

Figure 3.16. Effects of e-PEI/Alg film layer number and reducing agent concentration on the cell viability of *E coli*. $(e\text{-PEI/Alg})_{10}$, $(e\text{-PEI/Alg})_{30}$, $(e\text{-PEI/Alg})_{50}$, $(PEI/Alg)_{50}$ and glass slides control were placed in 10^5 CFU/mL *E. coli* for 2 h at 37.5 °C with and without GSH as the reducing agent.

Solution-based antimicrobial tests were used to investigate the factors related to the bactericidal effects of the annealed LbL films. $(e\text{-PEI/Alg})_n$, $(PEI/Alg)_{50}$ and glass controls were placed in PBS buffer containing 10^5 CFU/mL *E. coli* for 2 h at 37.5 °C and aliquots of the solution were taken out after the time period to determine the viable bacterial counts in the solutions. Given that the presence of a reducing agent is important for the production of the selenolate form of ebselen, which is required for generation of superoxide ($O_2^{\bullet-}$), the influence of reducing agent concentration was also studied. As shown in **Figure 3.16**, compared with the control glass slides, e-PEI/Alg films and

$(PEI/Alg)_{50}$ exhibit different levels of antimicrobial effects. Without the presence of a reducing agent, $(e\text{-}PEI/Alg)_{10}$, $(e\text{-}PEI/Alg)_{30}$ and $(e\text{-}PEI/Alg)_{50}$ are able to kill 66.1%, 95.6% and 98.2% of living *E-coli* cells in solution compared to a glass control that exhibits no killing effect. The killing efficacy increases with the number of bilayers that are incorporated into the e-PEI/Alg films, indicating a dose-dependent antimicrobial effect. An increase in the bilayer number provides more catalytic sites to produce superoxide ($O_2^{\bullet-}$), resulting in more bacteria killed in solution phase. A $(PEI/Alg)_{50}$ control film is able to kill 72.2% of bacterial cells under the same condition, indicating the contribution from the polyelectrolytes backbone to the antimicrobial properties of the e-PEI/Alg films. However, considering the viable bacterial counts after the treatment with $(e\text{-}PEI/Alg)_{50}$ film is only 6% of that for the $(PEI/Alg)_{50}$, the increased superoxide ($O_2^{\bullet-}$) production greatly improves the killing efficacy of the ebselen-based LbL films. In the presence of 20 μM GSH as the reducing agent, all the LbL films except the glass slide control exhibit better killing efficacy when compared to the case with no reducing agent added. For $(e\text{-}PEI/Alg)_{50}$ placed in bacteria solutions containing 0, 20 and 50 μM GSH, it is clear that the killing efficacy increases with the reducing agent concentration in the solution. While 2 logs of killing (i.e., the number of viable cells was reduced from $\sim 1.8\times10^5$ to $\sim 3\times10^3$ CFU/mL) is observed for $(e\text{-}PEI/Alg)_{50}$ film without reducing agent added, the killing effect is improved to 3 logs (i.e., the number of viable cells was reduced from $\sim 2.4\times10^5$ to $\sim 8\times10^2$ CFU/mL) with the addition of 50 μM GSH. The reducing agent that facilitates selenolate formation will also facilitate superoxide ($O_2^{\bullet-}$) production, thereby enhancing the antimicrobial properties of the coating.

Considering most of the antimicrobial effects of the films take place near the surface, the surface bacterial attachment on $(e\text{-}PEI/Alg)_{50}$, $(PEI/Alg)_{50}$ and a glass slide control were compared after soaking in 10^5 CFU/mL *E. coli* for 2 h at 37.5 °C in the presence of 50 μM GSH. As shown in **Figure 3.17**, although viable attached bacterial cells (indicated by green dots) are obvious on the surface of a bare glass (A) and $(PEI/Alg)_{50}$ (B), they are hardly observed on the $(e\text{-}PEI/Alg)_{50}$ (C) surface. Quantitative analysis indicates that $(e\text{-}PEI/Alg)_{50}$ and $(PEI/Alg)_{50}$ are able to reduce 87% (~8 times reduction) and 56% (~2 times reduction) of total bacterial surface coverage compared to a glass slide ($n=3$, $p<0.01$, see **Figure 3.18a**). For both $(e\text{-}PEI/Alg)_{50}$ and $(PEI/Alg)_{50}$ surfaces,

more than 92% (n=3, $p<0.01$, see **Figure 3.18b**) of total bacteria attached are dead or membrane damaged (indicated by red dots in **Figure 3.17**), demonstrating the killing effect at the surface. The difference between $(e\text{-PEI/Alg})_{50}$ and $(PEI/Alg)_{50}$ for total bacterial attachment, especially living bacterial attachment, clearly indicates that the ebselen segments and superoxide ($O_2^{\bullet-}$) production play important roles in improving the antimicrobial properties of the LbL films. It is likely that superoxide ($O_2^{\bullet-}$) present in the vicinity of the film kills the bacterial cells before they reach and attach onto the surface, and thus helps to repel living bacterial cells and reduce total bacterial surface coverage.

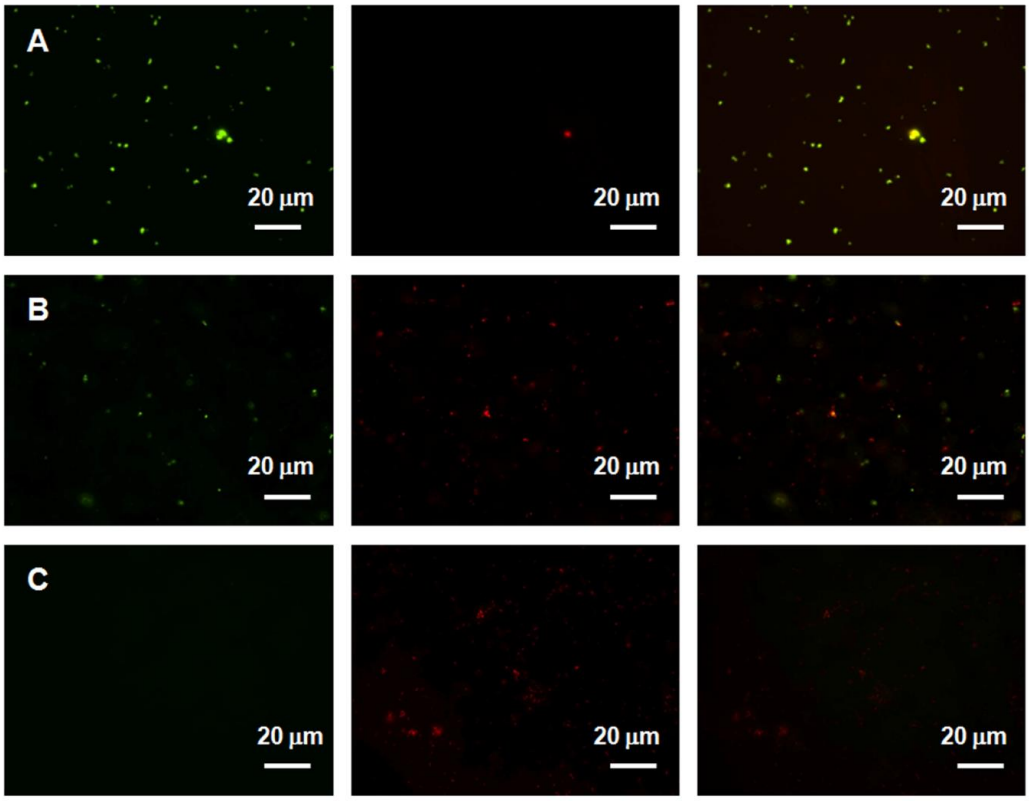

Figure 3.17. Representative fluorescent micrographs showing comparison of surfaces of A) bare glass; B) $(e\text{-PEI/Alg})_{50}$; C) $(PEI/Alg)_{50}$ after soaking in 10^5 CFU/mL *E coli* containing 50 µM GSH for 2 h at 37.5 °C. Bacterial cells were stained with Bacterial LIVE/DEAD staining dyes and viable cells shown green while dead or membrane damaged cells shown red fluorescence in the images.

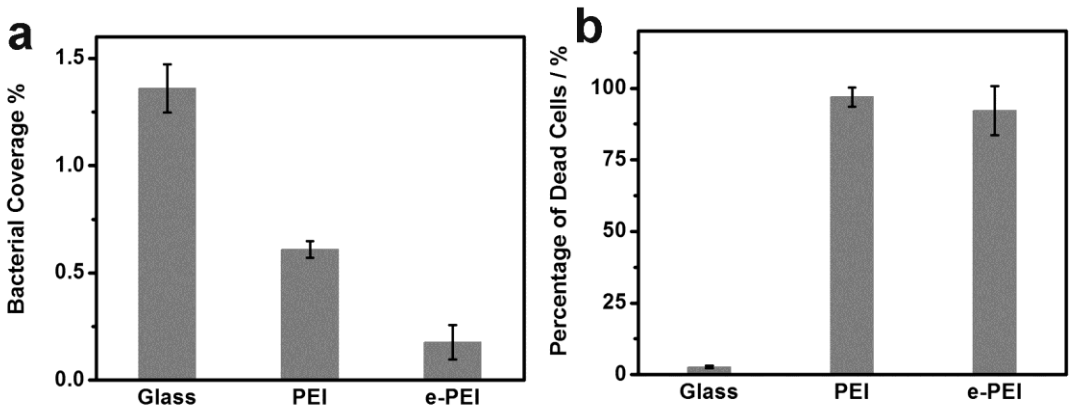

Figure 3.18. Quantitative analysis of a) bacterial surface coverage percentage; b) dead cell percentage of attached cells for glass slides, $(PEI/Alg)_{50}$ and $(e\text{-}PEI/Alg)_{50}$ surface after soaking in 10^5 CFU/mL *E. coli* containing 50 μM GSH for 2 h at 37.5 °C. Bacterial cells were stained with Bacterial LIVE/DEAD staining dyes and images from the same films were processed with COMSTAT software (n=3, $p<0.01$).

The antimicrobial effect of the LbL films was also found to be time and bacteria type dependent. When $(e\text{-}PEI/Alg)_{50}$ was placed in 10^5 CFU/mL *E. coli* at 37. 5 °C, it was found that all the bacteria were killed after 24 h (data not shown), indicating that a longer time exposure to superoxide ($O_2^{\bullet-}$) helps to kill more bacteria in solution. To determine whether the antimicrobial effect is universal, $(e\text{-}PEI/Alg)_{50}$ was placed in 10^8 CFU/mL of *E. coli*, *P. aeruginosa* and *S. aureus* for 24 h at 37.5 °C. As shown in **Figure 3.19**, the LbL films are able to kill a broad spectrum of bacteria with better killing efficacy observed for Gram positive *S. aureus* compared with Gram negative *E. coli* and *P. aeruginosa*, suggesting that the cell membrane structures of the given bacteria also influence the killing efficacy by the LbL films. Considering that *P. aeruginosa*, *S. aureus* and *E. coli* are highly related to wound, catheter or urinary tract infections,[20, 21] the C-ebselen based LbL films have promising prospects in biomedical applications where such infections occur.

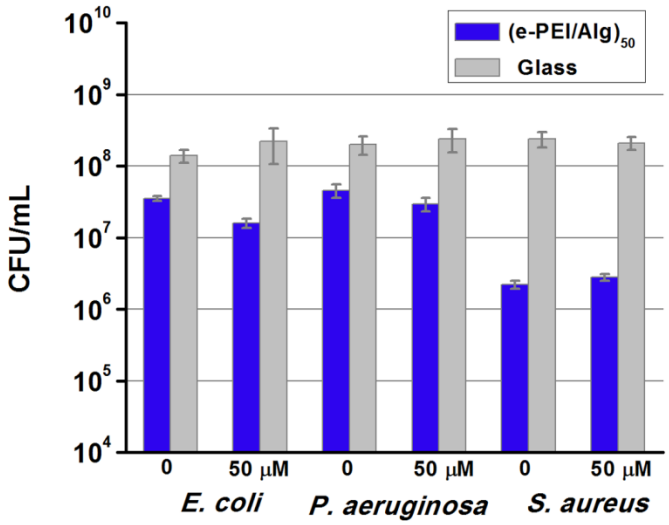

Figure 3.19. Antimicrobial properties of $(e\text{-PEI/Alg})_{50}$, in 10^8 CFU/mL of *E. coli*, *P. aeruginosa* or *S. aureus* for 24 h at 37.5 °C without and with 50 μM GSH as the reducing agent. Glass slides were used as controls.

3.3.8 Antibiofilm properties of annealed LbL films

To study the antibiofilm properties of the LbL coatings, a glass slide control and two glass slides with either the $(PEI/Alg)_{50}$ or $(e\text{-PEI/Alg})_{50}$ coatings were incubated in a CDC biofilm reactor containing GFP-labeled *E. coli* at RT (23 °C) for seven days. For the films to continuously produce superoxide ($O_2^{\bullet-}$), the GSH concentration in the circulating medium was kept at 50 μM. The antibiofilm properties of different surfaces are compared on the eighth day when the slides are removed from the reactor. As shown in **Figure 3.20**, although a biofilm has colonized the control glass slide surface after the one-week incubation, both the $(PEI/Alg)_{50}$ and $(e\text{-PEI/Alg})_{50}$ surfaces are clean, indicating significant antibiofilm properties. Unfortunately, it is difficult to distinguish the differences between the antibiofilm properties of these two LbL coatings using the current method.

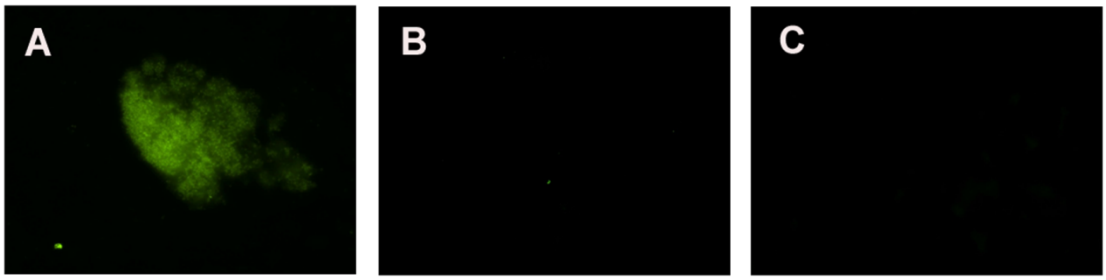

Figure 3.20. Fluorescent micrographs of *E. Coli* biofilm on the surface of A) glass slide; B) $(PEI/Alg)_{50}$; C) $(e\text{-}PEI/Alg)_{50}$ after 7 d antibiofilm test in a CDC biofim reactor, *E. Coli* was labeled by green fluorescence protein (GFP).

3.3.9 Scavenging effect of NO and superoxide ($O_2^{\bullet-}$)

Although the NO and superoxide ($O_2^{\bullet-}$) generation from the carboxyl-ebselen-based LbL film suggests that this type of film has potential application as both an anti-thrombus and antimicrobial coating, to use this type of film as a coating with dual functionality, it is necessary to consider the scavenging effect coming from the reaction of NO and superoxide ($O_2^{\bullet-}$). Recently, both modeling and experimental results suggest that the reaction between NO and superoxide ($O_2^{\bullet-}$), which is faster than the reaction between NO and oxygen, contributes to the reduced detection limit observed for a selenocystamine-based electrochemical RSNO sensor under ambient conditions compared to under nitrogen atmosphere.[5] To evaluate the "NO scavenging effect" from superoxide ($O_2^{\bullet-}$) production, the NO generation behaviors of the C-ebselen and $(e\text{-}PEI/Alg)_{50}$ in pH 7.4 PBS containing 100 μM EDTA, 20 μM CySH and 10 μM CysNO at 37.5°C under N_2 atmosphere or air flow were compared and the results are shown in **Figure 3.21a**. While in the presence of air, the superoxide ($O_2^{\bullet-}$) production scavenges ~30% of the total NO produced by the free C-ebselen, it also reduced the NO flux of $(e\text{-}PEI/Alg)_{50}$ to ~74% of the flux under the N_2 atmosphere. The microbial killing effects, on the other hand, are similar when $(e\text{-}PEI/Alg)_{50}$ films are placed in *E. coli* solution containing 100 μM EDTA, 20 μM CySH with or without 10 μM CysNO for 1 h (see **Figure 3.21b**) and this is attributed to the antimicrobial effect of both NO and peroxynitrite ($ONOO^-$), the product of NO and superoxide ($O_2^{\bullet-}$) reaction. Considering that significant levels of NO are still produced in the presence of ambient oxygen, it is likely that most of the anti-thrombotic

and antimicrobial properties of the LbL films will be retained even in the presence of this reaction. When $(e\text{-PEI/Alg})_{50}$ films are placed in *E. coli* solution containing 100 μM EDTA, 50 μM CySH with or without 50 μM CysNO for 1 h, however, a reduction in the antimicrobial property of the LbL films is observed when RSNO is added as shown in **Figure 3.21b**. This is due to the excess of RSNO that competes with oxygen for the selenolates that are critical for superoxide ($O_2^{\bullet-}$) production. It also suggests that superoxide ($O_2^{\bullet-}$) is a better antimicrobial agent compared with NO. Therefore, most of the antimicrobial properties of the LbL films are attributed to the superoxide ($O_2^{\bullet-}$) production from the immobilized ebselen segment. However, since most of the antimicrobial property of the film is retained, the C-ebselen-based LbL films have potential to be used as dual functional coatings to prevent both thrombus formation and bacterial infection.

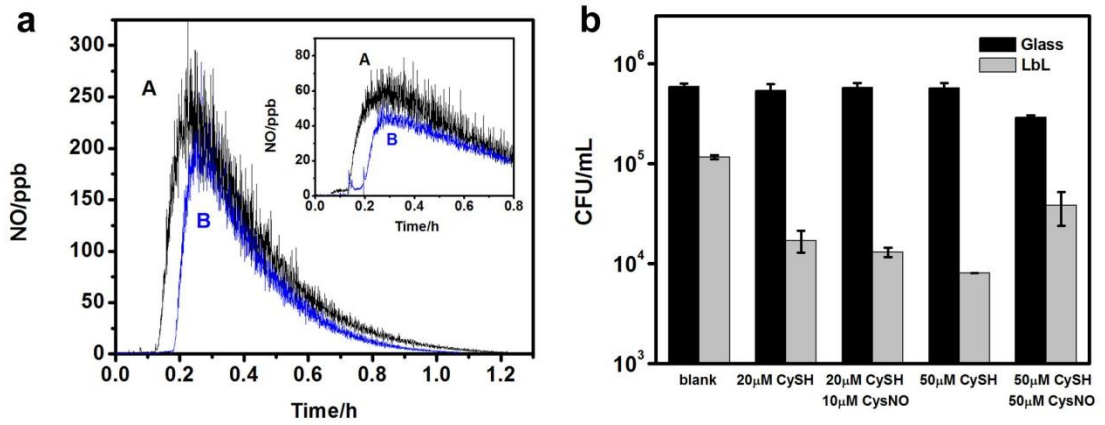

Figure 3.21. a) NO generation in pH 7.4 PBS containing 100 μM EDTA, 20 μM CySH, 10 μM CysNO, 10 μM C-ebselen at 37.5 °C under N_2 (A) or air (B) atmosphere. The integration indicates superoxide ($O_2^{\bullet-}$) production from ambient oxygen scavenges ~30% of total NO production. Inset shows the NO generation from $(e\text{-PEI/Alg})_{50}$ in pH 7.4 PBS containing 100 μM EDTA, 20 μM CySH, 10 μM CysNO at 37.5 °C under N_2 (A) or air (B) atmosphere; b) Antimicrobial properties of $(e\text{-PEI/Alg})_{50}$ in pH 7.4 PBS containing 10^5 CFU/mL *E. coli* and different amounts of CySH and CysNO for 1 h at 37.5 °C. Glass slides were used as controls.

3.4 Conclusions

Carboxyl-ebselen was used to generate NO from endogeneous RSNOs via a catalytic process. Further, a $(\text{e-PEI/Alg})_{50}$ coated polyurethane catheter, exhibiting minimal selenium leaching, was able to produce physiological levels of NO flux ($\sim 3\times10^{-10}$ mol cm^{-2} min^{-1}) from RSNOs after soaking in blood for one week. The LbL film was also able to prevent living bacterial surface attachment, reduce biofilm formation and exhibit promising antimicrobial effects for a broad spectrum of bacteria through the production of superoxide ($O_2^{\bullet -}$) as the antimicrobial agent. This type of film, exhibiting the potential for both antithrombotic and antimicrobial properties, may be useful to help resolve complications due to thrombus formation and bacterial infection associated with a wide range of biomedical devices such as catheters, vascular grafts and stents. In addition, the simplicity of the LbL method also facilitates the automatic mass production of the coatings.

3.5 References

1. Cha, W.; Meyerhoff, M. E. *Biomaterials* **2007,** 28, 19-27.
2. Mathee, K.; Ciofu, O.; Sternberg, C.; Lindum, P. W.; Campbell, J. I.; Jensen, P.; Johnsen, A. H.; Givskov, M.; Ohman, D. E.; Molin, S.; Hoiby, N.; Kharazmi, A. *Microbiology* **1999,** 145 (Pt 6), 1349-57.
3. Liu, Y.; Li, B.; Li, L.; Zhang, H. Y. *Helv. Chim. Acta* **2002,** 85, (1), 9-18.
4. Młochowski, J.; Kloc, K.; Syper, L.; Inglot, A. D.; Piasecki, E. *Liebigs Ann. Chem.* **1993,** 1993, 1239-1244.
5. Hofler, L.; Meyerhoff, M. E. *Anal. Chem.* **2011,** 83, (2), 619-624.
6. Heydorn, A.; Nielsen, A. T.; Hentzer, M.; Sternberg, C.; Givskov, M.; Ersboll, B. K.; Molin, S. *Microbiology* **2000,** 146, 2395-2407.
7. Cotgreave, I. a.; Morgenstern, R.; Engman, L.; Ahokas, J. *Chem.-Biol. Interact.* **1992,** 84, 69-76.
8. Haenen, G.; Derooij, B. M.; Vermeulen, N. P. E.; Bast, A. *Mol. Pharmacol.* **1990,** 37, (3), 412-422.
9. Yang, S.; Zhang, Y.; Zhang, X.; Guan, Y.; Xu, J.; Zhang, X. *ChemPhysChem* **2007,** 8, 418-24.
10. McAloney, R. a.; Dudnik, V.; Goh, M. C. *Langmuir* **2003,** 19, 3947-3952.
11. Fery, A.; Schöler, B.; Cassagneau, T.; Caruso, F. *Langmuir* **2001,** 17, 3779-3783.
12. Ghannoum, S.; Xin, Y.; Jaber, J.; Halaoui, L. I. *Langmuir* **2003,** 19, (11), 4804-4811.
13. Ji, J.; Shen, J. *Conf Proc IEEE Eng Med Biol Soc* **2005,** 1, 720-2.
14. Tran, P. L.; Hammond, A. a.; Mosley, T.; Cortez, J.; Gray, T.; Colmer-Hamood, J. a.; Shashtri, M.; Spallholz, J. E.; Hamood, A. N.; Reid, T. W. *Appl. Environ. Microbiol.* **2009,** 75, 3586-92.
15. Vaughn, M. W.; Kuo, L.; Liao, J. C. *Am J Physiol Heart Circ Physiol* **1998,** 274, (6), H2163-H2176.
16. Mugesh, G.; Singh, H. B. *Chem. Soc. Rev.* **2000,** 29, 347-357.
17. Pietka-Ottlik, M.; Wojtowicz-Mlociiowska, H.; Kolodziejczyk, K.; Piasecki, E.; Mlochowski, J. *Chem. Pharm. Bull.* **2008,** 56, (10), 1423-1427.
18. Billack, B.; Santoro, M.; Lau-Cam, C. *Microb Drug Resist* **2009,** 15, (2), 77-83.
19. Lichter, J. A.; Van Vliet, K. J.; Rubner, M. F. *Macromolecules* **2009,** 42, (22), 8573-8586.
20. Dwyer, A. *Semin. Dialysis.* **2008,** 21, (6), 542-546.
21. van der Starre, W. E.; van Nieuwkoop, C.; Paltansing, S.; van't Wout, J. W.; Groeneveld, G. H.; Becker, M. J.; Koster, T.; Wattel-Louis, G. H.; Delfos, N. M.; Ablij, H. C.; Leyten, E. M. S.; Blom, J. W.; van Dissel, J. T. *J. Antimicrob. Chemother.* **2011,** 66, (3), 650-656.

Chapter 4 Catalytic Activity of Cu(II)-Cyclen-Based Complexes and Copper Oxide Nanoparticles-Based Polymer Films Towards *S*-Nitrosothiols

4.1 Introduction

As described in Chapter 1, copper-based catalytic species including Cu(II)-complexes and Cu-based particles exhibit RSNO decomposition activity. The ligand cyclen, for example, with a binding constant of 10^{23} M^{-1} to Cu(II) ion,[1] has been covalently attached to different polymer backbones to fabricate NO generation polymers.[2-5] Due to the strong binding with Cu(II) ion and open coordination sites of Cu(II)-cyclen that are still capable of interacting with reducing agents and RSNOs, Cu(II)-cyclen-based polymers are expected to have minimal leaching of copper ion and good catalytic activity towards RSNOs. However, while the polymers exhibit good RSNO decomposition activity, their lifetimes are limited. In fact, the NO generation mechanism for Cu(II)-cyclen-based polymers needs to be re-investigated due to the following factors: 1) The reported redox potential (-0.642 V vs. SCE) of Cu(II)-cyclen complex[6] is very negative, so a strong reducing agent is needed for this Cu(II)-complex to be reduced into its Cu(I) form, which is the key intermediate for RSNO decomposition as described in detail in Chapter 1; and 2) The RSNO decomposition catalytic activity of Cu(II)-cyclen has not yet been reported, so it is difficult to compare the catalytic activity of Cu(II)-cyclen and Cu(II)-cyclen-based polymers.

In Chapter 1, the NO generation mechanism for copper-based particles was also described. This process relies on the corrosion of the particles in solution to produce Cu^{2+} ions that are the catalytic species to decompose RSNOs. Although Cu^{0} micro- or nanoparticles (NPs) have been utilized in NO generation coatings that have achieved *in*

vivo antithrombotic activity,[7, 8] the corrosion rates of these types of particles are fast due to the redeposition/reformation of the inert surface oxides,[9] which will further lead to toxicity issues and affect the lifetimes of copper particle-based NO generating coatings. In contrast to copper-based particles, which only have copper cores and thin layers of protective oxides, CuO NPs are homogeneously composed of inert copper (II) oxide and thus have slower corrosion rates.[9] Therefore, CuO NPs are expected to be attractive alternatives to the previously used catalysts to further extend the lifetime for copper-based NO generation materials.

In this chapter, a mechanistic study is carried out to compare the coordination geometry, reduction potential and RSNO decomposition catalytic activity of Cu(II)-cyclen, Cu(II)-cyclen derivative and Cu(II)-cyclen-tethered polymers. The RSNO decomposition catalytic activity and copper leaching from Cu^0 and CuO NPs-based polyurethane (PU) films is also studied and compared. The long-term NO generation activity of the CuO NPs-based PU film is further studied, and it turns out that the film appears to be quite promising for potential biomedical applications.

4.2 Experimental

4.2.1 Materials

1,4,7,10-Tetraazacyclododecane (cyclen) was purchased from Strem Chemicals Co (Newburyport, MA). $CuCl_2 \bullet 2H_2O$, anhydrous acetonitrile, glutathione (GSH), cysteine (CySH), CuO NPs (<50 nm, specific surface area (SSA): 29 m^2/g), N,N'-diisopropylcarbodiimide (DIC), N-hydroxysuccinimide (NHS), N-propylamine, 4-(2-hydroxyethyl)-1-piperazineethanesulfonic acid (HEPES) and all the other chemical reagents were from Sigma-Aldrich (St. Louis, MO). Ambersep®900, OH form ion exchange resin and all the other solvents were from Fisher Scientific (Fair Lawn, NJ). Cu^0 NPs (40-60 nm, SSA: ~12 m^2/g) were from SkySpring Nanomaterials, Inc. (Houston, TX). Hydrophilic PU (HPU; Tecophilic, SP-93A-100, SP-60D-60, SP-60D-20) and Tecoflex PU SG-80 were gifts from Lubrizol Advanced Materials, Inc. (Cleveland, OH) and Cu (II)-cyclen PU (modified from SP-93A-100 PU) was synthesized by Sang-yeul Hwang, a previous group member, using a reported method.[3] The copper content of

Cu(II)-cyclen PU was 0.4 wt%. DI water was prepared by a Milli-Q filter system (18 MΩ cm^{-1}, Millipore Corp., Billerica, MA). All the NMR reagents were from Cambridge Isotope Laboratories, Inc. (Andover, MA) and were used without further purification.

4.2.2 Measurements

^{1}H NMR spectra were recorded using a Varian 400 MHz spectrometer. Mass spectra were obtained using a Micromass LCT Time-of-Flight mass spectrometer. EPR spectra were taken with a Bruker EMX (Center field, 3300 G, Sweep Width, 2000 G, Frequency, 9.248 GHz). UV-Vis spectra were recorded on a UV-Vis spectrophotometer (Lambda 35, Perkin-Elmer, MA). The XRD diffraction patterns were obtained on a Bruker D8 Advance powder X-ray diffractometer with a 1.6 kW sealed tube X-ray source (Cu). Cyclic voltammograms (CVs) were recorded on a CHI electrochemical analyzer using a three-electrode system consisting of a glassy carbon electrode as the working electrode, a platinum counter electrode and a Ag/AgCl (3M KCl) as the reference electrode. A scan rate of 100 mV s^{-1} was used for all the CVs. A mixture of 67 mM Na_2HPO_4 and 0.1 M $NaClO_4$ was chosen as the supporting electrolyte, as previously reported.[6] The $CuCl_2$ and ligand ratio was kept at 1:2 to minimize the concentration of free copper ion in solution. NO generated from various polymer films was detected by purging N_2 into 2 mL pH 7.4 PBS solution in an NOA cell protected from light and monitored using a chemiluminescence NO analyzer (NOA) (Sievers 280, Boulder, CO). The leaching of copper from PU films containing different copper species was determined by inductively coupled plasma - optical emission spectroscopy (ICP-OES) on a Perkin-Elmer Optima 2000 DV system (Perkin-Elmer, Wellesley, MA).

4.2.3 Synthesis of amide derivative of cyclen

N-propyl-2-cyclen-acetamide :

$(Boc)_3$-cyclen-N-acetic acid was synthesized according a previously reported method.[3] Five hundred mg $(Boc)_3$-cyclen-N-acetic acid was dissolved in 50 mL anhydrous CH_3CN, and then 217 mg NHS and 292 μL DIC was added into the mixture and stirred until totally dissolved. Ninety three μL N-propylamine was then added to the mixture and the solution was bubbled with argon and stirred overnight. After the reaction, the

white precipitate was filtered and the residue was purified by a column chromatography using silica gel (EtOAC: Hexanes ratio gradually increased from 2:1, 3:1 to 4:1) to obtain $(Boc)_3$-N-propyl-2-cyclen-acetamide species.

^{1}H NMR (400 MHz, $CDCl_3$): δ= 0.89 (t, 3H, CH_3), 1.45 (27H, CH_3 from Boc), 1.65 (2H, CH_2 CH_3), 2.59 (4H, CH_2NCH_2CO in cyclen), 3.14 (4H, CH_2CO, CH_2NH), 3.43 (12 H, CH_2CH_2NBoc in cyclen)

MS: Calcd MW=571, found *m/z*: $[M+Na]^+$ 594.3, $[M+H]^+$ 572.3

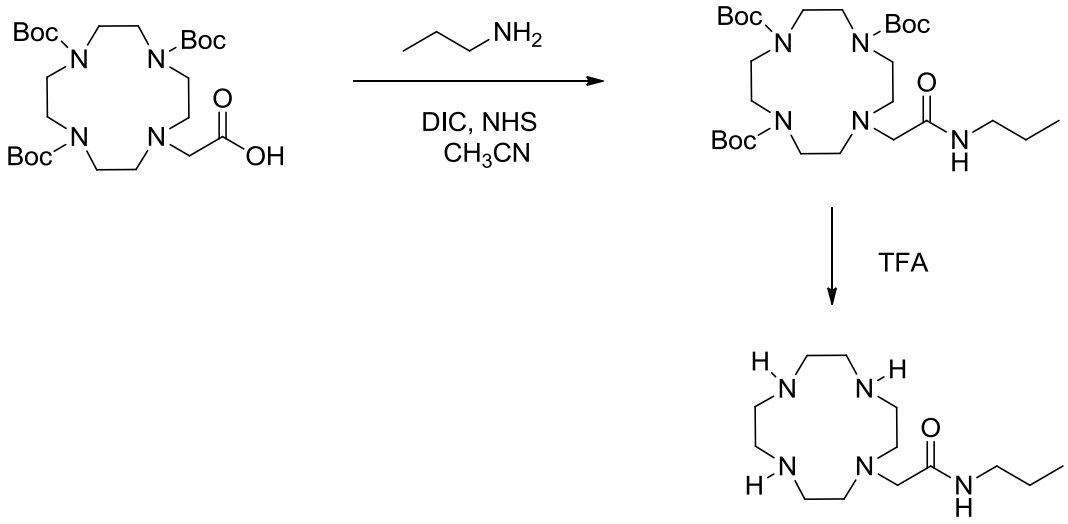

Scheme 4.1. The synthesis of N-propyl-2-cyclen-acetamide.

To remove the Boc groups, 350 mg $(Boc)_3$-cyclen-N-acetic acid was dissolved in a mixture of 2 mL CH_2Cl_2/TFA (trifluoroacetic acid) (1:19) and the reaction mixture was stirred for 4 h at RT. The solvent was then removed by a rotovap and the residue was then extracted with Et_2O/H_2O (20 mL/20 mL). The water layer was then passed through an ion-exchange column containing 54.6 mL Ambersep®900 and the final solution was collected and lyophilized to obtain the final product.

^{1}H NMR (400 MHz, D_2O): δ=0.71 (t, 3H, CH_3), 1.35 (m, 2H, CH_2CH_3), 2.54 (12 H, CH_2CH_2NH in cyclen), 2.64 (4H, CH_2NCH_2CO in cyclen), 3.04 (m, 4H, $CH_2CH_2CH_3$, NCH_2CO)

MS: MW calcd 271, found *m/z* $[M+H]^+$ 272.2

4.2.4 Pretreatment of CuO NPs

Twenty mg of CuO NPs were dispersed in 1.5 mL of 100 μM or 200 μM EDTA to obtain a homogeneous dispersion and then centrifuged at 4000 rpm for 5 min. The supernatant was then removed and this washing process was then repeated once using 100 μM or 200 μM EDTA and twice with distilled water.

4.2.5 Fabrication of CuO or Cu NPs-based PU film

Tecophilic or Tecoflex PUs were dissolved in THF to obtain a 20 mg mL^{-1} solution. CuO NPs were initially treated and washed using 100 μM EDTA as described in Section 4.2.4, and further dispersed into THF to obtain a 20 mg mL^{-1} dispersion. One mL of the CuO NP dispersion was then mixed with 5 mL PU solution and 3 mL of the mixture was then added into a Teflon microplate well (d=2.6 cm and h=0.5 cm, 1.5 mL of the dispersion was added at a time) and left to dry overnight. For comparison, Cu^0 NPs with the same pre-treatment were used and a concentration of 16 mg mL^{-1} was utilized for the Cu NP THF solution to obtain the final Cu NPs-PU film with the same copper content as the CuO NPs-PU films. Small pieces (d=9 mm) of the film were then used for further studies.

4.2.6 Copper leaching detection from copper-based PU films

To compare the influence of reducing agent on the leaching of copper from the Cu(II)-cyclen PU, the Cu(II)-cyclen PU films were prepared by adding 0.5 mL of 20 mg mL^{-1} Cu(II)-cyclen PU per well into teflon microplate wells (d=1 cm). The films were then placed in 2 mL PBS buffer or PBS buffer with 20 mM GSH at 37 °C and the soaking solutions were collected and replaced on the second, third, fifth and seventh days. GSH solution was freshly prepared each time during the replacement of the soaking solution. The collected soaking solutions were then combined and the accumulated copper leaching amounts over the six day period were then detected by ICP-OES. The leaching experiments were done in triplicate using three Cu(II)-cyclen PU films.

To compare the leaching of copper from Cu or CuO NP-based PU (SP-60D-60) films, the films (d=9 mm) were soaked in 5 mL PBS buffer containing 50 μM EDTA, 50 μM GSH and 50 μM GSNO at 37 °C. The soaking solutions were collected and replaced on

the second, third fifth and seventh day. The GSH/GSNO solution was freshly prepared each time during the replacement of the soaking solution. Two mL nitric acid was added into each collected soaking solution and the copper leaching amounts were then detected by ICP-OES. All the leaching experiments were done in triplicate utilizing three Cu or CuO NP-based PU films.

4.2.7 Long-term NO generation catalytic activity of CuO NPs-PU film

To evaluate the potential long-term NO generation catalytic activity of CuO NPs-PU films, a CuO NPs doped SP-60D-60 film was placed in solution containing 50 μM EDTA, 50 μM GSH and 50 μM GSNO at 37 °C and the NO that is generated from the film was then detected by the NO analyzer. The film was then removed from the reaction reservoir and was inserted and taken out repeatedly to evaluate the stability of the catalytic sites within the film. While not in use, the film was stored in PBS buffer containing 50 μM EDTA, 50 μM GSH and 50 μM GSNO at 37 °C. The NO flux was monitored periodically over sixteen days in freshly prepared test solution with the same compositions. The soaking solution was replaced after each evaluation of the film's catalytic activity.

4.3 Results and Discussion

4.3.1 RSNO decomposition catalytic activity of Cu (II)-cyclen complexes and Cu(II)-cyclen PU film

Initially, the catalytic activity of a previously developed Cu(II)-cyclen PU film was studied and as shown in **Figure 4.1A**, the film exhibits good catalytic activity for converting GSNO into NO when GSH is used as the reducing agent and this is consistent with previously reported results.[3] However, when Cu(II)-cyclen (not linked to polymer) is utilized under the same conditions, hardly any NO is generated (data not shown). Therefore, different reducing agents and RSNOs were further employed to reinvestigate the RSNO decomposition catalytic activity of Cu(II)-cyclen and the results are shown in **Figure 4.2**. In all the studies, EDTA and an excess of cyclen were added to minimize the

presence of free copper ion in solution. As shown in **Figure 4.2a-B**, the Cu(II)-complex exhibits catalytic activity towards GSNO in the presence of CySH, a stronger reducing agent compared with GSH.[3] This is consistent with the hypothesis that a strong reducing agent is needed to convert the Cu(II)-complex into its Cu(I) form due to the negative redox potential of Cu(II)-cyclen.[6] When CySNO, a RSNO with reduced steric hindrance is used instead of GSNO, better RSNO decomposition catalytic activity is observed for the Cu(II)-cyclen (see **Figure 4.2a-A** and **Figure 4.2b-A)**. The catalytic activity towards CySNO is decreased when GSH, a weaker reducing agent is employed, as shown in **Figure 4.2b-B**.

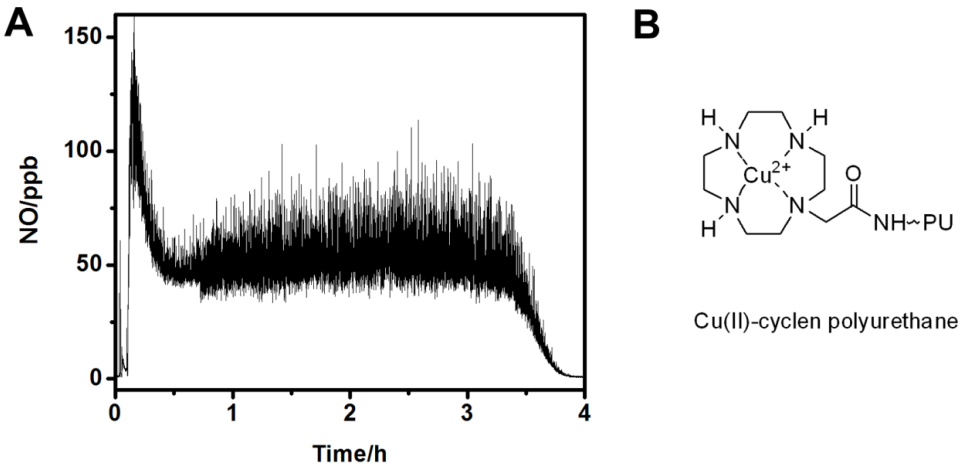

Figure 4.1. A) NO generation from a Cu(II)-cyclen PU film (d=1.4 cm, prepared from 1 mL 4 wt% Cu(II)-cyclen-PU) in pH 7.4 PBS buffer containing 20 μM EDTA, 50 μM GSH, 50 μM GSNO; B) structure of Cu(II)-cyclen PU.

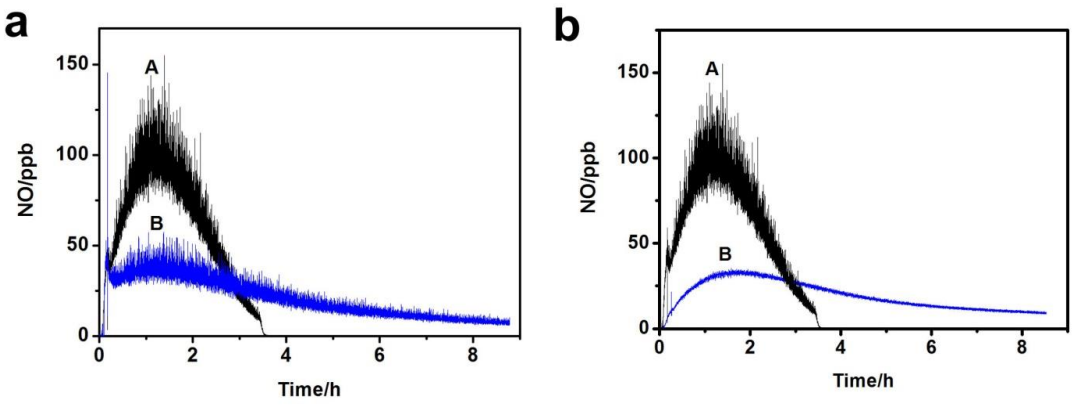

Figure 4.2. a) Catalytic NO generation from HEPES buffer (pH=7.04) containing 20 μM EDTA, 50 μM CySH, 50 μM Cu(II)-Cyclen (1:1.5) with 50 μM CySNO (A) or 50 μM GSNO (B); b) Catalytic NO generation from HEPES buffer (pH=7.04) containing 20 μM EDTA, 50 μM CySNO, 50 μM Cu(II)-Cyclen (1:1.5) with 50 μM CySH (A) or 50 μM GSH (B).

4.3.2 Comparing the reduction potential, coordination geometry and catalytic activity between Cu (II)-cyclen and Cu(II)-cyclen amide complexes

The above studies suggest that Cu(II)-cyclen PU has better catalytic activity when compared to the Cu(II)-cyclen complex. Since an amide bond is formed between the cyclen derivative and polyurethane backbone during the Cu(II)-cyclen PU synthesis, the amide bond might contribute to the improved catalytic activity of Cu(II)-cyclen PU. Therefore, N-propyl-2-cyclen-acetamide, an amide derivative of cyclen was synthesized to investigate the influence of the addition of amide bond on the catalytic activity of the Cu(II)-cyclen complex.

Firstly, to investigate whether the amide bond will shift the reduction potential of Cu(II)-cyclen, the cyclic voltammograms (CVs) of free copper salt, Cu(II)-cyclen and Cu(II)-cyclen amide derivative on a glassy carbon electrode were examined and are shown in **Figure 4.3**. The CV for free $CuCl_2$ on the glassy carbon electrode under a N_2 atmosphere at a scan rate of 100 mV s^{-1} is shown in **Figure 4.3a-A** and two pairs of peaks are observed corresponding to Cu(II)/Cu(I) and Cu(I)/Cu(0) redox couples as previously reported.[10] The cathodic peak corresponding to Cu(II)/Cu(I) reduction (c_1) is located at -0.0475 V (vs. Ag/AgCl). In the presence of air, however, the cathodic peak

corresponding to Cu(I)/Cu(0) (c_2) disappears as shown in **Figure 4.3a-B**, which is probably due to the instability of Cu(I) under ambient conditions. Therefore, all the CVs for Cu(II)-complexes were recorded under a N_2 atmosphere.

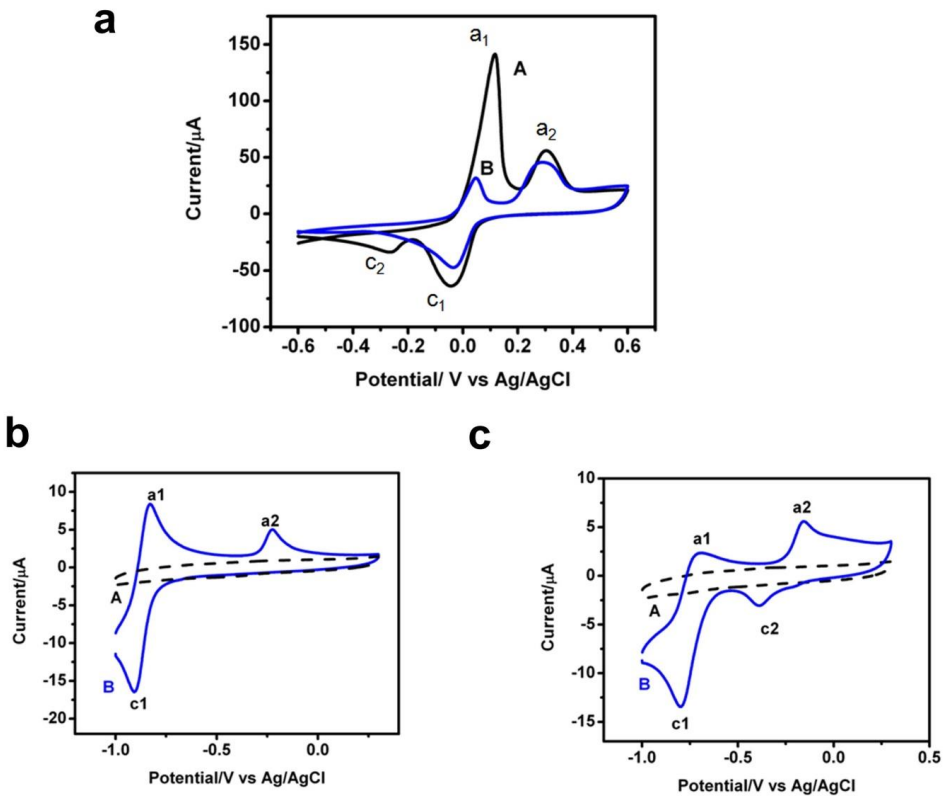

Figure 4.3. a) Cyclic voltammograms (CVs) of 1 mM $CuCl_2$ in solution containing 0.1 M $NaClO_4$, 67 mM Na_2HPO_4 under N_2 (A) or air (B) atmosphere at 100 mV/s on glassy carbon electrode; b) CVs of 2 mM cyclen (A) or 1 mM Cu-cyclen ($CuCl_2$: cyclen=1:2) (B) on glassy carbon electrode at 100 mV/s under N_2. Supporting electrolytes 0.1 M $NaClO_4$, 67 mM Na_2HPO_4; c) CVs of 2 mM cyclen amide (A) or 1 mM Cu-cyclen amide ($CuCl_2$:cyclen amide=1:2) (B) on glassy carbon electrode at 100 mV/s under N_2. Supporting electrolytes 0.1 M $NaClO_4$, 67 mM Na_2HPO_4.

The CVs of cyclen and Cu(II)-cyclen on the glassy carbon electrode under a N_2 atmosphere at a scan rate of 100 mV s^{-1} are compared and shown in **Figure 4.3b-A** and **Figure 4.3b-B**, respectively. The cathodic peak corresponding to Cu(II)-cyclen/Cu(I)-cyclen reduction (c_1) is located at -0.902 V (vs. Ag/AgCl), indicating Cu(II)-cyclen is very difficult to be reduced compared to free copper ion, which is consistent with

previous observations.[6] The cathodic peak corresponding to Cu(II)-cyclen amide/Cu(I)-cyclen amide reduction (c_1), on the other hand, is located at -0.800 V (vs. Ag/AgCl) (see **Figure 4.3c-B**). The 100 mV positive shift might result from the electron withdrawing effect of the amide bond which weakens the binding of cyclen with Cu(II) and facilitates the reduction of the Cu(II) complex into its Cu(I) form.

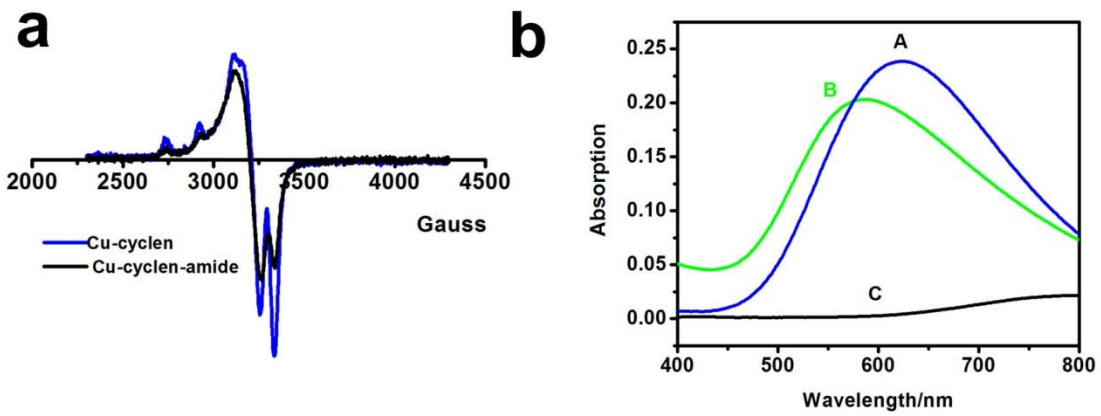

Figure 4.4. a) EPR spectra of Cu(II)-cyclen and Cu(II)-cyclen-amide in solution containing 0.1 M $NaClO_4$ and 67 mM Na_2HPO_4 at 77K: Center field, 3300 G; Sweep width, 2000 G; Frequency, 9.248 GHz; b) UV-Vis spectra of 1 mM Cu(II)-cyclen (1:2) in 0.1 M $NaClO_4$, 67 mM Na_2HPO_4 (A), Cu(II)-cyclen-amide (1:2) in 0.1 M $NaClO_4$, 67 mM Na_2HPO_4 (B) and 1 mM $CuCl_2$ in 0.1 M $NaClO_4$ (C).

To evaluate whether the introduction of the amide bond causes any changes in the coordination geometry of Cu(II)-cyclen, the EPR spectra and UV-Vis spectra of Cu(II)-cyclen and Cu(II)-cyclen amide are compared in **Figure 4.4a** and **Figure 4.4b**. The same supporting electrolytes used in the CV studies were added to the solutions used for EPR and UV-Vis spectra to ensure the consistency of all the comparisons. As shown in **Figure 4.4a**, the EPR spectra of both Cu(II)-cyclen and Cu(II)-cyclen amide exhibit the typical four-line patterns as previously reported for Cu(II)-cyclen and Cu(II)-cyclen polyurethane,[3] indicating the addition of the amide bond does not cause any changes in the coordination geometry for the Cu(II)-cyclen complex. For both Cu(II)-cyclen and Cu(II)-cyclen amide, the g values are 1.99, 2.03 and 2.13 for g_x, g_y and g_z, respectively, indicating a square pyramidal symmetry with the ground state of dx^2-y^2.[11] The UV-Vis

spectra of Cu(II)-cyclen and Cu(II)-cyclen amide exhibit maximum absorption at $\lambda_{max} = 621$ nm and $\lambda_{max} = 586$ nm which are consistent with previously reported five-coordinate geometry for the copper ion center.[11] Therefore, both Cu(II)-cyclen and Cu(II)-cyclen amide derivative have five-coordinated square pyramidal structures and a water molecule or a solution ion such as Cl^- might act as the fifth ligand.

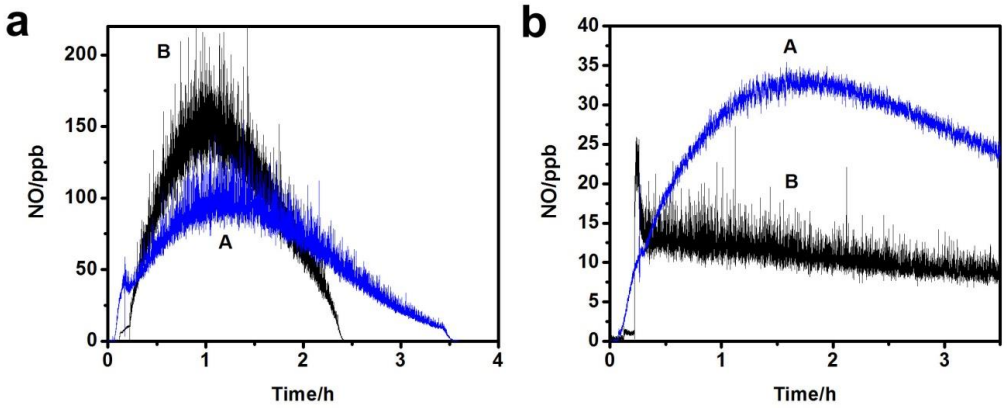

Figure 4.5. a) Catalytic NO generation profiles from solution of 20 μM EDTA, 50 μM CySH, 50 μM CySNO with 50 μM Cu(II)-Cyclen (1:1.5) (A) and 50 μM Cu(II)-cyclen-amide (1:10) (B) in HEPES buffer pH=7.4; b) NOA from solution of 20 μM EDTA, 50 μM CySH, 50 μM GSNO with 50 μM Cu(II)-Cyclen (1:1.5) (A) and 50 μM Cu(II)-cyclen-amide (1:10) (B) in HEPES buffer pH=7.04

The RSNO decomposition catalytic activity of Cu(II)-cyclen amide was also studied and compared with Cu(II)-cyclen. Initially, when GSH is used as the reducing agent, similar to Cu(II)-cyclen, no catalytic activity is observed for Cu(II)-cyclen amide towards GSNO. The RSNO decomposition catalytic activity is observed only when CySH is used as the reducing agent and the comparison towards CySNO and GSNO are shown in **Figure 4.5a** and **Figure 4.5b**, respectively. Although the 100 mV positive shift of the reduction potential of Cu(II)-cyclen amide contributes to the improved catalytic activity of this complex towards CySNO, the improvement is not very significant as shown in **Figure 4.5a**. When GSNO is used as the RSNO substrate, due to the steric hindrance, Cu(II)-cyclen exhibits even better catalytic activity compared to the amide derivative. Therefore, the introduction of an amide bond hardly improves the RSNO decomposition catalytic activity for the Cu(II)-cyclen complex.

4.3.3 Proposed mechanism for improved RSNO decomposition catalytic activity for Cu(II)-cyclen-based polyurethanes

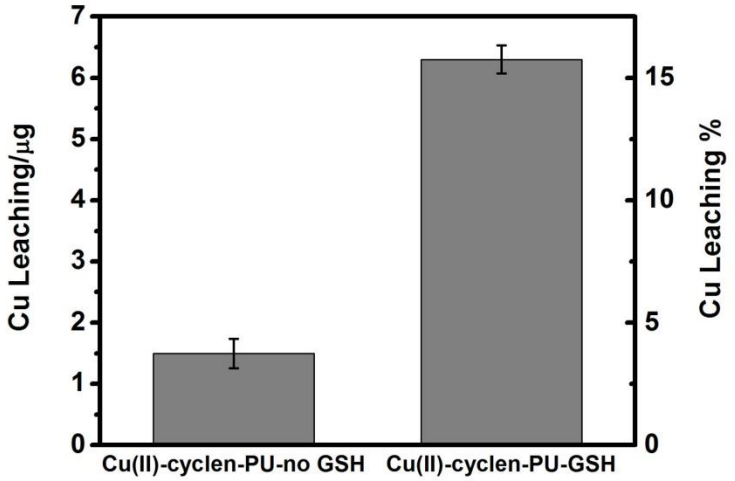

Figure 4.6. Six day accumulated copper leaching for Cu(II)-cyclen-PU film in PBS buffer without or with 20 mM GSH (n=3), the copper content of each film used is 40 μg.

The above comparison studies between the Cu(II)-cyclen and Cu(II)-cyclen amide complexes rule out the possibility that the introduction of the amide bond is contributing to the improved RSNO decomposition catalytic activity of Cu(II)-cyclen PU films. Since it is reported that the cyclen structure is not able to trap coordinated Cu^{+} due to its increased ionic size (from 72 pm to 96 pm) and electron repulsion (from d^{9} to d^{10}),[12, 13] when the Cu(II)-cyclen PU is in contact with a reducing agent, it is very likely that Cu^{+} will leach out of the cyclen ring. To prove that the cyclen ring is unable to stabilize Cu^{+}, the accumulated copper leaching amounts of Cu(II)-cyclen-PU films soaked in PBS buffer with or without reducing agent were compared and the results are shown in **Figure 4.6**. In the presence of 20 mM GSH as the reducing agent, the accumulated copper leaching amount increases from 3.8% to 15.8%, which is ~4 times higher than the copper leaching amount in the absence of a reducing agent. This result supports the hypothesis that the cyclen ring and the PU matrix are unable to fully stabilize Cu^{+}. When the Cu^{+} leaches out from the cyclen ring, it may loosely bind to the urethane groups within the polymer matrix and eventually leach out. The loosely bound Cu^{+} is then likely

responsible for the improved RSNO decomposition catalytic activity and short lifetime of the NO generation polymer.

4.3.4 RSNO decomposition catalytic activity of CuO NPs

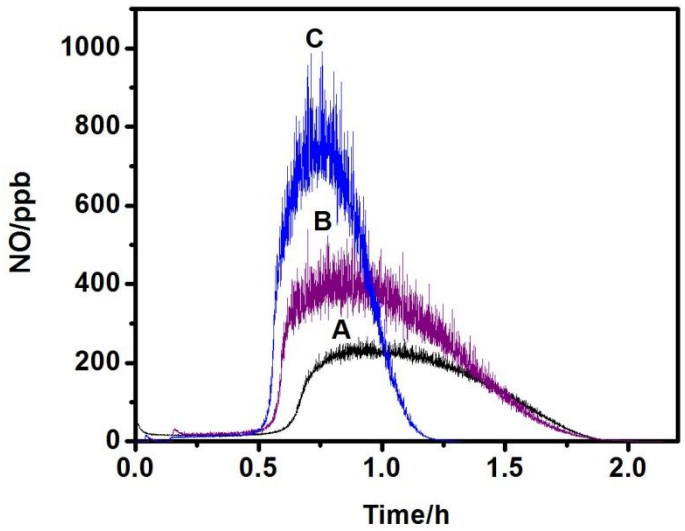

Figure 4.7. Catalytic NO generation profiles of 50 μM CuO NPs A) without EDTA pre-wash treatment; B) with 100 μM EDTA pre-wash treatment; C) with 200 μM EDTA pre-wash treatment in PBS buffer containing 20 μM EDTA, 50 μM GSH and 50 μM GSNO at 37°C. CuO NPs were prepared in PBS buffer as a 5 mM dispersion and aliquots were added into the reaction reservoir to reach a concentration of 50 μM.

To improve the lifetime of copper-based NO generation materials, CuO NPs, with a larger reservoir of copper compared to Cu(II)-cyclen complexes and slower corrosion rate compared to Cu NPs, were investigated as a novel catalyst for RSNO decomposition. The catalytic activities of CuO NPs with different treatments were first studied in PBS buffer containing 20 μM EDTA, 50 μM GSH and 50 μM GSNO at 37 °C. As shown in **Figure 4.7**, the CuO NPs exhibit good catalytic activity towards GSNO when GSH is used as the reducing agent. Improved catalytic activity for CuO NPs is observed when the particles are prewashed by EDTA solutions, and the higher the EDTA concentration in the washing solution, the better the catalytic activity of the particles after such treatment. This improvement might come from the dissolution of the outer layers of the

NPs, which further facilitates the corrosion of the particles in solution. However, an excess of EDTA will totally dissolve the CuO NPs. Since both RSNO decomposition catalytic activity and lifetime are important for NO generation materials, 100 μM was chosen as the EDTA wash concentration to improve the catalytic activity and retain most of the copper reservoir.

4.3.5 RSNO decomposition catalytic activity of CuO NPs doped PU films

To evaluate whether the CuO NPs can be incorporated into a polymer film for NO generation, the particles were dispersed into a SP-60D-60 PU matrix and the RSNO decomposition catalytic activity of CuO NPs-based PU film was studied and compared with a film containing Cu NPs with the same pre-treatment. As shown in **Figure 4.8A**, when a Cu NPs-SP-60D-60 film is placed into a solution containing 100 μM EDTA, 50 μM GSH and 50 μM GSNO at 37 °C, all the GSNO is decomposed within 10 min with a burst of NO generation, indicating a fast corrosion rate and high catalytic activity of Cu NPs-SP-60D-60 films. Since both the burst of NO and fast corrosion of Cu NPs will lead to toxicity issues, alternative catalysts need to be developed.

When a CuO NPs-SP-60D-60 film is inserted into PBS solution containing 50 μM EDTA, 50 μM GSNO, 50 μM GSH at 37 ºC, due to the much slower corrosion of the more inert CuO surface, a steady NO flux is observed as shown in **Figure 4.8B and C**. When the film is removed from the reaction reservoir, the NO generation immediately ceases, indicating minimized leaching of catalytic species from the film. Without the EDTA washing pretreatment, the NO flux of the CuO NPs-PU film is ~57% (**Figure 4.8B**) of the film containing particles with the pretreatment (**Figure 4.8C**), which is consistent with the previous observations of the influence of EDTA on the catalytic activity of CuO NPs. The effect of the water uptake of the polyurethane matrices was also evaluated. The water uptake values of SP-60D-60, SP-60D-20 and SG-80A are 60 wt%, 20 wt% and <1 wt%, respectively.[14] As shown in **Figure 4.8C**, **D and E**, the NO flux of the films decrease with a decrease of the water uptake of the polymer matrices. For SG-80A with barely any water uptake, the RSNO decomposition catalytic activity is poor because only the CuO NPs on the surface are accessible for the RSNO in the

substrate. The higher the water uptake of the polymer, the more catalytic sites within the film will be accessible to low molecular weight GSH and GSNO, and, therefore, the better the catalytic activity of the CuO NPs-PU film. To evaluate whether the CuO NPs-PU film is capable of generating physiological levels of NO flux, a CuO NPs-SP-60D-60 film was placed in a reservoir containing 50 μM EDTA, 20 μM GSH and 1 μM GSNO and the result is shown in **Figure 4.8F**. An NO flux of ~1.7×10^{-10} mol cm^{-2} min^{-1} is observed, which is comparable to that produced by the healthy endothelial cell surfaces,[15] indicating the potential antithrombotic activity of the CuO NPs-PU film.

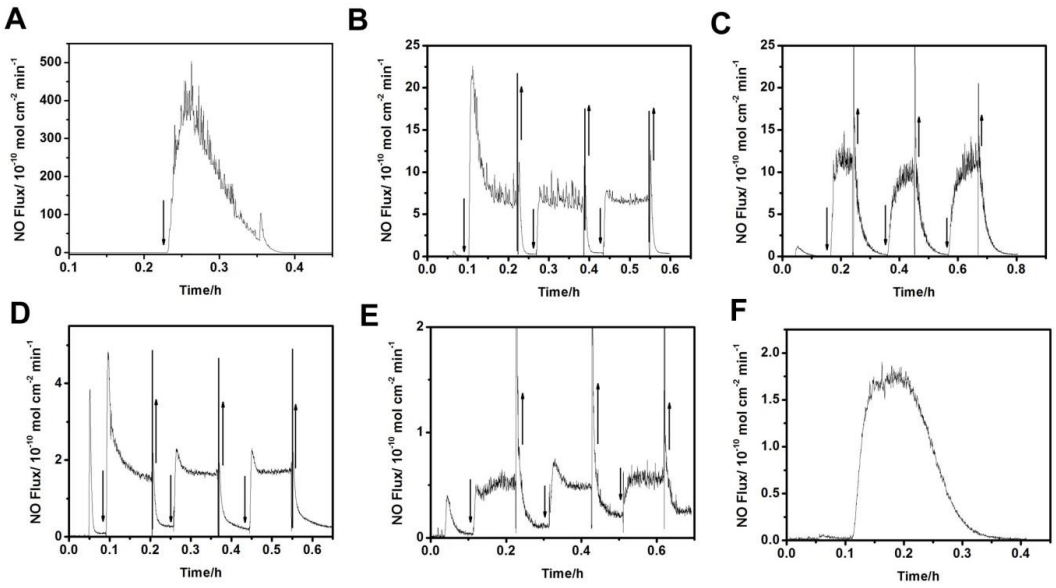

Figure 4.8. Catalytic activity of A) Cu NPs-SP-60D-60 film in 2 mL PBS (10 mM, pH=7.04) buffer containing 100 μM EDTA, 50 μM GSNO, 50 μM GSH at 37 ºC; B) CuO NPs-SP-60D-60 film (CuO NPs without EDTA pre-wash treatment); C) CuO NPs-SP-60D-60 film; D) CuO NPs-SP-60D-20 film; E) CuO NPs-SG-80 film in 2mL PBS (10 mM, pH=7.04) buffer containing 100 μM EDTA, 50 μM GSNO, 50 μM GSH at 37 ºC ; F) CuO NPs-SP-60D-60 film in 2 mL PBS (10 mM, pH=7.04) buffer containing 50 μM EDTA, 1 μM GSNO, 20 μM GSH at 37 ºC. Films were repeatedly inserting and taken out of the solution as indicated by the ↑and ↓arrows.

4.3.6 Long-term catalytic activity from CuO NPs doped PU film

The long-term catalytic activity of the CuO NPs-SP-60D-60 film was further evaluated in solution containing 50 μM EDTA, 50 μM GSNO, 50 μM GSH at 37 ºC. As shown in **Figure 4.9**, the film exhibits a gradually decreased NO flux over time for sixteen days with the depletion of the copper reservoir. The decreased NO flux of the film on the first day (**Figure 4.9A**) compared to the previous result (**Figure 4.8C**) is due to the loss of catalytic sites during storage in the soaking solution and the NOA test. Due to the ease of the fabrication of the CuO NPs-PU film, the lifetime of the coating is expected to be further controlled by controlling the CuO NPs composition and film thickness.

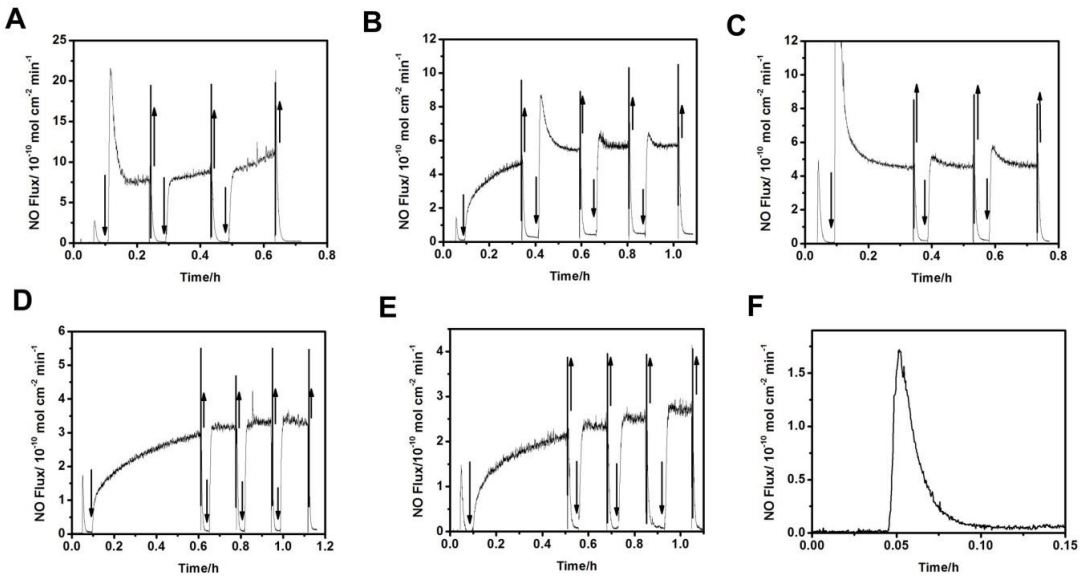

Figure 4.9. Catalytic activity of CuO NPs-SP-60D-60 film in 2 mL PBS (10 mM, PH=7.04) buffer containing 50 μM EDTA, 50 μM GSNO, 50 μM GSH at 37 ºC on the A) first; B) third; C) fifth; D) eighth; E) twelfth; F) sixteenth day. The film was repeatedly inserting and taken out of the solution as indicated by the ↑and ↓arrows. The film was stored in 10 mL PBS buffer containing 50 μM EDTA, 50 μM GSNO, 50 μM GSH at 37 ºC and the storage solution was freshly prepared and replaced after each NOA test.

4.3.7 Copper leaching from the Cu or CuO NPs doped PU film

The leaching of copper from SP-60D-60 PU films containing CuO or Cu NPs was monitored over a six day period using ICP-OES and the copper daily leaching values of the two types of films are shown in **Figure 4.10**. Considering the average daily uptake of

Cu by humans is 0.6~1.6 mg/day[7] and the small area of most medical devices, none of the films are considered to leach toxic levels of copper. However, the CuO NPs doped PU film, with a slower corrosion rate, obviously exhibits less leaching of copper compared with films containing Cu NPs loaded with the same copper weight percentage (calculated to be 13.8 wt%). In addition, considering that the specific surface area of CuO NPs (29 m^2/g) is higher than the Cu NPs (12 m^2/g), their smaller sizes (active surface area per mass) can lead to more corrosion. Therefore, when CuO NPs with the same size as the Cu NPs are utilized, less leaching should be observed than shown in **Figure 4.10**. In addition, this result is consistent with a previously observed trend that CuO NPs with a larger surface compared with Cu NPs exhibit less leaching of copper in PBS buffer.[9]

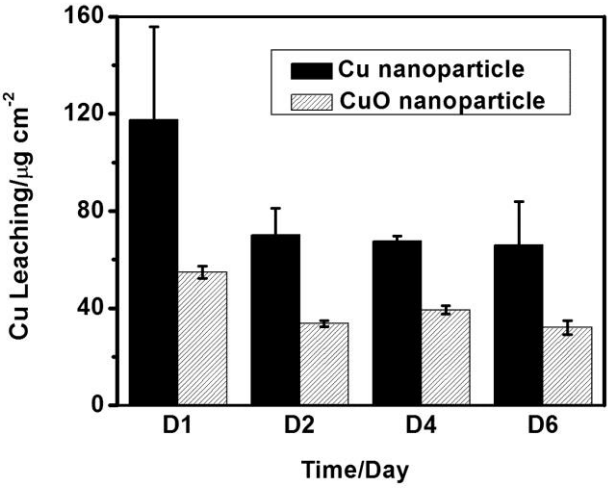

Figure 4.10. Copper leaching from CuO NPs or Cu NPs-doped SP-60D-60 film (D=9 mm) on the first, second, fourth and sixth day (n=3).

4.3.8 XRD patterns of CuO and Cu NPs

To better understand the particle compositions utilized in these experiments, the XRD patterns of the CuO and Cu NPs employed herein are compared in **Figure 4.11.** The XRD pattern of CuO NPs shown in **Figure 4.11A** can be indexed to monoclinic tenorite CuO, as previously reported.[16] The XRD pattern of Cu NPs, in contrast, is complicated due to the presence of a surface oxide layer.[9] As shown in **Figure 4.11B**, while most of

the peaks in the XRD pattern match the reported data for cubic copper, peaks for cubic Cu_2O are also observable as reported previously for Cu NPs.[17] A magnification of the oxide region is shown in the **Figure 4.11B** inset, which indicates the presence of both Cu_2O and CuO on the surface of the copper NPs, as has been reported elsewhere.[9] According to the intensity of the strongest peak for each species, the relative proportions of Cu_2O, CuO and Cu core are 3.9%, 1.9% and 94.2%, respectively. The presence of Cu_2O on the surface and the limited coverage of oxide layer on the surface of the Cu NPs contribute to the burst of NO generation from the reaction reservoir and faster corrosion rate of the copper NPs.

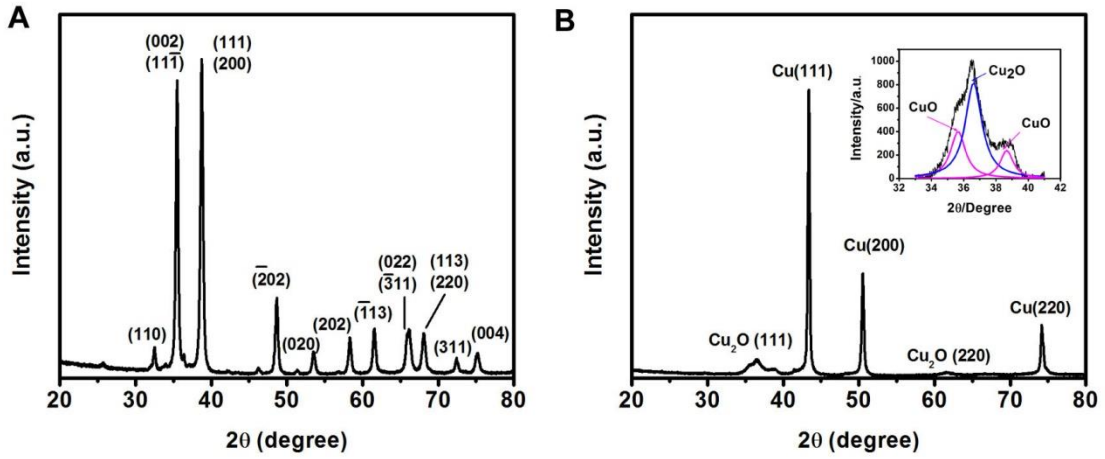

Figure 4.11. XRD patterns of A) CuO NPs and B) Cu NPs. The inset shows the magnification and peak deconvolution of the oxide region which contains two peaks from CuO and one peak from Cu_2O. The presence of surface Cu_2O and CuO due to slow oxidation causes the peak broadening.

4.4 Conclusions

A mechanistic study suggests the better RSNO decomposition catalytic activity and the short lifetime of the Cu(II)-cyclen PU polymer material results from the inability of the cyclen cavity to hold Cu^+. In contrast, a CuO NPs-based PU film is capable of generating physiological levels of NO and its catalytic activity lasts for sixteen days due to the slow corrosion and release of Cu^{2+} from the film. This type of film, with minimal copper

leaching and long-term catalytic activity, is expected to be an alternative to the previously developed Cu(II)-cyclen-based NO generation coatings.

4.5 References

1. Thom, V. J.; Hosken, G. D.; Hancock, R. D. *Inorg. Chem.* **1985,** 24, (21), 3378-3381.
2. Hwang, S.; Cha, W.; Meyerhoff, M. E. *Angew. Chem., Int. Ed.* **2006,** 45, (17), 2745-2748.
3. Hwang, S.; Meyerhoff, M. E. *Biomaterials* **2008,** 29, (16), 2443-2452.
4. Puiu, S. C.; Zhou, Z. R.; White, C. C.; Neubauer, L. J.; Zhang, Z. F.; Lange, L. E.; Mansfield, J. A.; Meyerhoff, M. E.; Reynolds, M. M. *J. Biomed. Mater. Res., Part B* **2009,** 91B, (1), 203-212.
5. Liu, K.; Meyerhoff, M. E. *J. Mater. Chem.* **2012,** 22, (36), 18784-18787.
6. Miyoshi, K.; Tanaka, H.; Kimura, E.; Tsuboyama, S.; Murata, S.; Shimizu, H.; Ishizu, K. *Inorg. Chim. A-Bioninor.* **1983,** 78, (1), 23-30.
7. Wu, Y.; Rojas, a.; Griffith, G.; Skrzypchak, a.; Lafayette, N.; Bartlett, R.; Meyerhoff, M. *Sens. Actuators, B* **2007,** 121, 36-46.
8. Major, T. C.; Brant, D. O.; Burney, C. P.; Amoako, K. A.; Annich, G. M.; Meyerhoff, M. E.; Handa, H.; Bartlett, R. H. *Biomaterials* **2011,** 32, (26), 5957-5969.
9. Midander, K.; Cronholm, P.; Karlsson, H. L.; Elihn, K.; Moller, L.; Leygraf, C.; Wallinder, I. O. *Small* **2009,** 5, (3), 389-399.
10. Popescu, A. M.; Constantin, V.; Cojocaru, A.; Olteanu, M. *Rev. Chim.* **2011,** 62, (2), 206-211.
11. Lacerda, S.; Campello, M. P.; Santos, I. C.; Santos, I.; Delgado, R. *Polyhedron* **2007,** 26, (14), 3763-3773.
12. Tabata, M.; Babasaki, M. *Inorg. Chem.* **1992,** 31, (25), 5268-5271.
13. Gasser, G.; Belousoff, M. J.; Bond, A. M.; Spiccia, L. *Inorg. Chem.* **2007,** 46, (10), 3876-3888.
14. http://www.lubrizol.com/Medical/Products/Tecophilic.html
15. Vaughn, M. W.; Kuo, L.; Liao, J. C. *Am J Physiol Heart Circ Physiol* **1998,** 274, (6), H2163-H2176.
16. Lee, S. C.; Park, S. H.; Lee, S. M.; Lee, J. B.; Kim, H. J. *Catal. Today* **2007,** 120, (3-4), 358-362.
17. Cheng, Z. P.; Zhong, H.; Xu, J. M.; Chu, X. Z.; Song, Y. Z.; Xu, M.; Huang, H. *Mater. Lett.* **2011,** 65, (19-20), 3005-3008.

Chapter 5 Conclusions and Future Directions

5.1 Conclusions

The research in this dissertation focused on developing antithrombotic and antimicrobial coatings based on two strategies: nitric oxide (NO) release and NO generation. While previously developed NO release materials have been widely utilized for antithrombotic applications,[1-3] in this dissertation, a focus was on investigating the antibiofilm properties of NO release coatings. In Chapter 2, it was demonstrated that diazeniumdiolate (NONOate)-doped poly(lactic-*co*-glycolic) acid (PLGA)-based NO release films with controllable NO release patterns are capable of preventing biofilm formation under various conditions in a CDC biofilm reactor. Specifically, an NO releasing film with a base layer of 30 wt% dibutyhexyldiamine diazeniumdiolate (DBHD/N_2O_2) mixed with poly(lactic acid) (PLL), is capable of NO release for 10 d at 37 °C and exhibited ~ 98.4% reduction in biofilm biomass of *S. aureus* and ~ 99.9% reduction for *E. coli* at 37 °C when compared with a silicone rubber control surface after one week of testing. This type of coating is thus expected to be applied as a potentially coating on short-term indwelling devices such as catheters to reduce infection rates. Since the influence of NO release profiles on the antibiofilm properties of the NO coatings in a flowing system has hardly been reported, this work also serves as a model for fundamental studies.

NO release coatings, however, have short lifetimes due to a limited NO donor reservoir that can be incorporated into the polymeric coatings. To solve this problem, various NO generation coatings with covalently attached organodiselenides[4, 5] and Cu(II)-cyclen segments[6, 7] or doped Cu nanoparticles (NPs)[8] have been developed in this group to convert endogenous NO donors such as *S*-nitrosothiols (RSNOs) into NO. The previously developed NO generation coatings, however, have had limited applications

due to the following factors: 1) the aliphatic selenium species utilized in previous NO generation coatings can exhibit cytotoxicity issues; 2) the Cu(II)-cyclen complex-based NO generation polymers have limited lifetimes and the NO generation mechanism is not clear; and 3) the corrosion rate of Cu NPs are too fast and will lead to potential toxicity issues and shorten the lifetimes of Cu NPs-based NO generation coatings. Therefore, in this dissertation, two new types of NO generation coatings based on aromatic selenium species and CuO NPs were explored to reduce the toxicity issue and improve the lifetimes of previously developed NO generation coatings.

In Chapter 3, a carboxyl derivative of the drug ebselen, an antioxidant drug that is currently undergoing Phase III clinic trial in Japan due to its low toxicity,[9] was successfully synthesized. By attaching this derivative onto polyethylenimine (PEI), a Layer-by-Layer (LbL) coating was then fabricated by using the ebselen-PEI as the polycation and alginate as the polyanion. After a two-step annealing treatment, the LbL film exhibits significantly reduced selenium leaching. The potential antithrombotic and antimicrobial properties of the annealed films were further evaluated. A polyurethane catheter coated with 50 bilayers of the annealed LbL films exhibits an NO flux of 3×10^{-10} mol cm^{-2} min^{-1} when bathed in physiological levels of RSNOs and thiols, indicating the potential antithrombotic properties of the LbL coatings. *In vitro* antimicrobial tests also proved the capability of the LbL films in reducing bacterial surface attachment and killing a broad spectrum of bacterial species through superoxide production. This type of coating, with reduced toxicity, is expected to be a dual functional coating that can be further applied to indwelling devices to solve thrombus and infection related complications. In addition, due to the utilization of covalently attached ebselen segment and endogenous NO donors, this type of coating is expected to be applied for both short-term indwelling devices such as catheters and long-term indwelling devices such as vascular grafts and stents, and *in-vivo* studies need to be performed in the future before the potential applications.

The previous mechanism for the catalytic activity of Cu(II)-cyclen-based polymers are vague. Therefore, in Chapter 4, it was first demonstrated that Cu(II)-cyclen-based polyurethane (PU) has better catalytic activity compared with the Cu(II)-cyclen complexes or its derivative through a series of mechanistic studies. The improved

catalytic activity likely comes from the leaching of Cu(I) from the polymer due to the inability of the cyclen ring to stabilize Cu(I). Based on these findings, copper particle-based NO generation materials, with a larger copper reservoir, are expected to be the alternatives to improve the lifetime of copper-based NO generation materials. The RSNO catalytic decomposition activities and leaching of copper from CuO NPs-doped PU films were studied and compared with Cu^0 NPs-doped PU films. The CuO NPs-based PU films with a slower corrosion rate exhibit lower leaching of copper without a "burst" of NO generation compared with the Cu^0 NPs-based PU films, and greatly reduced the toxicity issues. In addition, the catalytic activity of the CuO NPs-based PU film lasts for sixteen days and the lifetime is expected to be further extended by changing the film formulation. This type of coating, with CuO NPs as the novel catalyst, is expected to be an alternative to previously developed NO generation coatings based on various copper species. Compared to the organoselenium species-based NO generation coatings, the CuO NPs-based NO generation coating developed in this dissertation work has limited lifetime and can only be applied on short-term indwelling devices such as catheters. However, the advantage of this type of coating lies in its cheap cost and simplicity of fabrication. Since ParaGard IUD (intrauterine device) based on copper releasing has been commercialized and approved by FDA,[10] additional properties and applications of the CuO NPs-based polyurethane coatings need to be further examined in the future.

5.2 Future Directions

5.2.1 Ebselen-based polyurethane for NO generation

In Chapter 3, a carboxyl-ebselen-based LbL film was shown to exhibit potential antithrombotic and proven antimicrobial properties. In addition to LbL coatings, elastomers, such as PUs, are widely utilized in biomedical applications due to their good mechanical strength, ease for modification for biocompatibility improvement and flexibility in processing.[11] Therefore, it should be possible to attach ebselen derivatives onto different PU matrices to fabricate selenium-based NO generation coatings. The resulting materials are expected to exhibit potential antithrombotic and antimicrobial

properties as previously observed for the ebselen-based LbL coatings as described in Chapter 3.

To attach the carboxyl-ebselen segment to PU, one approach would be to aminate the PU matrix using a previously reported method[6] followed by reacting the carboxyl-ebselen with the amino group in the modified PU as shown in **Scheme 5.1**. This approach, attempted in preliminary studies of this dissertation research, resulted in a polymer with only 0.08 wt% Se content (experimental data from ICP-OES), indicating limited attachment of the ebselen segments onto the polymer matrix.

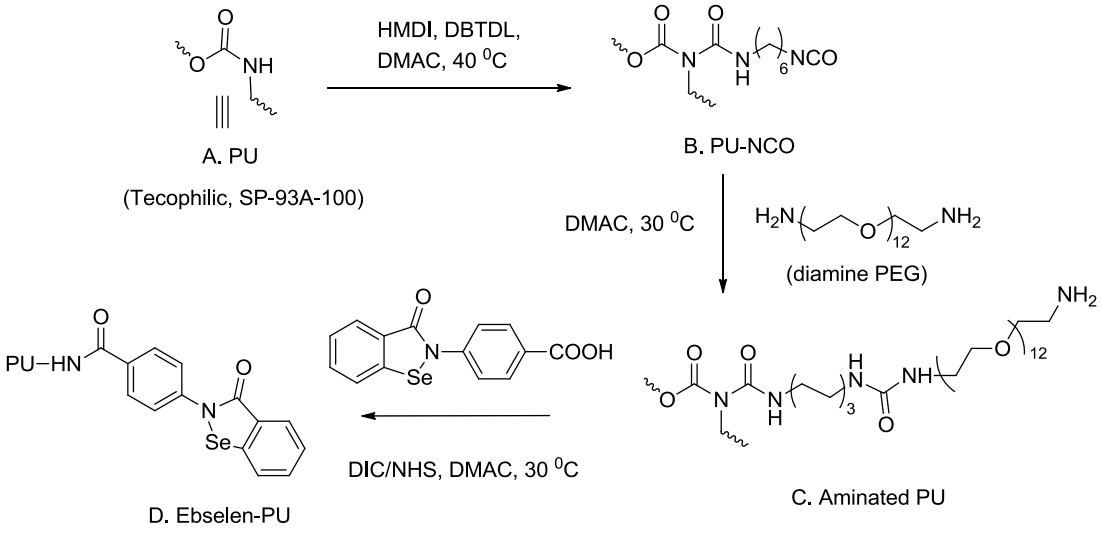

Scheme 5.1. Synthesis of ebselen-PU utilizing a three-step approach similar to that is previously reported.[6]

The poor attachment rate of carboxyl-ebselen in the previous attempts might be due to the cross-linking reactions that take place during the two-step synthesis of the aminated PU. Therefore, to reduce cross-linking before the attachment of the ebselen derivative, an improved two-step synthesis route is proposed, as shown in **Scheme 5.2**. In reducing the synthesis route from three steps to two steps, this proposed approach is expected to reduce the cross-linking during the PU modification and improve the attachment of catalytic sites onto the PU matrix.

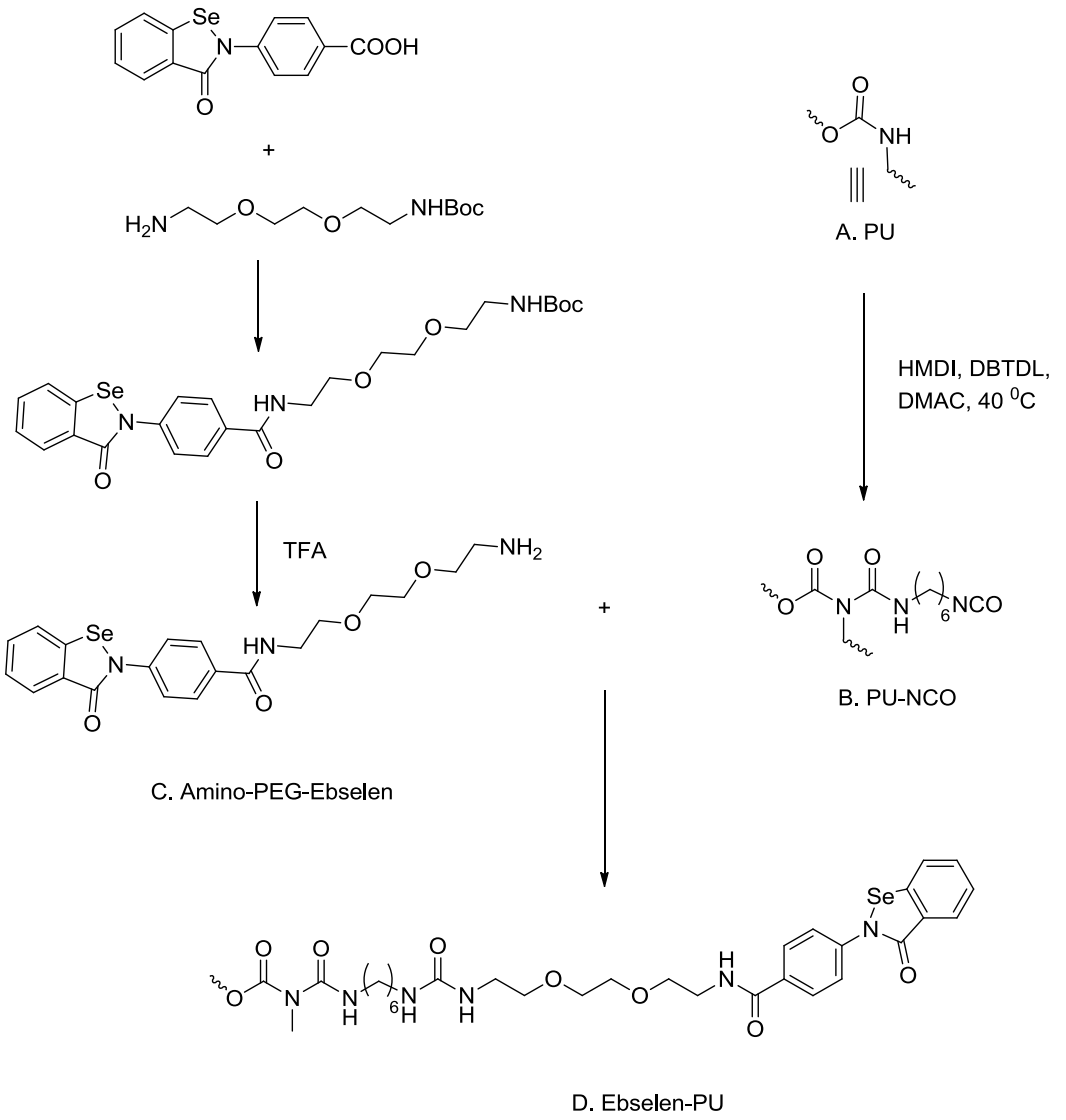

Scheme 5.2. Proposed two-step synthesis route for ebselen-PU.

5.2.2 Cu(II)-tris(2-pyridylmethyl)amine-based polymers for NO generation

In Chapter 4, it was demonstrated that neither Cu(II)-cyclen or the Cu(II)-cyclen amide derivative has good catalytic activity towards RSNOs due to their very negative reduction potentials. In addition, the cyclen structure is unable to stabilize Cu(I) as reported previously.[12] Therefore, better chelating agents should be developed to incorporate Cu(II)-complexes into a polymer phase. There are several requirements for a good chelating agent: a) the chelating agent should be able to stabilize Cu(I) to prevent any

leaching problems; b) the reduction potential of the Cu(II)-complex should not be too negative to cause a significant loss of catalytic activity; and c) the Cu(II)-complex should still have open sites to interact with reducing agents and RSNOs. Different from Cu(II)-cyclen, a Cu(II)-TPA (see structure in **Figure 5.1A,** TPA= tris(2-pyridylmethyl)amine) complex that has been reported to exhibit a more positive reduction potential of -0.34V (vs. Ag/AgCl)[13] and it has also been reported that that d-π transfer can help to stabilize Cu(I).[14] The catalytic activity of Cu(II)-TPA complexes towards RSNOs was examined in HEPES buffer containing 20 μM EDTA, 50 μM GSH and 50 μM GSNO and shown in **Figure 5.1B**. The complex exhibits good catalytic activity towards RSNOs and the conversion rate is ~100%, which is much better than those observed with the Cu(II)-cycle complex or its derivative, that hardly exhibit any catalytic activity under the same conditions.

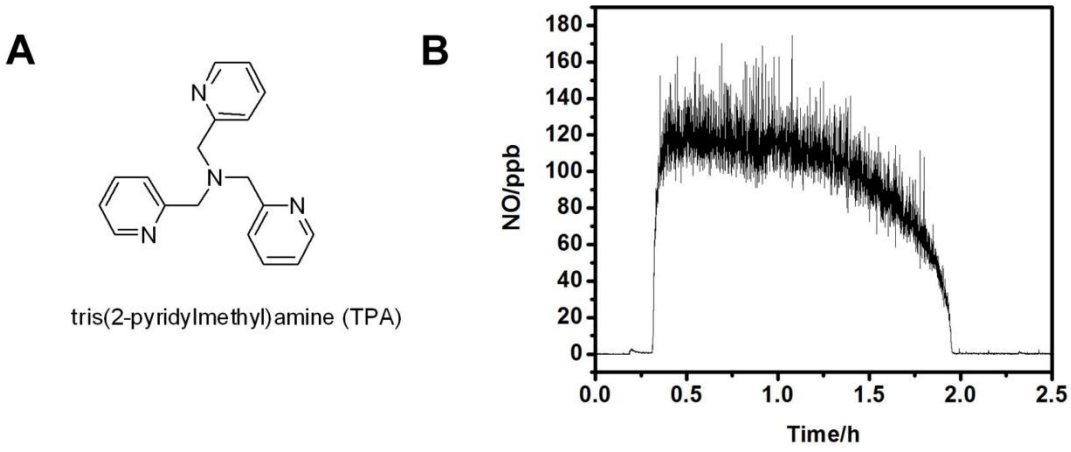

Figure 5.1. A) Structure of tris(2-pyridylmethyl) amine (TPA); B) Catalytic NO generation in a solution of 20 μM EDTA, 50 μM GSH, 50 μM GSNO, 50 μM Cu(II)-TPA (1:5, TPA in excess) in 0.1 M HEPES buffer (pH=7.4).

Based on the above observation, TPA derivatives, such as an amine derivative that can be synthesized using a reported method[15] (and potentially attached onto polymers) may provide the best approach to develop Cu(II)-complex-based NO generation materials with enhanced catalytic activity and longer lifetimes compared with Cu(II)-cyclen-based polymers. A proposed schematic synthesis route for such polymers is shown in **Scheme 5.3**. Copper (II) can be incorporated onto the TPA-based polymer to develop NO

generation polymers based on the immobilized Cu(II)-TPA complexes using a previously reported method. [6]

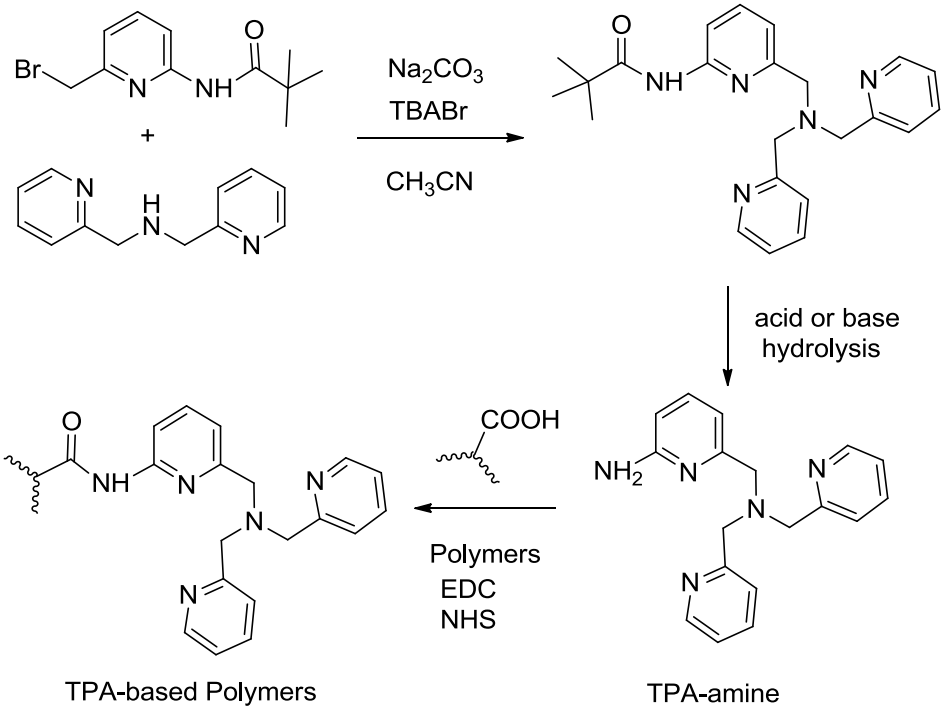

Scheme 5.3. Schematic illustration of synthetic route of TPA-based polymers with the amine derivative of TPA being synthesized using a reported method.[15]

5.2.3 Combined coating based on NO generation and RSNO release materials

One of the limitations of utilizing NO generation materials for biomedical applications lies in the limited and variable amounts of the RSNO reservoirs in human blood.[16] Although it has been previously demonstrated that RSNOs, such as *S*-nitroso-*N*-acetylpenicillamine (SNAP), can be infused to improve the antithrombotic performance of NO generation coatings,[8] a more convenient method will be to combine the NO generation material with a RSNO release material into one coating.

As described in Chapter 1, RSNOs can be doped[17] within or covalently[18-20] attached to polymers to fabricate NO release coatings. The NO release of the RSNO release coatings can then be trigged through heat or light. Despite the known catalytic activity towards

RSNO, the NO generation polymeric materials that have been developed previously, have not been combined with the RSNO release materials.

In Chapter 4, it was demonstrated that a CuO nanoparticles (NPs)-doped polyurethane (PU) film can potentially be utilized as an alternative to previously developed copper-based NO generation materials. This coating can be further utilized as a model system to devise a combination coating that has an RSNO release under-layer and a top layer composed of CuO NPs to generate NO from the RSNO species released from the under-layer.

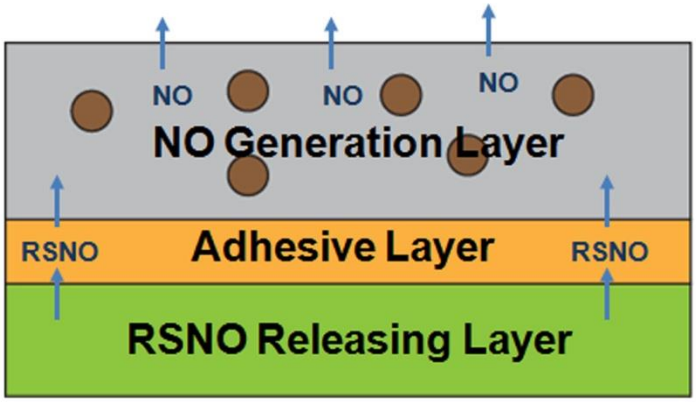

Figure 5.2. Configuration of a coating that combines RSNO release and NO generation materials. The coating contains a RSNO release layer as the base layer, an adhesive layer and an NO generation layer-based on CuO NPs-doped PU films.

A proposed coating configuration is shown in **Figure 5.2**. First, the coating contains a RSNO release coating as the base layer. This layer can be composed of the previously developed RSNO release materials[17-20] or a SNAP-doped Elast-Eon™ 2As (E2As, from AorTech Biomaterials) film that have been developed recently by Elizabeth Brisbois in the Meyerhoff group. An NO generation film is utilized as the top coating. For example, it can be the CuO NPs doped SP-60D-60 PU film. The polymer matrix applied in the top coating should have adequate water uptake so that reducing agents and released RSNO can further enter the top layer and interact with the catalytic sites within the top coating. Since the water uptake of the base layer, such as the SNAP releasing film, is normally much lower when compared with the polymer utilized in the top coating, an adhesive layer is necessary to combine the base layer and top coating as well as to prevent direct

contact of the catalytic sites with RSNOs to reduce the burst of NO at the initial stage of NO release. The adhesive layer can be comprised of silane compounds such as γ-aminopropyltrimethoxysilane as previously utilized in commercial glucose sensors.[21]

In summary, this thesis has laid the foundation for developing antithrombotic and antimicrobial coatings based on NO release or generation. The developed coatings are expected to be applied to short-term indwelling devices such as catheters to solve thrombus or infection related biocompatibility issues. The NO generation coatings, with improvements as indicated in the future directions, are expected to be further applied to long-term implants, such as vascular grafts, stents, etc.

5.3 References

1. Major, T. C.; Brant, D. O.; Reynolds, M. M.; Bartlett, R. H.; Meyerhoff, M. E.; Handa, H.; Annich, G. M. *Biomaterials* **2010,** 31, (10), 2736-2745.
2. Batchelor, M. M.; Reoma, S. L.; Fleser, P. S.; Nuthakki, V. K.; Callahan, R. E.; Shanley, C. J.; Politis, J. K.; Elmore, J.; Merz, S. I.; Meyerhoff, M. E. *J. Med. Chem.* **2003,** 46, (24), 5153-5161.
3. Yan, Q. Y.; Major, T. C.; Bartlett, R. H.; Meyerhoff, M. E. *Biosens. Bioelectron.* **2011,** 26, (11), 4276-4282.
4. Cha, W.; Meyerhoff, M. E. *Biomaterials* **2007,** 28, 19-27.
5. Yang, J.; Welby, J. L.; Meyerhoff, M. E. *Langmuir* **2008,** 24, (18), 10265-10272.
6. Hwang, S.; Meyerhoff, M. E. *Biomaterials* **2008,** 29, (16), 2443-2452.
7. Hwang, S.; Cha, W.; Meyerhoff, M. E. *Angew. Chem., Int. Ed.* **2006,** 45, (17), 2745-2748.
8. Major, T. C.; Brant, D. O.; Burney, C. P.; Amoako, K. A.; Annich, G. M.; Meyerhoff, M. E.; Handa, H.; Bartlett, R. H. *Biomaterials* **2011,** 32, (26), 5957-5969.
9. Mugesh, G.; Singh, H. B. *Chem. Soc. Rev.* **2000,** 29, 347-357.
10. http://www.paragard.com/what-is-paragard/Default.aspx
11. McMillin, C. R. *Rubber Chem. Technol.* **2006,** 79, (3), 500-519.
12. Gasser, G.; Belousoff, M. J.; Bond, A. M.; Spiccia, L. *Inorg. Chem.* **2007,** 46, (10), 3876-3888.
13. Kunishita, A.; Kubo, M.; Ishimaru, H.; Ogura, T.; Sugimoto, H.; Itoh, S. *Inorg. Chem.* **2008,** 47, (24), 12032-12039.
14. Navon, N.; Golub, G.; Cohen, H.; Paoletti, P.; Valtancoli, B.; Bencini, A.; Meyerstein, D. *Inorg. Chem.* **1999,** 38, (15), 3484-3488.
15. Szajna, E.; Makowska-Grzyska, M. M.; Wasden, C. C.; Arif, A. M.; Berreau, L. M. *Inorg. Chem.* **2005,** 44, (21), 7595-7605.
16. Giustarini, D.; Milzani, A.; Dalle-Donne, I.; Rossi, R. *Journal of Chromatography B-Analytical Technologies in the Biomedical and Life Sciences* **2007,** 851, (1-2), 124-139.
17. Amadeu, T. P.; Seabra, A. B.; de Oliveira, M. G.; Costa, A. M. A. *J. Eur. Acad. Dermatol. Venereol.* **2007,** 21, (5), 629-637.
18. Seabra, A. B.; da Silva, R.; de Oliveira, M. G. *Biomacromolecules* **2005,** 6, (5), 2512-2520.
19. Li, Y.; Lee, P. I. *Mol. Pharm.* **2010,** 7, (1), 254-266.
20. Hetrick, E. M.; Schoenfisch, M. H. *Biomaterials* **2007,** 28, (11), 1948-1956.
21. Wang, J.-H. L.; Dang, T. T.; Cochran, B. B.; Mastrototaro, J. J.; Shah, R. Analyte sensors comprising blended memberane compositions and methods for making and using them. US Patent 20110152654A1, 2011.

Appendix Diazeniumdiolate-Doped Poly(lactic acid)-Based Biodegradable Nitric Oxide Release Film

A.1 Introduction

Metals, such as titanium, titanium alloys and magesium alloys have been widely used in biomedical applications.[1, 2] For example, due to their good fatigue strength, relative low modulus and shape memory phenomenon, titanium and its alloys have been utilized in the fabrication of prosthetics such as artifical hip joints (shown in **Figure A.1A**) and cadiovascular devices such as stents (shown in **Figure A.1B**).[1]

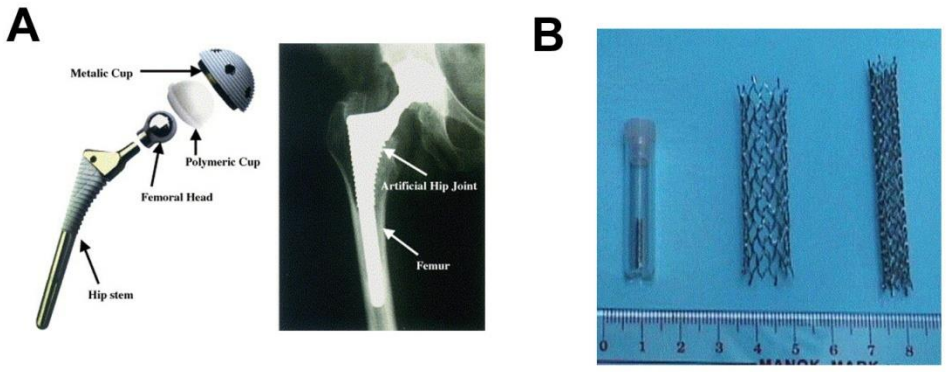

Figure A.1. Schematic diagram of A) artificial hip joint; B) vascular stents.[1]

As described in Chapter 1, bacterial infection is a common problem for indwelling devices. The annual infection rate in the United States is reported to be 4.3% for orthopedic implants and 7.4% for cardiovascular implants.[3] In Chapter 2, it was demonstrated that diazeniumdiolate-doped poly(lactic-*co*-glycolic acid) (PLGA)-based NO release films are capable of preventing biofilm formation. PLGA or PLGA-based

drug-eluting coatings have also been applied on metal implants to slow down the corrosion of the implants, improve fracture healing and prevent restenosis.[4-6] Therefore, in this appendix, effors to create a totally biodegradable NO releasing film based on diazeniumdiolate of spermine (SPER/NONOate) and poly(lactic acid) (PLL) can be fabricated and this type of film is expected to be further applied on indwelling metal implants to prevent bacterial infection problems after implantation. Diazeniumdiolated spermine is chosen because the degradation product spermine is a naturally occruing polyamine, which greatly reduces toxicity concerns for the films developed here.

A.2 Experimental

A.2.1 Materials

Poly(lactic acid) (PLL) (100 DL 7E) was purchased from Lakeshore Biomaterials (Birmingham, AL). The residual monomers were determined as 2 wt% (information provided by the vendor). $Ca(OH)_2$, $Mg(OH)_2$, L-arginine (free base), bromothymol blue (BB) and anhydrous THF were purchased from Sigma-Aldrich (St. Louis, MO). Spermine NONOate (SPER/NONOate) was obtained from Cayman Chemical (Ann Arbor, MI). SPER/NONOate and PLL were stored in a desiccator at -20 °C before use.

A.2.2 Evaluation of film pH change of PLL films doped with different bases

Two hundred mg of PLL was dissolved in 3 mL THF and different bases including $Ca(OH)_2$, $Mg(OH)_2$ and arginine were then dispersed into the PLL solution to reach a final base concentration of 5 wt%, 10 wt% or 20 wt%. The dispersions were sonicated until homogeneous dispersions were formed. A solution of bromothymol blue (BB) in THF (5 mM) was then added into the dispersions to reach a final indicator concentration of 10 mmol kg^{-1} as previously described in Chapter 2.[7] Glass slides (0.9 × 5 cm) were cleaned by sonicating in acetone, deionized water and acetone sequentially and dried before use. Two hundred μL of each of the PLL-base dispersions was then cast onto a glass slide and the films were then left dry overnight in a desiccator. The films were then placed into PBS buffer and the colors of the films were evaluated at different time intervals.

A.2.3 Preparation of biodegradable NO release films

Two hundred mg of PLL was dissolved in 3 mL anhydrous THF, and $Ca(OH)_2$ was then added into the solution to reach a final base percentage of 10 wt%. The dispersion was sonicated to obtain a homogeneous dispersion and 200 μL of the dispersion was then cast onto a glass slide as a base layer (100 μL of the dispersion was added at a time). SPER/NONOate (2.13 mg) was added into 500 μL of the dispersion of 10 wt% $Ca(OH)_2$ in PLL to obtain a dispersion containing 5 wt% of SPER/NONOate. The dispersion was then sonicated and 25 μL of the dispersion was added into an O-ring (d=7 mm) onto the base layer. The film was then dried in a desciccator and this procedure was repeated another three times until 100 μL of the total dispersion was cast on top of the base layer as the NO release layer. Two hundred μL of the dispersion of 10 wt% $Ca(OH)_2$ in PLL was then added as a top coating (100 μL of the dispersion was added at a time) to fabricate the final multilayer film (film A). A comparison film (film B) was also prepared using the same method except a solution of 600 mg PLL in 3 mL THF with 10 wt% $Ca(OH)_2$ was used to prepare the base layer and the top coating. The films were dried in a desciccator for 6 h and then in vacuum for 2 d before use.

A.2.4 NO release measurement

The NO release profiles of the film were measured by purging N_2 into 2 mL PBS buffer solution, pH 7.4, in a glass cell protected from light and monitored using a chemiluminescence NO analyzer (NOA) (Sievers 280, Boulder, CO) as previously described in Chapter 2.

A.3 Result and Discussion

A.3.1 Comparison of pH changes of PLL films containing different bases

As described in Chapter 1, in previous reports, small molecular diazeniumdiolates (NONOates) such as proli/NONOate and SPER/NONOate (see structures in **Figure 1.5B**) have been infused into animals due to the non-toxic amino acids or polyamines generated once NO is released from these two NONOates.[8] Without the presence of any base, the lifetimes of the NONOates are very short (2 s for proli/NONOate and 5-50 min

for SPER/NONOate in PBS buffer at 37 °C).[9] Therefore, basic solutions such as NaOH solution[10] or solid bases such as $Mg(OH)_2$ [11] need to be utilized to further extend the lifetimes of such NONOates.

In this experiment, SPER/NONOate was chosen because of its relatively long half-life. In Chapter 2, it was demonstrated that there is a correlation between the NO release lifetime and the film pH change utilizing bromothymol blue (BB) as the pH indicator. The higher the film pH, the slower the depletion of the NO donors within the NO release film and thus the longer the NO release lifetime. Therefore, before the addition of SPER/NONOate, the pH changes of films of the PLL matrix doped with different bases were evaluated.

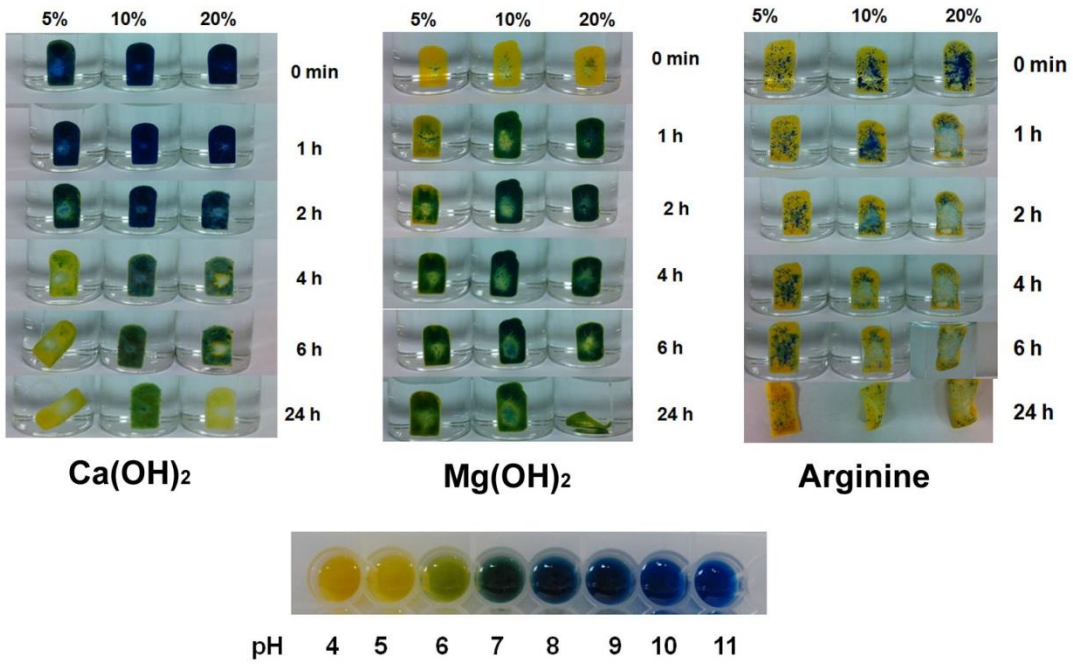

Figure A.2. Comparison of color changes of bromothymol blue (BB) doped films containing 5 wt%, 10 wt% or 20 wt% of $Ca(OH)_2$, $Mg(OH)_2$ or arginine (free base) at 37 °C in PBS buffer for 0 min, 1 h, 2 h, 4 h, 6 h and 24 h, respectively.

As shown in the comparison of the film colors in **Figure A.2**, only the PLL films with $Ca(OH)_2$ doped within exhibit a basic environment when the films are placed into PBS buffer. This basic environment is important to reduce the "burst" of NO at the initial stage of NO release and stabilize the NONOate within the film once SPER/NONOate is

added. Although the PLL film containing 20 wt% of arginine also exhibits observable basic regions, the soluble base of arginine quickly leaches out into the solution within 1 h as can be observed in **Figure A.2**. Compared to $Ca(OH)_2$, $Mg(OH)_2$, a weaker base, is only able to create a neutral environment after gradual water uptake of the film after ~1 h, which is not enough to maintain the stability of the NONOate at the initial stage of the NO release. As demonstrated in Chapter 2, the addition of a base into the PLL matrix is also able to facilitate the hydrolysis of the ester groups of the polymer matrix. Therefore, while too little $Ca(OH)_2$ will not fully neutralize the acid after its hydrolysis, too much base will also over-expedite the hydrolysis of the PLL matrix. Therefore, the ratio of $Ca(OH)_2$ and PLL have to be optimized to obtain the film that can maintain a basic condition for the longest time before the addition of SPER/NONOate. From the comparisons of the pH induced color changes shown in **Figure A.2** for the PLL films doped with different weight percentages of $Ca(OH)_2$, a film containing 10 wt% $Ca(OH)_2$ is the optimal.

A.3.2 NO release profiles of biodegradable NO release films

The NO release profiles of the biodegradable NO release films with different top coating thicknesses are compared and shown in **Figure A.3A and Figure A.3B.** Both films contain an NO releasing layer containing 5 wt% of SPER/NONOate doped in a matrix also containing 10 wt% of $Ca(OH)_2$ in PLL that is sandwiched between two layers of 10 wt% $Ca(OH)_2$ in PLL. Both the base layer and top coating of film B are three times thicker than those of film A. The NO release profiles of the films, however, are similar. According to the integration of the total amount of NO that is released from the films, only ~13% of the SPER/NONOate is fully converted to NO. The low efficiency is observed for both films and might be attributed to the preparation method used during which the SPER/NONOate has to be exposed to ambient moisture for a long time, resulting in loss of NO during the drying process.

To further evaluate the pH changes within the film during the NO release period, a film containing the pH probe in the sandwiched layer was prepared utilizing the same method as film A and the color change of the film was monitored over 24 h and compared with

the previously observed result in **Figure A.2** for a film with 10 wt% $Ca(OH)_2$ doped in PLL without the sandwich configuration. As shown in **Figure A.3C**, the color changes of both films are almost identical and the degradation of the PLL matrix begins to be observed between the 4 h and 6 h period of incubation. This trend is consistent with the NO release pattern of the film. As shown in **Figure A.3A**, the NO flux is low at the initial stage due to the high film pH, but increases significantly after 5 h due to the degradation of the PLL matrix, which produces more protons to facilitate the NO release of the NONOate. Film B, with a thicker top coating and base layer, does not show any observable NO release until after 5 h. The thicker barrier is responsible for slower water uptake into the middle layer and releases the NO from the NONOate. The film appearance after the pH experiment is shown in **Figure A.3D** with no significant leaching of the pH probe into the PBS buffer is observed.

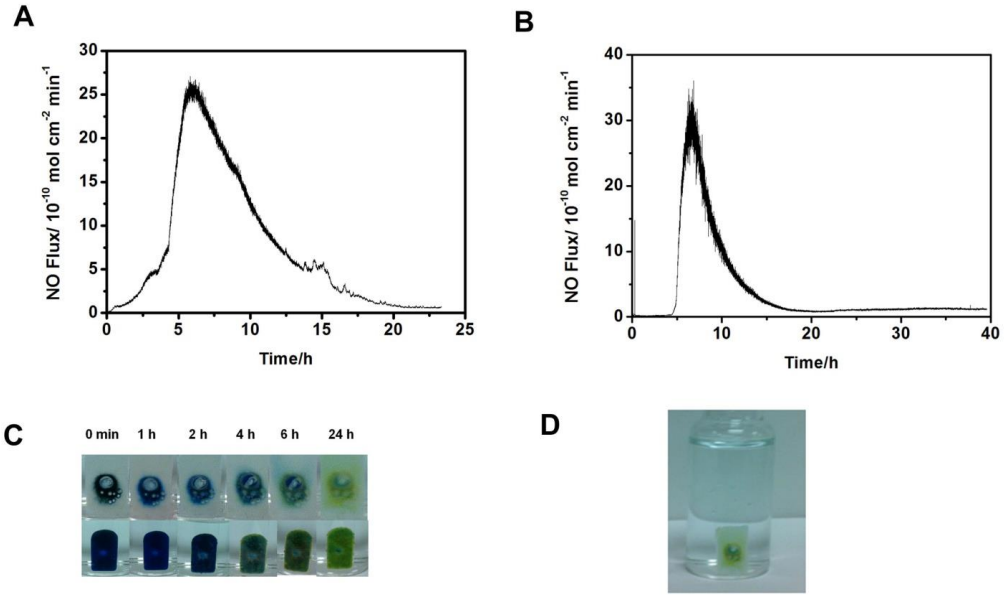

Figure A.3. NO release profiles of A) film A and B) film B in PBS buffer at 37 °C. Both biodegradable NO release films containing a sandwiched middle layer of 5 wt% SPER/NONOate in 10 wt% $Ca(OH)_2$ doped in PLL matrix (see section A.2.3 for details of film preparation). The thickness of the top coating and base layer of film B are three times that of film A; C) comparison of film pH changes overtime for films with a sandwich configuration and film used in **Figure A.2**; D) appearance of the film with a sandwich configuration after the pH experiment in PBS buffer for 24 h at 37 °C.

A.4 Conclusions

Firstly, biodegradable matrices with basic environments can be created by doping bases into PLL and this approach can be utilized to extend the NO release lifetimes of embedded NONOates. A completely biodegradable NO release film was fabricated by doping spermine NONOate into a matrix composed of 10 wt% $Ca(OH)_2$ in PLL. The film is capable of releasing NO for 20 h at 37 °C and is thus expected to be potentially applied on metal implants to help solving the bacterial infection issues associated with conventional orthopedic implants.

A.5 References

1. Liu, X. Y.; Chu, P. K.; Ding, C. X. *Mater. Sci. Eng. R-Rep.* **2004,** 47, (3-4), 49-121.
2. Hornberger, H.; Virtanen, S.; Boccaccini, A. R. *Acta Biomater.* **2012,** 8, (7), 2442-2455.
3. Hetrick, E. M.; Schoenfisch, M. H. *Chem. Soc. Rev.* **2006,** 35, (9), 780-789.
4. Ostrowski, N. J.; Lee, B.; Roy, A.; Ramanathan, M.; Kumta, P. N. *J. Mater. Sci.-Mater. Med.* **2013,** 24, (1), 85-96.
5. Schmidmaier, G.; Wildemann, B.; Stemberger, A.; Haas, N. P.; Raschke, M. *J Biomed Mater Res* **2001,** 58, (4), 449-455.
6. Raval, A.; Parikh, J.; Engineer, C. *Ind. Eng. Chem. Res.* **2011,** 50, (16), 9539-9549.
7. Cai, W. Y.; Wu, J. F.; Xi, C. W.; Meyerhoff, M. E. *Biomaterials* **2012,** 33, (32), 7933-7944.
8. Miller, M. R.; Megson, I. L. *Br. J. Pharmacol.* **2007,** 151, 305-21.
9. Keefer, L. K. *ACS Chem. Biol.* **2011,** 6, (11), 1147-1155.
10. Jeh, H. S.; Lu, S.; George, S. C. *J. Microencapsulation* **2004,** 21, (1), 3-13.
11. Kaul, S.; Cercek, B.; Rengstrom, J.; Xu, X. P.; Molloy, M. D.; Dimayuga, P.; Parikh, A. K.; Fishbein, M. C.; Nilsson, J.; Rajavashisth, T. B.; Shah, P. K. *J Am Coll Cardiol* **2000,** 35, (2), 493-501.